論文 / 著書情報
Article / Book Information

題目(和文)	
Title(English)	Color metallography of Al alloys using Weck ’ s reagent: applications and coloring mechanism
著者(和文)	高立
Author(English)	Li Gao
出典(和文)	学位:博士（工学）, 学位授与機関:東京工業大学, 報告番号:甲第9837号, 授与年月日:2015年3月26日, 学位の種別:課程博士, 審査員:熊井　真次,里　達雄,木村　好里,曽根　正人,村石　信二
Citation(English)	Degree:, Conferring organization: Tokyo Institute of Technology, Report number:甲第9837号, Conferred date:2015/3/26, Degree Type:Course doctor, Examiner:,,,,
学位種別(和文)	博士論文
Type(English)	Doctoral Thesis

Tokyo Institute of Technology

Color metallography of Al alloys using Weck's reagent: applications and coloring mechanism

A Dissertation for the Degree of
Doctor of Engineering
Field of Materials Science and Engineering

By
Li Gao

December, 2014

Contents

Chapter 1

General introduction of this thesis

1.1. History and recent development of color etching metallography

Color etching is an effective technique to characterize the microstructures for various metals or alloys. The history of color etching is very long. Color micrographs were published as early as over ninety-some years ago [1]. The human eye can only distinguish about sixty levels of gray shades from white to black, but can distinguish a large number of colors. That is why color etchants can reveal more features in the microstructure compared to normal black and white etchants. However, the use of color etchants was quite limited in metallography due to several reasons. First of all, in the old times, the cost of film and prints were high so reproducing color images was difficult. Although the development of digital imaging has made the reproduction cheaper and easier, color micrographs are still hardly seen in recent published articles, which is due to the second reason: the insufficient understanding of color etching method. In the history of color etching metallurgy, many color etchants were invented. Some of them are believed to be sensitive to crystallographic orientation and some of them are said to be able to reveal

variations in composition. However, unfortunately most of these abilities or potentials have not been proved rigorously. The third reason is the fast popularization of electron microscopy. With the development of techniques such as electron backscattered diffraction (EBSD) and electron probe micro-analysis (EPMA), quantitative characterization of crystallographic orientation and distribution of solute distribution has been realized. As a result, Color etching, this “old” technology seems to be more and more unnecessary.

Nevertheless, the endeavor to use and understand color etching method has never been stopped. Recently, several studies were carried out for cast iron or steels applying color etching method [2-7]. Among those studies, some had made an effort in explaining the coloration mechanisms or the relationship between color and materials properties [4, 6and 7]. It was found that the color difference could qualitatively represent the difference in chemical compositions [4] or grain orientations [6, 7]. Maltais et al [8] summarized three well-known coloring mechanisms which are shown in Fig. 1-1. In many cases, a thin (usually several hundred micrometers) film is formed on the surface of specimen after color etching which can lead to light interference when observed by optical microscope. The difference in the thickness from location to location therefore can yield to a difference in color (Fig. 1-1 (a)). One example is given in Fig. 1-2 with reference to [9]. The author contributes

the color difference in austenite to the Si micro-segregation, which causes a difference in film thickness formed after etching by alkaline solution. Not only the thickness, but also the film's optical anisotropy can lead to a color difference even if the thickness is uniform (Fig. 1-1 (b)). In this case, the orientation of the granular substrate and the film are related, so that the color difference observed can always reflect the difference in the crystallographic orientation of the grains in the specimen (substrate) as experimentally proved by Szabo and Kardos [7], Fig. 1-3. In the case of aluminum and its alloys, anodizing using Barker's reagent (1.8% HBF_4 in distilled water) is widely applied to reveal the grain structure, as shown in Fig. 1-4, [1]. Despite the fact that in many cases, a film is formed on the specimen's surface after anodizing, no film is formed on aluminum alloys when anodized by Barker's reagent. As shown in Fig. 1-1 (c), instead, the surface is furrowed with two sets of parallel faces, which causes coloration effects under polarized light [1]. The color difference comes from the different face orientation which is directly related to the grain orientation. However, not all the coloration can be explained by the above three mechanisms. Maltais *et al*. also developed a new color etching technique called "line etching" for Magnesium alloy [10], where the birefringence coming from a linearly crackled surface is responsible for the color observed under polarized light.

From the history and recent research of color etching metallography it is

clear that understanding the coloring mechanism is the prerequisite for the wider use of a certain color etchant. Different color etchant can have different coloring mechanism and the meaning of color or color difference also changes from etchant to etchant.

1.2. Weck's reagent

In 1980s, Weck and Leistner developed a color etchant that could detect segregations in cast aluminum alloys [11]. The chemical compositions are 4g $KMnO_4$, 1g NaOH and 100mL distilled water. One example was given in Fig. 1-5 from [1]. The material is as-cast Al alloy (Al-4.4%Cu-0.3%Mg-0.3%Mn). After etching the dendritic Al phase is colored with a vivid contrast. The color difference in one grain correlates with the micro-segregation occurred during casting. Suárez-Peña and co-authors explained the mechanism of this etching process in detail [12] by referring other studies concerning aluminum's chemical activity [13,14] and permanganate conversion coating on 2024 Al alloy [15]:

1) Aluminum is a very active metal. The initial product of the corrosion of aluminum in an aqueous environment is the hydroxide aluminum, namely $Al(OH)_3$. Then, $Al(OH)_3$ creates a hydrated oxide ($Al_2O_3 \cdot H_2O$).

2) When the sample is immersed in Weck's reagent, based on an alkaline solution of potassium permanganate (pH value is 13 approximately), the oxide layer will be dissolved. Therefore the fresh aluminum is exposed.
3) The freshly exposed aluminum reacts with $KMnO_4$ thus a colored film (MnO_2) is formed on the surface:

$$Al + MnO_4^- + 2\ H_2O \rightarrow Al(OH)_4^- + MnO_2 \qquad (1)$$

For a branch of Al alloy dendrite, due to the different electrochemical potentials of edge and center regions resulting from segregation, a difference of color intensities is caused [12].

However, it should be mentioned that the above explanation is insufficient of experimental support. Furthermore, there is no detailed investigation of the relationship between micro-segregation and the color difference after etching.

1.3. Objectives of this study

The present study has been carried out to understand better about Weck's reagent. Specifically speaking, the following three topics are studied in detail:

1) The detailed correlation between micro-segregation and color difference
2) The applications of Weck's reagent using its ability of detecting micro-segregations
3) The coloring mechanism of Weck's reagent

The first topic was chosen because this is the most basic function of Weck's reagent, namely detecting the micro-segregation in Al alloys. However, most of the etching examples with Weck's reagent are provided using commercial Al alloys containing more than two added elements. This makes it difficult to judge which element segregates and as a result, causes the color difference. Without knowing the detailed influence of a single element's micro-segregation in Al phase on the coloration, it is meaningless to use Weck's reagent to characterize the micro-segregation. In this study, two methods are applied to investigate this issue. One is using strictly controlled binary Al alloys so the color difference revealed by Weck's reagent can be convincingly attributed to the added element's segregation. The other one is EPMA analysis especially the concentration mapping of the solutes in Al alloy. The mapping is compared to the micrograph observed after etching so that the relationship between color and micro-segregation can be intuitively

studied.

The second topic needs to be studied because the present application of Weck's reagent is still restrained to as-cast Al alloys with a dendritic structure. As is well known, dendritic structure is an uncontrolled or weakly controlled cast (solidified) microstructure for alloys. In many practical foundry cases, coarse dendritic structure is not expected compared with refined spheroidal or equiaxed structure in order to obtain better mechanical properties of the later types of microstructure. Therefore, it is significant to investigate if Weck's reagent can be applied to characterize the micro-segregation in the Al phase with various types of structure. Also, after studying the first topic, the segregation-detection ability of Weck's reagent is known better. Taking the advantage of this ability, if more information can be obtained is of great interest. Finally, besides micro-segregations in Al phase, if the grain structure can be revealed by Weck's reagent or not is also important since most of the other existing chemical etchants such as Keller's reagent are usually applied to attack grain boundaries.

The last main objective of this study is to understand the coloring mechanism. This is the topic of the biggest challenge since it requires knowledge and experimental results of various fields such as surface characterization, film characterization and color science. As mentioned before, Suárez-Peña et al. suggest that during etching, Al reacts with

Weck's reagent producing a film of Manganese oxide on the specimen's surface. Our first task concerning this topic is to confirm the existence of this Manganese oxide film. If the film does exist, then we focus on the characterization of this film, especially on those observations such as surface morphology, thickness which can affect the optical properties of the film.

1.4. Construction of the thesis

The present thesis is entitled "Color metallography of Al alloys using Weck's reagent: applications and coloring mechanism", which consists of 6 chapters as follows.

Chapter 1 "General introduction of this thesis"

Background of both color etching metallography and Weck's reagent, objectives of this study are provided.

Chapter 2 "Correlation between the micro-segregation in Al phase and the color revealed by Weck's reagent"

In this chapter, the detailed correlation between color and micro-segregation in Al alloys is studied. Various Al alloys including A356 (with or without Ti added) alloy, Al-Si and Al-Mg binary alloys are

used. EPMA mapping mode is applied to characterize the solute distribution and compared to optical micrograph after etching with Weck's reagent. The results show that micro-segregations of Ti, Si and Mg in Al phase can all lead to a color difference. Besides dendritic Al structure, micro-segregation also exists in spheroidal Al grains obtained by semi-solid process. Surprisingly, the spheroidal grain growth occurred when cooling it from semi-solid state to room temperature can also be visualized by Weck's reagent. Discussion about different solutes' micro-segregation in Al phase is also provided in this chapter.

Chapter 3 "accurate solid fraction evaluation of Al alloy at semi-solid state by Weck's reagent"

As a result shown in chapter 2, grain growth during quenching from semi-solid state could be visualized by Weck's reagent. This finding can help to evaluate solid fraction at semi-solid state with a better accuracy by excluding this part when calculating the area fraction of solid particles in the optical micrograph. The results of A356 Al alloy using this method are compared with both the traditional method without excluding the grain growth during solidification and the results from level rule referring to Al-Si binary phase diagram.

Chapter 4 "spheroidization mechanism of Al phase at semi-solid state by

compression and partial re-melting process”

In this chapter, the microstructural evolution of Al grains from dendritic to spheroidal is focused. Since the materials was deformed and heated to semi-solid state, recrystallization occurred during heating. As a result, Al grains are refined compared to the specimen without deformation before heating. Weck’s reagent finds its application again in this study. By etching the specimen which is transforming from dendritic to spheroidal, compressed dendritic Al grains are found separated and when the eutectic structure starts to melt, liquid phase penetrates into those separation sites and spheroidized Al grains are formed. According to EBSD analysis, high angle grain boundaries are found inside Al phase when the compressed specimen is heated. This suggests that Weck’s reagent is also able to reveal grain boundaries in Al phase.

Chapter 5 “coloring mechanism of Weck’s reagent studied by characterization of the etched surface”

Coloring mechanism of Weck’s reagent was studied by various characterizations and analyses of the etched surface. It was confirmed by electron scanning microscopy (SEM) that a film whose morphology changes from location to location is formed during etching. Compositional analysis shows that the film consists of Manganese oxide and the structure is amorphous. With the detailed observation by laser

microscopy and atomic force microscopy (AFM), the relationship between the color and etched surface is investigated. The results show that the film surface is flat while the interface between film and substrate is relatively rough. The film thickness and the roughness between film and substrate are strongly influenced by the concentration of Ti in Al. The higher concentration of Ti can promote the film growth, which is confirmed by the surface observation. It is concluded that the color of the film is basically brown. But the brightness of brown is strongly influenced by the film's thickness and the roughness of interface between film and substrate.

Chapter 6 "Summary and general conclusions"

A summary of the applications of Weck's reagent which have been found by this study and the coloring mechanism concluded from experimental results are provided.

References

[1] G.F Vander Voort, Metallography and Microstructures, ASM Handbook. Ohio: ASM International, 2004.

[2] S.M.A Boutorabi and J. Campbell, An etching technique for primary austenite dendrites in ductile cast iron, Mater. Charact. 31(1993) 127-132.

[3] A. Ray and S. Dhua, Microstructural manifestations in color: some applications for steels, Mater. Charact. 37(1996) 1-8.

[4] C.F Yeung, H. Zhao and W.B. Lee, The morphology of solidification of thin-section ductile iron castings, Mater. Charact. 40(1998) 201-208.

[5] J. Zhou, Colour metallography of cast iron, Chapter 1, China Foundry 9(2009) 152-157.

[6] P.J Szabó and A. Bonyár, Effect of grain orientation on chemical etching, Micron 43(2012) 349-351.

[7] P.J. Szabó and I. Kardos, Correlation between grain orientation and the shade of color etching, Mater. Charact. 61(2010) 814-817.

[8] A. Maltais, D. Dubé, F. Roy, M. Fiset, Optical anisotropy of a color-etched AZ91 magnesium alloy, Mater. Charact. 54 (2005) 315-326.

[9] J. Zhou, Colour metallography of cast iron, China Foundry 6 (2009):

152-157.

[10] A. Maltais, M. Fiset, G. Laroche, S. Turgeon, D. Dubé, Improvement in metallography of As-Cast AZ91 alloy, Mater. Charact., 52 (2004) 103–119.

[11] E. Weck, E. Leistner, Metallographic instructions for colour etching by immersion, part iii: non-ferrous metals, cemented carbides and ferrous metals, nickel-base and cobalt-base alloys. DVS GmbH, Düsseldorf, 1986.

[12] B. Suárez-Peña, J. Asensio-Lozano, G.F. Vander-Voort, Colour metallography in commercial Al-Si alloys. Optimization of the microstructural characterization techniques in light optical microscopy. Rev. Metal 46(2010) 469-476.

[13] H.P. Godard, W.P. Jepson, M.R. Bothwell, R.L. Kane, The corrosion of light metals. John Wiley and Sons, New York, 1967.

[14] M. Pourbaix, Aluminium atlas of electrochemical equilibrium in aqueous solutions. Pergamon, Oxford, 1966.

[15] S.A. Kulinich, A.S Akhtar, P.C. Wong, K.C. Wong, K.A.R. Mitchell, Growth Of Permanganate Conversion Coating On 2024-Al Alloy. Thin Solid Films 515 (2007) 8386-8392.

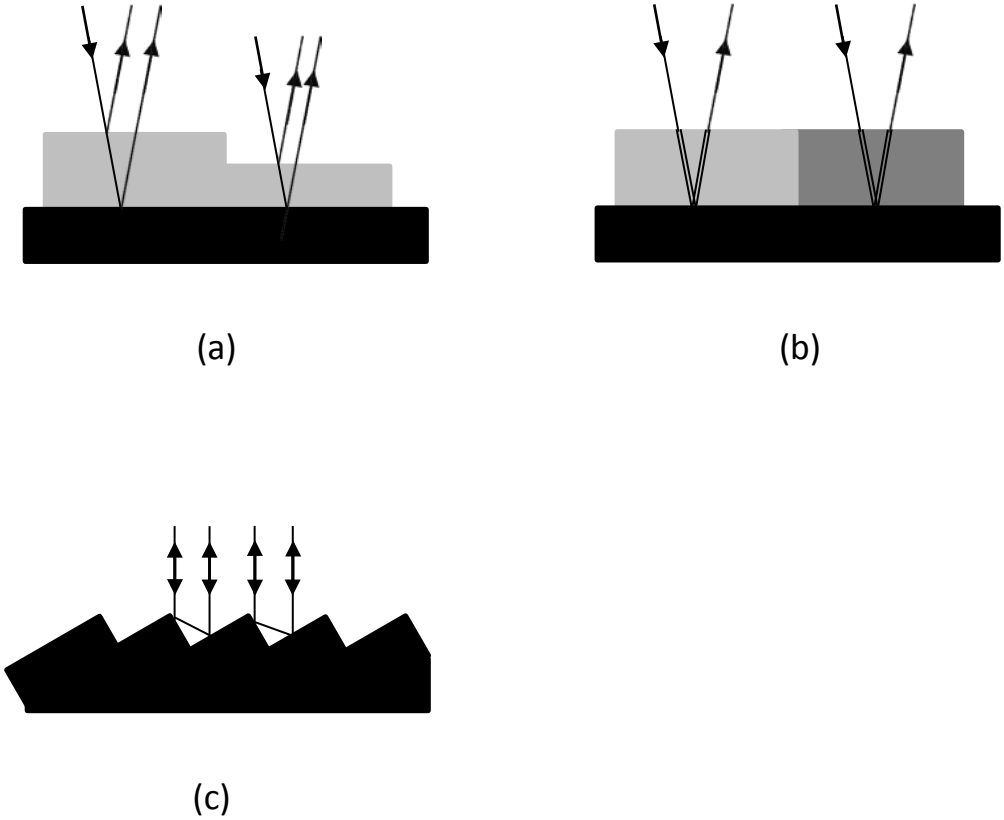

Fig. 1-1. Schematics of surfaces producing color after etching summarized by Maltais et al. [9]: (a) Interference film with different thickness. (b) Anisotropic film with the same thickness. (c) Etching pitting after anodizing of Al alloy.

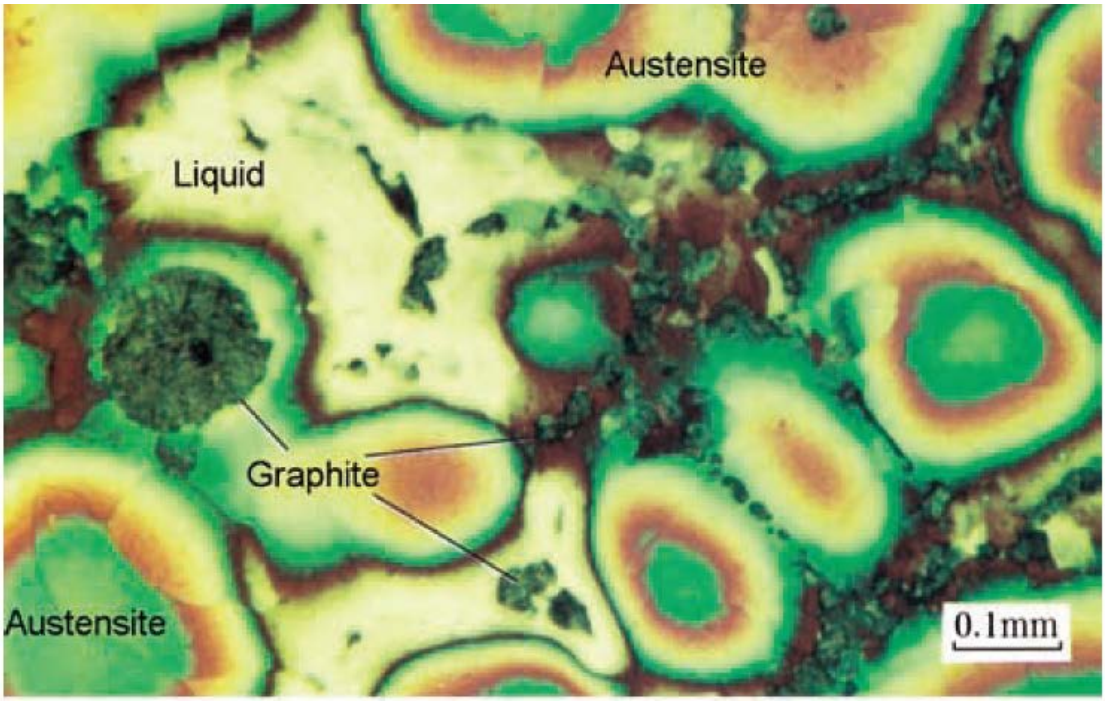

Fig. 1-2. An example of color etching showing different color in austenite which is caused by Si micro-segregation [9].

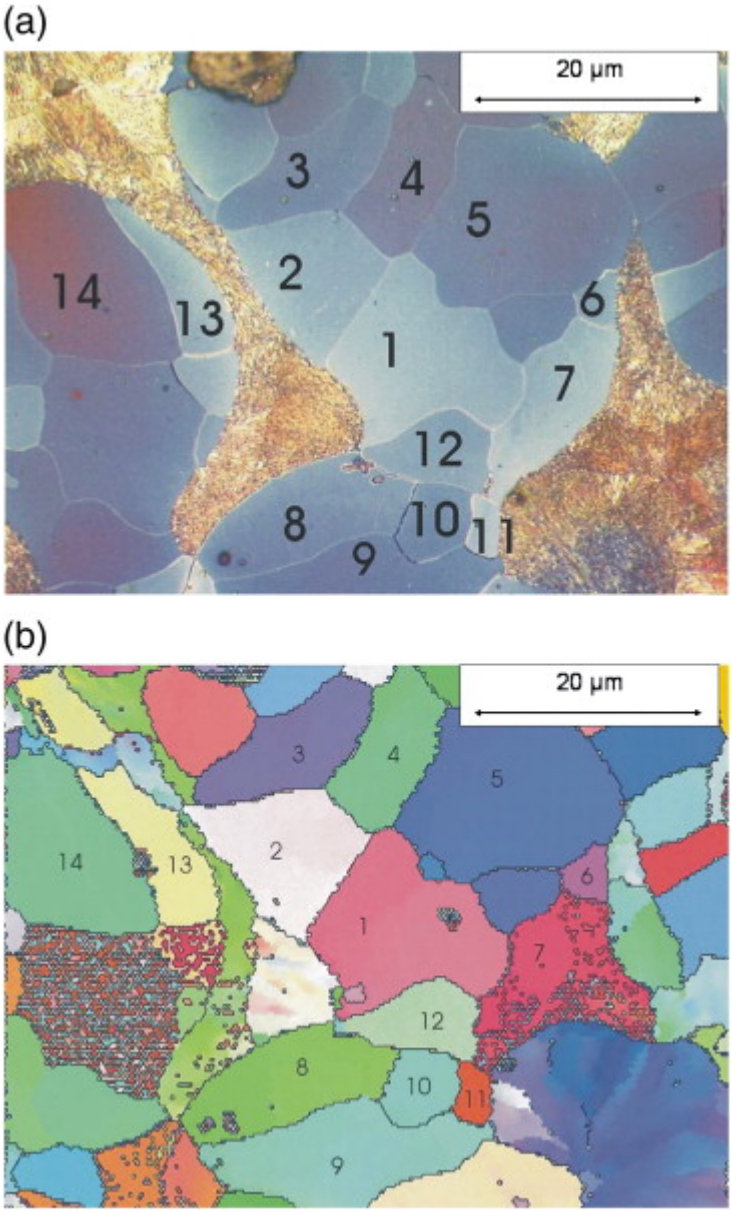

Fig. 1-3. An example showing the correlation between the (a) shade of color etching obtained by etching a cast iron specimen and (b) grain orientation by EBSD analysis [7].

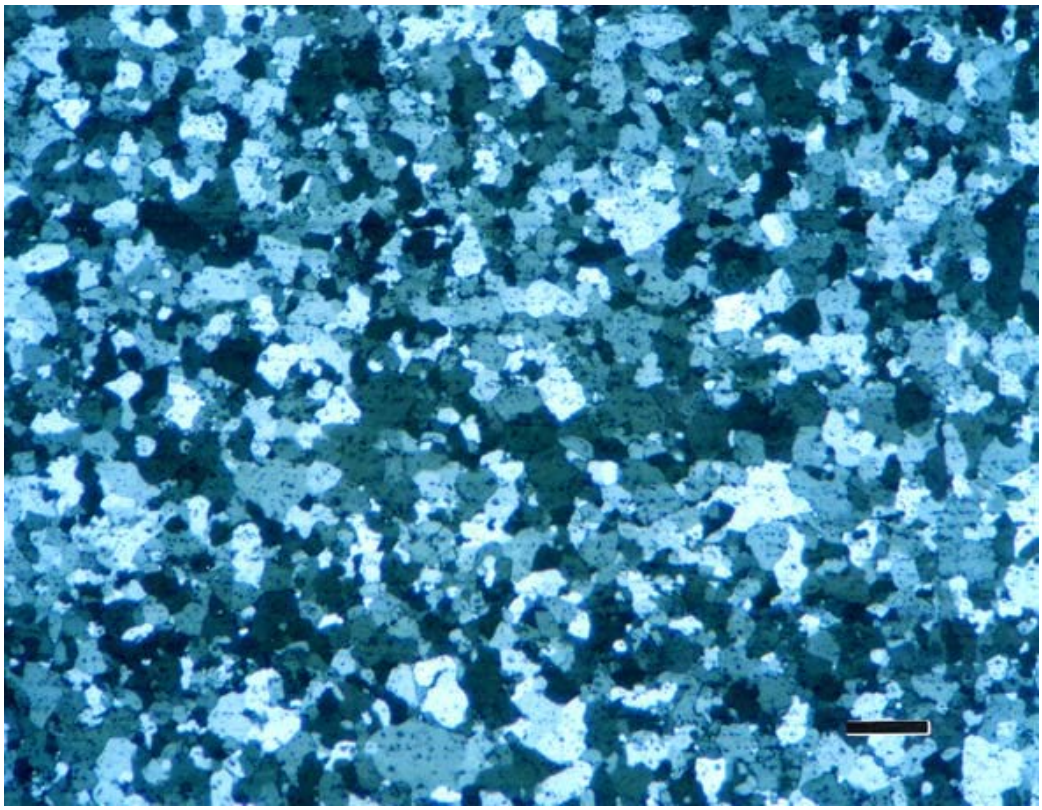

Fig. 1-4. An example showing the grain structure of wrought Al alloy after anodizing [1]. The microstructure was observed under polarized light and the magnification bar is 100 μm long

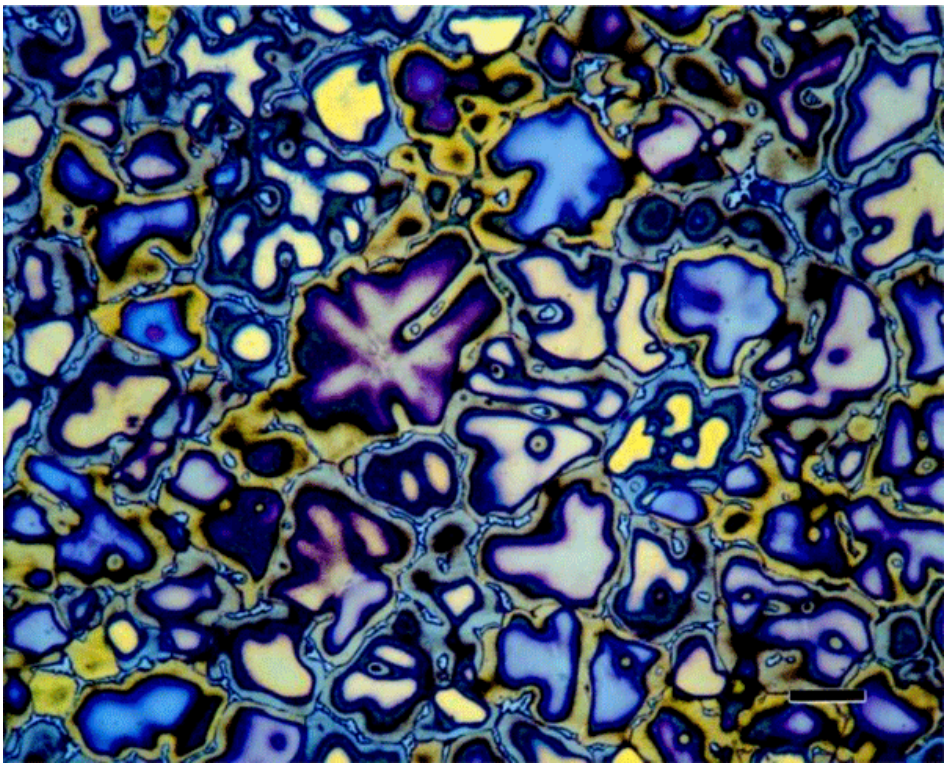

Fig. 1-5. An example of color etching provided in [1]. The micrograph is observed with crossed polarized light and sensitive tint so the color contrast is strengthened. Magnification bar is 50 μm long.

Chapter 2

Correlation between the micro-segregation in Al phase and the color revealed by Weck's reagent

2.1. Introduction

The partitioning of solute elements between liquid and solid leads to micro-segregation during solidification. Since micro-segregation can significantly affect a cast product's mechanical property [1], the understanding and characterization of micro-segregation is of great importance. For binary alloys, such partitioning data for the equilibrium state can be obtained from phase diagram. However, if the alloy is multi-component or at unequilibrium state, numerical or experimental analysis is needed to characterize the micro-segregation. In the case of experimental analysis, EPMA analysis is frequently used because of its satisfying accuracy [2-6]. As mentioned in Section 1.2, Chapter 1, Weck's reagent is said to be able to detect micro-segregations in Al alloys although there is not enough experimental support. Therefore, in this chapter, color etching using Weck's reagent will be directly compared with traditional EPMA analysis. Both of these two methods succeeded in charactering micro-segregations in different Al alloys and color etching has its advantages over EPMA analysis.

Also in chapter, binary Al alloys with the chemical composition strictly

controlled are used. Al-7% (mass %) Si and Al-5% (mass %) Mg as cast alloy show color difference inside dendritic Al gains after etching, which supports strongly that Si and Mg's segregation during solidification is the reason for the color difference revealed by Weck's reagent.

Not only inside dendritic Al grains, but also the micro-segregation in spheroidal Al grains is an important topic in this chapter, which is investigated by both EPMA analysis and color etching with Weck's reagent. In this case, multi-component alloys that have commercial compositions are used.

By these experiments and comparison between color etching method and EPMA analysis, the advantages of each method can be more clearly seen. Moreover, the most important role that Weck's reagent plays, micro-segregation detection can be better understood.

2.2. Experimental

There are in total four alloys used in this chapter. All of these four alloys' compositions are list in Table 2-1. The compositions of Al-7%Si binary alloy and A356 Al alloys (Ti-contained and Ti-free) were measured by an Optical Emission Spectrometer while Al-5%Mg binary alloy's composition was measured by a Sequential Type ICP Emission Spectrometer. Al-7%Si and Al-5%Mg binary alloy billets were made by

casting using Cu-mold while A356 alloys were DC-cast.

Spheroidization of Al grains in A356 Al alloys with or without Ti added was obtained by re-melting those alloys to semi-solid state after cold compression by 33%. The appearance and size of Ti-contained A356 alloy billets are shown in Fig. 2-1 as an example. The cold compression was done in Nissan Motor Co., Ltd's factory. To avoid buckling, the billet was cut into small ones (Φ105×150mm). Compression was carried out axially by a 500 ton compressing machine. The compressing rate is 0.2mm/sec. The billet's temperature was increased to about 44 ^{o}C when the target height (100mm, 33% reduction) was reached. After compression, small specimens were cut from the billet and heated to semi-solid temperatures. Specimens were quickly water quenched when the target semi-solid temperature was reached in order to restrain the homogenization of solute in Al phase by diffusion.

Specimens were polished via standard metallographic techniques, finished using Struers OPS colloidal silica. Subsequently, specimens were immersed in Weck's reagent for approximately 12 s at room temperature. Then the microstructure was observed by optical microscopy (OM) without any filters or analyzers.

EPMA analyses by X-ray Wavelength Dispersive Spectroscopy (WDS) were carried out to evaluate the micro-segregations of Ti, Mg and Si for the Ti-contained and Ti-free A356 Al alloys. The analyzed locations were

the same with where the optical micrographs were taken. The acceleration voltage was set to 15 kV for all the measurements. Electron beam current was set to 18 nA for the measurements of Si and 180 nA for Ti, Mg. Distribution mappings were made by measuring the intensities of characteristic X-rays, after which the intensity was converted into atomic percent using the calibration standards.

2.3. Results

2.3.1. Microstructures of Al-7%Si and Al-5%Mg binary alloys before and after etching with Weck's reagent

The as-cast microstructures of Al-7%Si and Al-5%Mg binary alloys before and after etching are shown in Fig. 2-2. The microstructures before etching (Fig. 2-2 (a) and (c)) indicate the dendritic shape of Al phase. As shown in Fig. 2-2 (b) and (d), due to the binary composition, the color difference observed after etching could be attributed to the micro-segregations of Si and Mg, respectively. In Al-7%Si binary alloy, even before etching, the dendritic Al phase is clearly distinguishable because of the existence of eutectic phase (Fig. 2-2 (a)). While in Al-5%Mg alloy, most of the microstructure is Al phase so that without etching, it is difficult to observe the shape of dendritic phase (Fig. 2-2 (c)). After etching with Weck's reagent as indicated in Fig. 2-2 (d), it is very

interesting that the first arm as well as secondary arm is clearly revealed simultaneously color difference inside the dendrites corresponds to the micro-segregation of Mg occurred during solidification. Comparing Fig. 2-2 (b) with Fig. 2-2 (d), it is indicated that the dendrites are differently colored (more brown in Al-7%Si alloy while blue in Al-5%Mg alloy). In order to explain this phenomenon, it is necessary to consider the coloring mechanism of Weck's reagent. Suárez-Peña and co-authors [7] explained the mechanism of this etching process by the following chemical reaction by referring other studies concerning aluminum's chemical activity [8, 9] and permanganate conversion coating on 2024 Al alloy [10]:

$$Al + MnO_4^- + 2H_2O \rightarrow Al(OH)_4^- + MnO_2 \quad (1)$$

Therefore, a MnO_2 film responsible for the color observed by OM is formed on the surface after etching with Weck's reagent. According to this theory, it can be inferred that the addition of different kinds of solutes (Si or Mg, for instance) can also affect the reaction so that the MnO_2 film may have different optical properties. As a result, the color will also change.

2.3.2. Microstructure of Ti-contained A356 Al alloy and EPMA analysis

Fig. 2-3 shows the microstructures of as-received (DC-cast) Ti-contained Al alloy both before and after etching by Weck's reagent. Micrographs were taken at this location because there was an intact

dendritic Al grain. It can be seen that after etching with Weck's reagent, inside the dendrite, color differences are visible. In line with the results of Suárez-Peña et al. [7], the central part of the dendrite branches has a darker color than the peripheral part.

After compressing and partially re-melting the as-received alloy, spheroidization of Al grains could be achieved. Spheroidal microstructures before and after etching are shown in Fig. 2-4. The specimen was water quenched when the temperature reached 581 ^{o}C (as shown in Fig. 2-3 (a), (b) and (c)), the Al-Si eutectic structure which is located among spheroidal Al grains was completely melted and solidified again during quenching. Inside Al grains (Fig. 2-4 (a) and (b)), there are several round spots which used to be entrapped liquid (droplets) in the semi-solid state and then solidified into very fine eutectic structure. There are two interesting results present in as-etched state (Fig. 2-4 (b)). First, a ring-shaped structure is visualized in the peripheral part of the spheroidal grain located at the center of Fig. 2-4 (b). This ring-shaped structure corresponds to the grain growth during water quenching. Second, a dendritic structure was also clearly revealed inside the spheroidal grain. Considering the fact that this spheroidal grain comes from a compressed dendritic Al grain, it is reasonable to regard this dendritic structure as the reflection of the as-compressed dendrite.

Since there are more that two alloying elements in A356 Al alloy, it is

difficult to judge which one is the cause of the color difference revealed by Weck’re reagent in both the case of dendritic and spheroidal Al grain. That is why EPMA analyses were carried out.

Solute distributions of Ti, Mg, Fe and Si in the dendritic grain are shown in Fig. 2-5. The data analysis system of the EPMA device automatically converts the atomic concentrations from high level to low level into different colors from light pink to dark purple, respectively (see the color bars next to the mappings). For convenience, the upper and lower limit of concentration that is converted into color can be decided manually. Consequently the region where the concentration is higher than the upper limit will be displayed in white while the region where the concentration is lower than the lower limit will be displayed in black. Fig. 2-5 (a) displays the Ti distribution before changing the upper and lower limit for concentrations. It should be noted that there is a point where the Ti concentration is much higher than in the other regions, which is probably a Ti compound that acted as a nucleation site during DC casting. Compared with the as-etched microstructure shown in Fig. 2-5 (f), which magnifies Fig. 2-3 (b), it can be seen that at the same location there is also a diminutive point indicated by the arrow. Moreover, in Fig. 2-5 (a), it is clear that a dendritic region (with dark blue color) exists which has a higher concentration of Ti than the other region. However, due to the influence of the very high Ti concentration of the Ti compound, the

contrast of the rest of the dendritic region is suppressed. By lowering the upper limit of Ti concentration displayed in light pink, the region which contains the Ti compound is displayed in white. However the reminder of the region shows much better contrast, as shown in Fig. 2-5 (b). Comparing Fig. 2-5 (b) with the as-etched microstructure in Fig. 2-5 (f), one observes a very strong correlation between the solute distribution of Ti and the color difference revealed by Weck's reagent. Specifically, the red region, which contains more Ti in Fig. 2-5 (b), has almost the same shape as the black and brown region in Fig. 2-5 (f).

Solute distributions of Ti, Mg, and Si inside the spheroidal grain are shown in Fig. 2-6 (concentration of Fe was not measured). Comparing Fig. 2-6 (a) with Fig. 2-4 (b), it is clear that a close correlation exists between the color difference in the as-etched microstructure and the distribution of Ti. Specifically, the dendritic region is rich in Ti while the entrapped eutectic regions contain the lowest concentration of Ti. As displayed in Fig. 2-6 (b) and (c), Mg, as well as Si are evenly distributed inside the spheroidal grain, except for the region of entrapped liquid. Furthermore, with a magnification of the grain growth during quenching, the micro-segregations of both Ti and Si were confirmed (Fig. 2-6 (d) and (e)). Comparing with Fig. 2-4 (b), the dashed line drawn in Fig. 2-6 (d) indicates the original liquid-solid interface at semi-solid state, which is also the location where the grain started to grow during water quenching.

As indicated by the mapping result, during water quenching, the concentration of Ti in the earlier solidified region is higher than that in the region which solidified later, which is very similar to the distribution in dendritic Al grain in Fig. 2-5 (b). The distribution of Si was also measured, and is shown in Fig. 2-6 (e). However, the location is not exactly the same with the one indicated in Fig. 2-6 (d). Owing to the existence of eutectic particles where Si has the highest concentrations, it is easy to distinguish the boundary of the spheroidal grain. Inside the spheroidal grain, it is clear that Si were enriched as the grain grew towards liquid phase.

2.3.3. Microstructure of Ti-free A356 Al alloy and EPMA analysis

Fig. 2-7 shows the microstructure as well as Si and Mg distributions measured by EPMA in Ti-free A356 Al alloys in dendritic state. We can find that after etching with Weck's reagent, a color difference was revealed inside the dendritic Al grain. Since this alloy is Ti-free, certainly Ti could not be detected (mapping was not shown here). But both the micro-segregations of Si and Mg were confirmed by EPMA mapping. From Fig. 2-7 (c) and (d), it is clear that both Si and Mg concentrate in the eutectic region, at the same time, they also segregate inside the dendrite Al grain. Both of them dilute in the center region of the dendrite and concentrate gradually toward eutectic region, which is in agreement

with their partition coefficients (smaller than 1) indicated by both Al-Si and Al-Mg binary phase diagrams (Fig. 2-8). Comparing the solute distributions with the micrograph after etching, one can see the strong correlation between the solute distribution and color difference revealed by Weck's reagent.

After compression and partial re-melting, the spheroidization of Al grains was realized as exhibited in Fig. 2-9. Please note that the scale of Fig. 2-9 (a) is different from Fig. 2-4 (a) and (b). By showing this relatively low magnification micrograph, we want to emphasize that in most of the spheroidal grains, it is difficult to see the dendritic structure as observed in Ti-contained A356 Al alloy (Fig. 2-4 (b)). Only the spheroidal grain located in the very center part of this micrograph shows an obscure shape of dendrite inside itself. In the peripheral region (also magnified in Fig. 2-9 (d)), same with the Ti-contained alloy, we can distinguish the grain growth during water quenching visualized after etching. EPMA mapping was carried out for the spheroidal grain located in the center part of Fig. 2-9 (a) and the grain growth occurred during water quenching. As indicated in Fig. 2-9 (b) and (c), Si, as well as Mg, concentrates in the eutectic region, including the entrapped eutectic region with a round shape inside the spheroidal grain. The dendritic distribution similar to Ti's distribution in Fig. 2-6 (a) was not detected in neither the case of Si nor Mg. However, in the area where spheroidal

grain grew during water quenching, Si segregated (Fig. 2-9 (e)) while Mg (Fig. 2-9 (f)) did not segregate.

From those results exhibited in Fig. 2-7 and Fig. 2-9, it can be concluded that Ti was not the only element whose micro-segregation can cause the color difference after etching with Weck's reagent. However, devoid of Ti, in the spheroidal case, the color contrast is much lowered compared to Ti-contained alloy shown in Fig. 2-4 (b). The detailed discussion focusing on Ti's micro-segregation will be given in the following section.

2.4. Discussion

2.4.1. Detection of micro-segregations by Weck's reagent

The results coming from Al-7%Si and Al-5%Mg binary alloys etched by Weck's reagent proved that micro-segregations of Si or Mg in Al phase are correlated to the color difference revealed by Weck's reagent. Although in some cases color difference is related to difference grain orientation [11, 12], since the color difference is inside one single dendritic grain, it can be concluded that the color difference signifies micro-segregations caused during solidification.

In the case of A356 Al alloys with Ti added, micro-segregations in the as-received dendritic Al phase could be visualized after etching. The micro-segregations of both Si and Ti were confirmed by EPMA mapping.

And Mg should also segregate but not detected by EPMA due to its small amount. Therefore, the color difference in Fig. 2-3 (b) cannot represent a single alloying element's segregation, but the "sum" of all the elements that segregated inside the Al phase during solidification. After spheroidization by semi-solid heat treatment, according to EPMA analysis, only Ti's micro-segregation remained and its distribution matches the color difference in optical micrograph very well, thus the color difference inside spheroidal grain should be the reflection of Ti's micro-segregation.

When Ti is eliminated from the alloy, the color contrast inside spheroidal grain is also decreased as a result. However, in some grains there is still a color difference. EPMA analysis could not detect any micro-segregation in this case probably because that the micro-segregation was too small that EPMA is not sensitive enough to detect it. In other words, color etching with Weck's reagent is more sensitive in detecting compositional difference.

2.4.2. Micro-segregation of Ti in Al phase

Al end of Al-Ti binary phase diagram is shown in Fig. 2-10 which was given by McCartney [13]. From the phase diagram it can be seen that the partition coefficient of Ti in Al is larger than one, which indicates that the concentration of Ti in Al phase at the beginning of solidification is the

highest. This is in accordance with the result of EPMA mapping in Fig. 2-5 (b). At the same time, Si's micro-segregation was also detected in EPMA mapping, having the opposite distribution with Ti which is also in accordance with the Al-Si phase diagram.

However, after semi-solid treatment, Ti's micro-segregation still existed in spheroidal Al phase while the micro-segregation of Si disappeared. In order to explain this phenomenon, the diffusion speed of different solute in Al is considered. The data collected from previous researches are summarized in Fig. 2-11 with reference to [14-18]. From the chat it can be seen that Ti's diffusion coefficient in Al is much lower than other solutes such as Si, Mg and Fe. Therefore, after being heated to semi-solid temperature, the micro-segregation of Si and other elements, namely the uneven distribution could be smoothened by the diffusion of them in Al phase. While for Ti, its micro-segregation could be preserved after semi-solid heat treatment.

The unique distribution of Ti in the spheroidal Al grains is also of interest. This kind of microstructure was called "cored microstructure" whose micrographs were provided by Kamio et al. [14] and Easton and St. John et al. [15] showing a color or grey level difference with dendritic shape inside coarsened Al grains. As shown in Fig. 2-6 (a), the dendritic region which corresponds to the original deformed dendrites before heating and partial re-melting, has a high concentration of Ti because this

region was firstly solidified from liquid during DC casting and remained after heating and partial re-melting. The area which enwraps the dendritic region has the lowest concentration of Ti. This could be explained by considering the coarsening of dendritic grains at the early stage of heating. At this early stage, dendritic grains coarsen toward the eutectic region. Since the eutectic region contains a very low level of Ti, which can be seen in Fig. 2-5 (b), the coarsened part of the dendrites is low in Ti. However, outside of this area, the concentration of Ti again increases, which can be explained as follows. At semi-solid state, spheroidal Al grains flow in liquid. At this state, Ostwald ripening occurs and, as a result, larger grains will grow at the expense of smaller grains. This may be a consequence of the smaller grains being melted and then solidified on other larger grains. It can be seen from Fig. 2-6 (a) that the region with blue color in the spheroidal grain has almost the same concentration of Ti as the eutectic region. On the average, however, spheroidal grains contain higher concentration of Ti than the eutectic region. Thus, the Ti concentration in the region belongs to the outer part of spheroidal grain, namely the grain growth led by Ostwald ripening, is higher.

2.5. Conclusions

Using Al-7%Si and Al-5%Mg binary alloys, the color difference was

revealed inside dendritic Al grains after etching by Weck's reagent. The binary composition of the specimen has proved that micro-segregation of either Si or Mg can be visualized by Weck's reagent.

If the material is multi-component, the color revealed by Weck's reagent should be the result of the all the micro-segregations inside Al phase. In the case of Ti-contained A356 Al alloy, both micro-segregations of Ti and Si exist in dendritic Al grain.

Not only dendritic structure, micro-segregations in spheroidal grains can also be characterized by Weck's reagent. However, in the case of Ti-contained A356 Al alloy, Si's micro-segregation disappeared while Ti's micro-segregation still remained, which can be revealed by Weck's reagent. The extremely low diffusion speed of Ti contributes to the preservation of Ti's micro-segregation at semi-solid state. In the case of Ti-free spheroidal grain, no micro-segregations could be detected by EPMA. But color difference can still be seen after etching although the contrast was low. Probably because color etching is more sensitive compared with EPMA therefore a weak micro-segregation was visualized by Weck's reagent.

Reference

[1] J. Lacaze and G. Lesoult, in Nature and Properties of Semi-solid Materials, TMS, Warrendale, Pennsylvania, 1991.

[2] F.-Y. Xie, X.-Y. Yan, L. Ding, F. Zhang, S.-L. Chen, M.-G. Chu, Y. A. Chang, A study of microstructure and microsegregation o aluminum 7050 alloy. Mater. Sci. Eng. A 355 (2003) 144-153

[3] F.-Y. Xie, T. Kraft, Y. Zuo, C.-H. Moon, Y.A. Chang, Microstructure and microsegregation in Al rich Al-Cu-Mg alloys. Acta Mater. 47 (1999) 489-500.

[4] X.-Y. Yan, S.-L. Chen, F.-Y. Xie, Y.A. Chang, Computational and experimental investigation of microsegregation in an Al-rich Al–Cu–Mg–Si quaternary alloy. Acta Mater., 50 (2002) 2199-2207.

[5] D. G. Eskin, D. Ruvalcaba, C. Kwakernaak and L. Katgerman, Different grain morphologies in grain-refined 7075 billet. Mater. Sci. Tech. 25 (2009) 1175-1182.

[6] Brij K. Dhindawa, L. Kumara, N.C. Amer Alkarkhib, H. Fredriksson, Microstructure development and solute redistribution in aluminium alloys under low and moderate shear rates during rheo processing. Mater. Sci. Eng. A 413-414 (2005) 156-164.

[7] B. Suárez-Peña, J. Asensio-Lozano, G.F. Vander-Voort, Colour metallography in commercial Al-Si alloys. Optimization of the microstructural characterization techniques in light optical

microscopy. Rev. Metal 46(2010) 469-476.

[8] H.P. Godard, W.P. Jepson, M.R. Bothwell, R.L. Kane, The corrosion of light metals. John Wiley and Sons, New York, 1967.

[9] M. Pourbaix, Aluminium atlas of electrochemical equilibrium in aqueous solutions. Pergamon, Oxford, 1966.

[10] S.A. Kulinich, A.S Akhtar, P.C. Wong, K.C. Wong, K.A.R. Mitchell, Growth Of Permanganate Conversion Coating On 2024-Al Alloy. Thin Solid Films 515 (2007) 8386-8392.

[11] P.J Szabó and A. Bonyár, Effect of grain orientation on chemical etching, Micron 43(2012) 349-351.

[12] P.J. Szabó and I. Kardos, Correlation between grain orientation and the shade of color etching, Mater. Charact. 61(2010) 814-817.

[13] D.G McCartney, Grain refining of aluminium and its alloys using inoculants, Int. Mater. Rev. 34(1989) 247-260.

[14] S. Fujikawa, K. Hirano, Y. Fukushima, Diffusion of silicon in aluminum, Metall. Trans. A 9A(1978) 1811-1815.

[15] S. Fujikawa, K. Hirano, Diffusion of ^{28}Mg in aluminum, Mater. Sci. Eng. 27(1977) 25-33.

[16] W.B. Alexander, L.M. Slifkin, Diffusion of Solutes in Aluminum and Dilute Aluminum Alloys, Phys. Rev. B 1(1970) 3274-3282.

[17] D. Bergner, Diffusion of foreign atoms in aluminum, Neue Hutte 29(1984) 207-210.

[18] D.H. St. John, L.M. Hogan, Thermal stability in the Al-Al3Ti system, J. Mater. Sci. 15(1980) 2369-2375.

[19] A. Kamio, H. Tezuka, J-C. Choi, T. Takahashi, Influence of vanadium and titanium on microsegregation and homogenization in Al-6.5%Cu alloys J. Jpn. Inst. of Light Met. (in Japanese) 35(1984) 133-139.

[20] M.A. Easton, D.H. St. John, Partitioning of titanium during solidification of aluminium alloys. Mater Sci Technol 16(2000) 993-1000.

Table 2-1. Main chemical compositions of the materials used in this chapter (wt.%)

Alloy	Si	Mg	Fe	Ti	Sr	Mn	Al
Al-7%Si	7.23	0.003	0.053	0.009	0.0001	0.008	Bal.
Al-5%Mg	ND	5.22	0.094	ND	ND	ND	Bal.
Ti-contained A356	6.90	0.39	0.10	0.14	0.025	<0.10	Bal.
Ti-free A356	7.04	0.43	0.13	0.0006	0.0024	0.006	Bal.

ND: Not detected by ICP

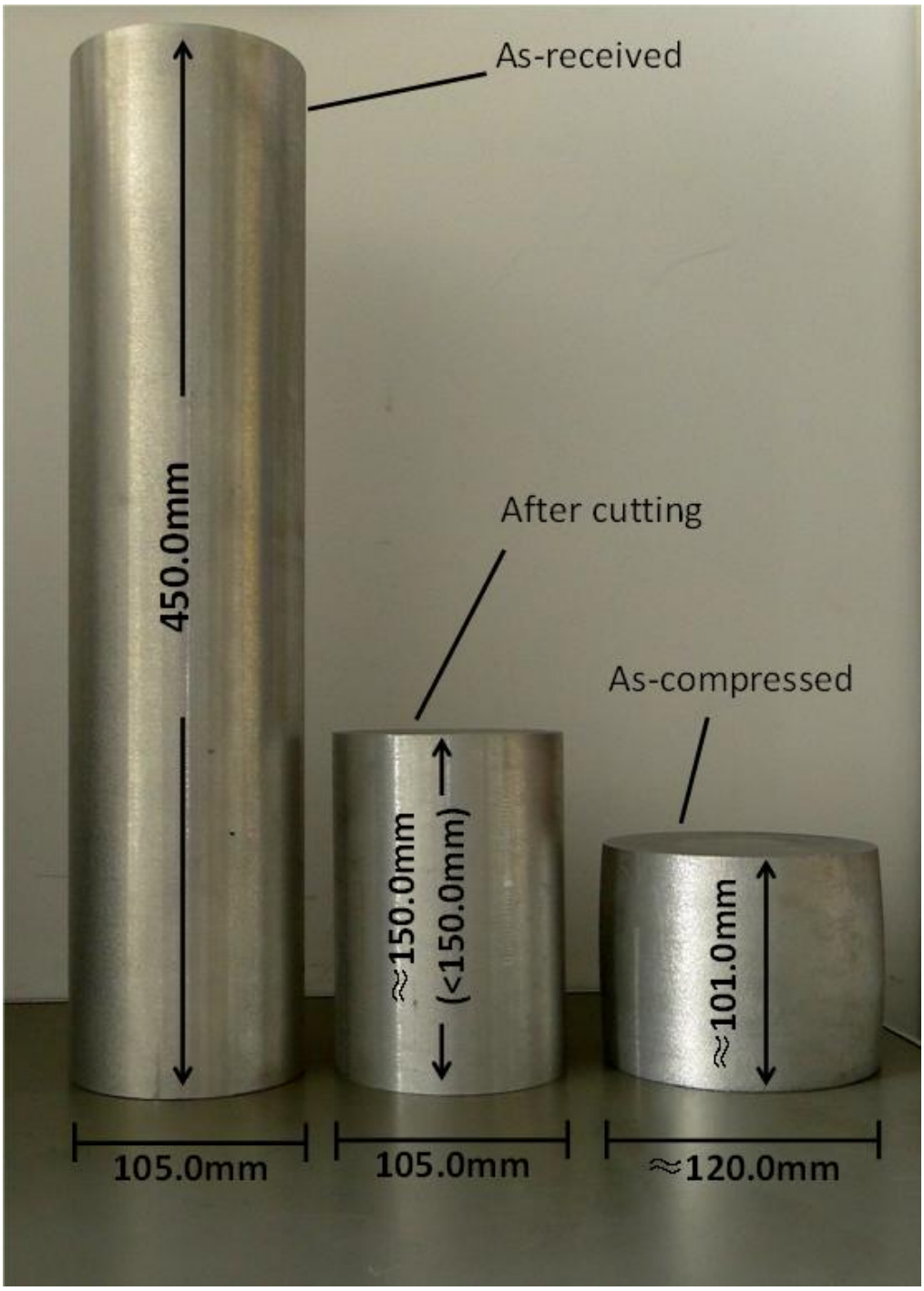

Fig. 2-1. Picture of the A356 aluminum billets used in this chapter, the as received billet was cut before compression in order to avoid buckling.

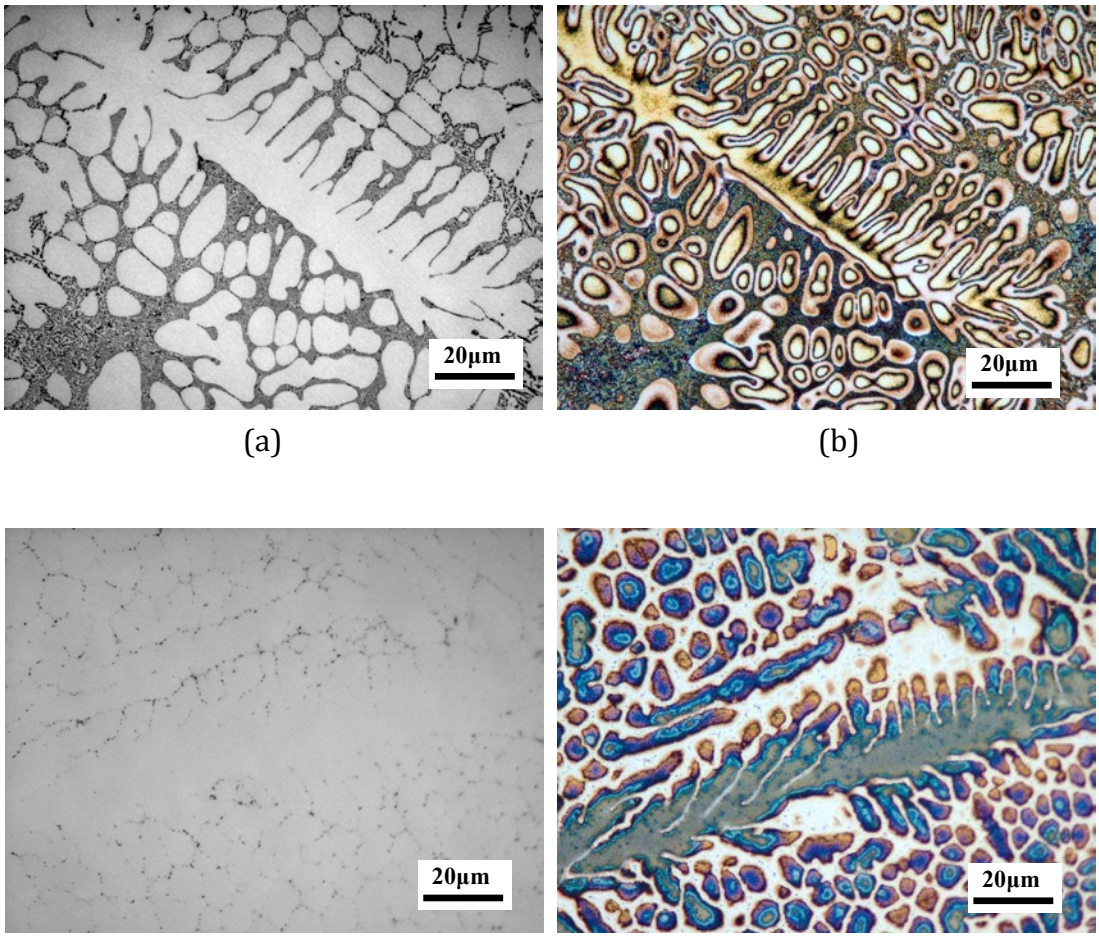

Fig. 2-2. As cast microstructures of Al-7%Si binary alloy before (a) and after (b) etching with Weck's reagent, as well as those of Al-5%Mg binary alloy before (c) and after (d) etching.

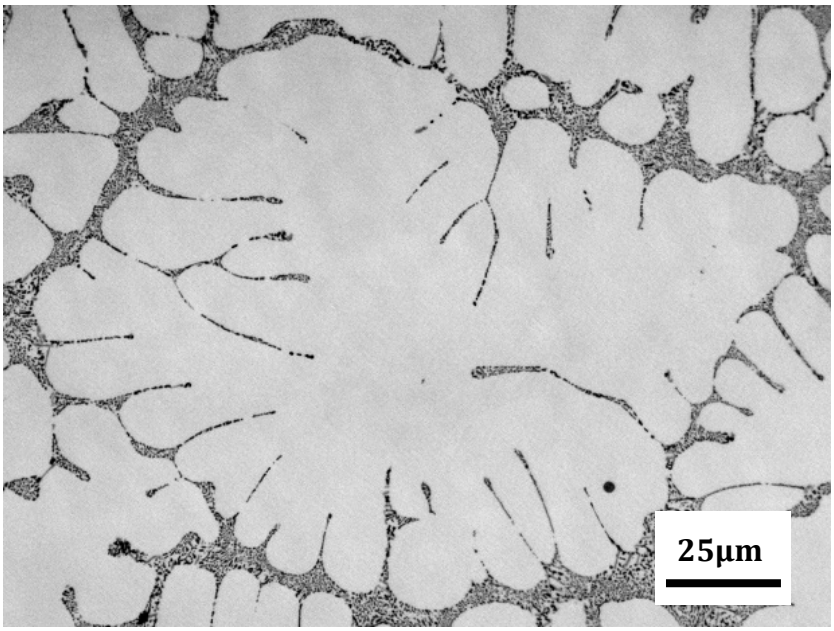

(a)

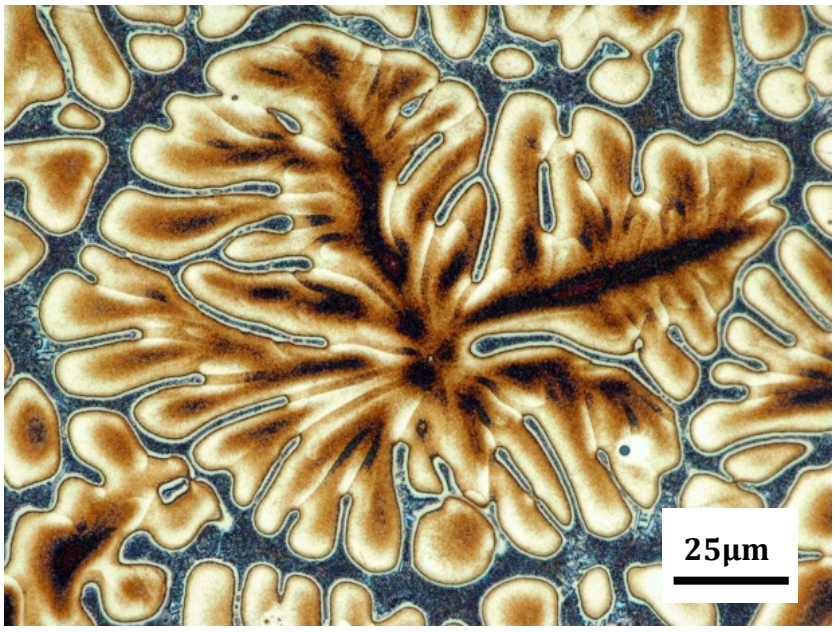

(b)

Fig. 2-3. Microstructure of as-received Ti-contained A356 billet before (a) and after etching (b) by Weck's reagent

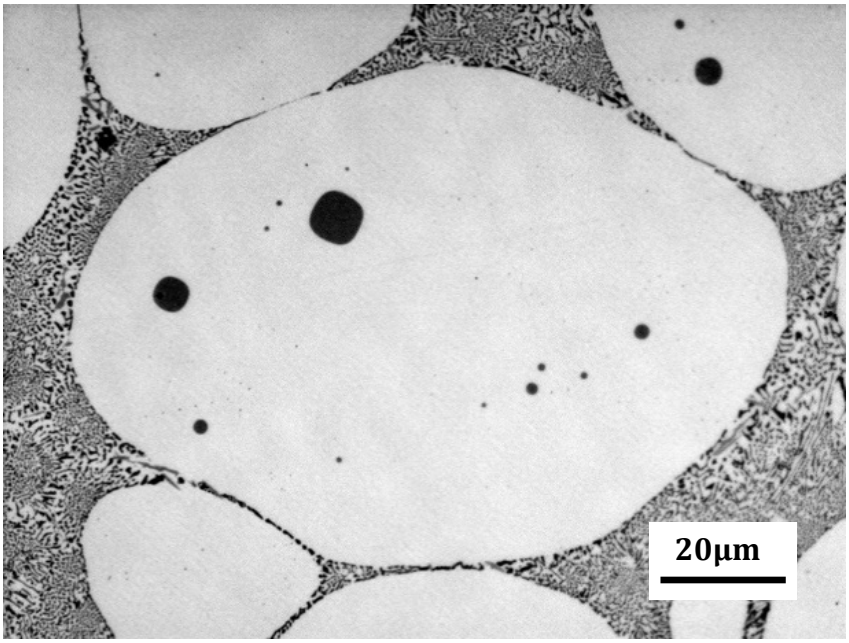

(a)

(b)

Fig. 2-4. Spheroidal microstructure of Ti-contained A356 billet before (a) and after etching (b) by Weck's reagent

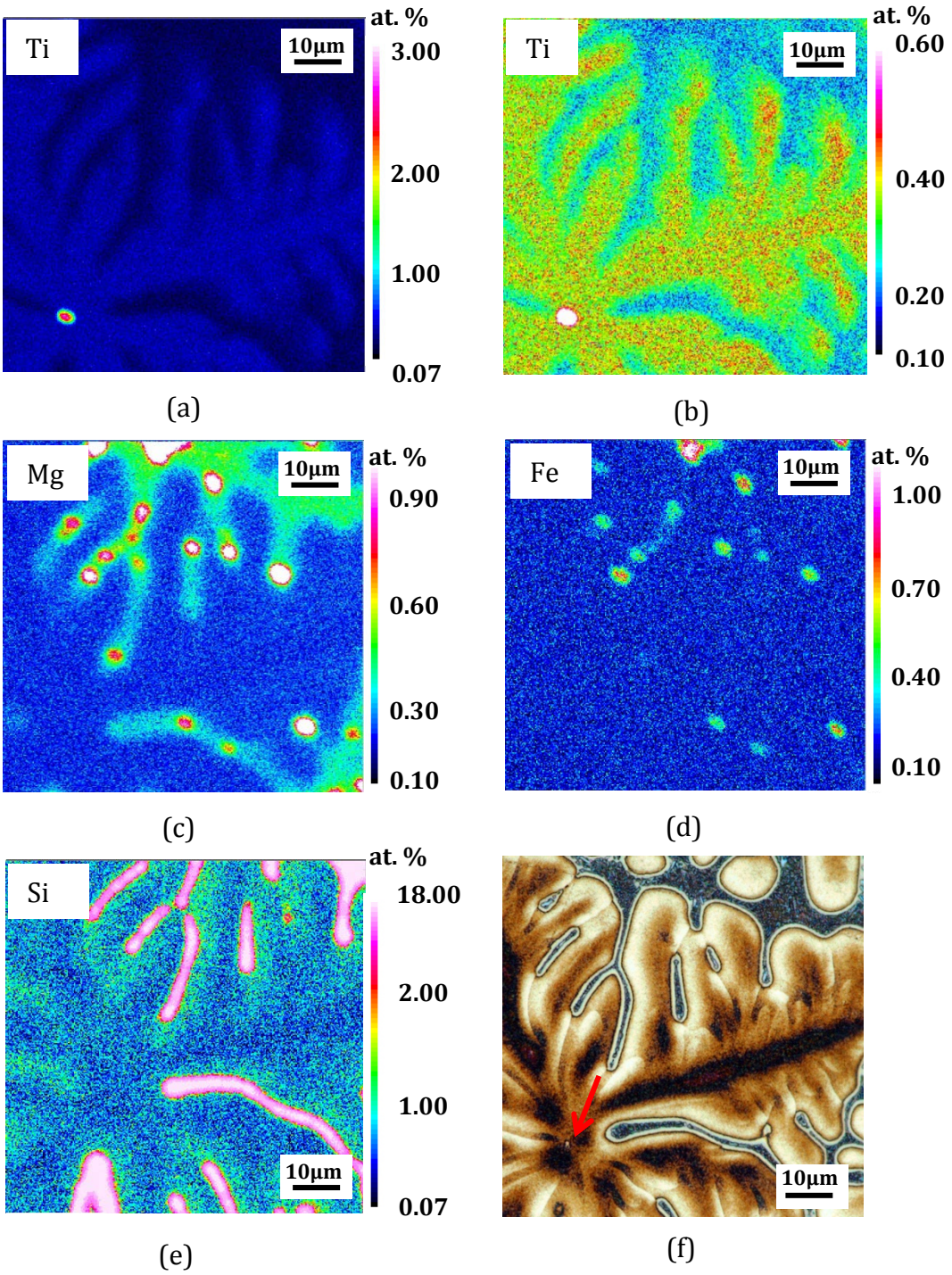

Fig. 2-5. Solute distribution of Ti (a), (b), Mg (c), Fe (d) and Si (e), together with a magnification (f) of Fig. 2 (b) showing the location where the EMPA analyses were carried out

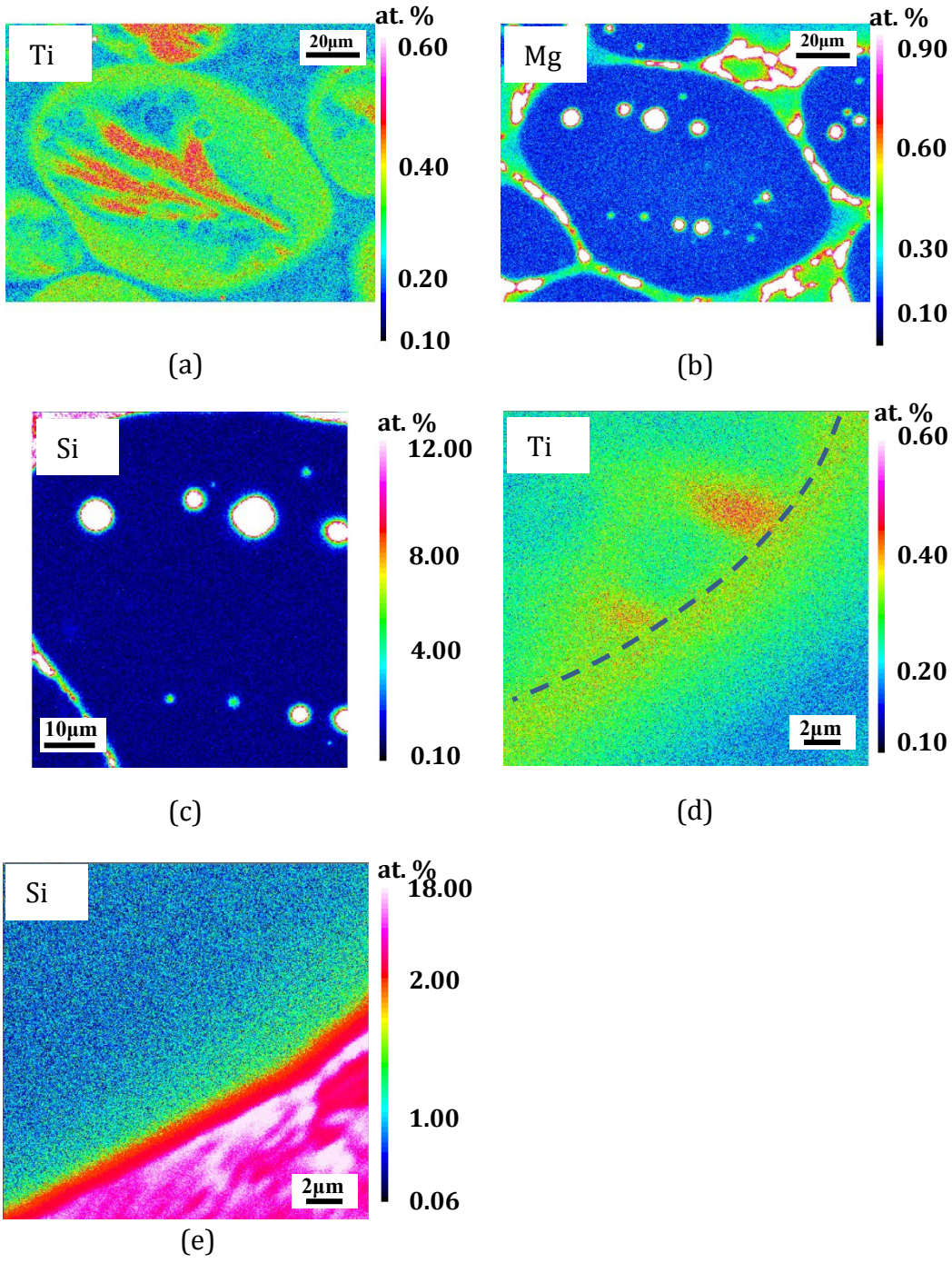

Fig. 2-6. Solute distributions of Ti (a) Mg (b) and Si (c) in the spheroidal gain and Ti (d), Si (c) in the grain growth during water quenching of Spec. 2 measured by EPMA

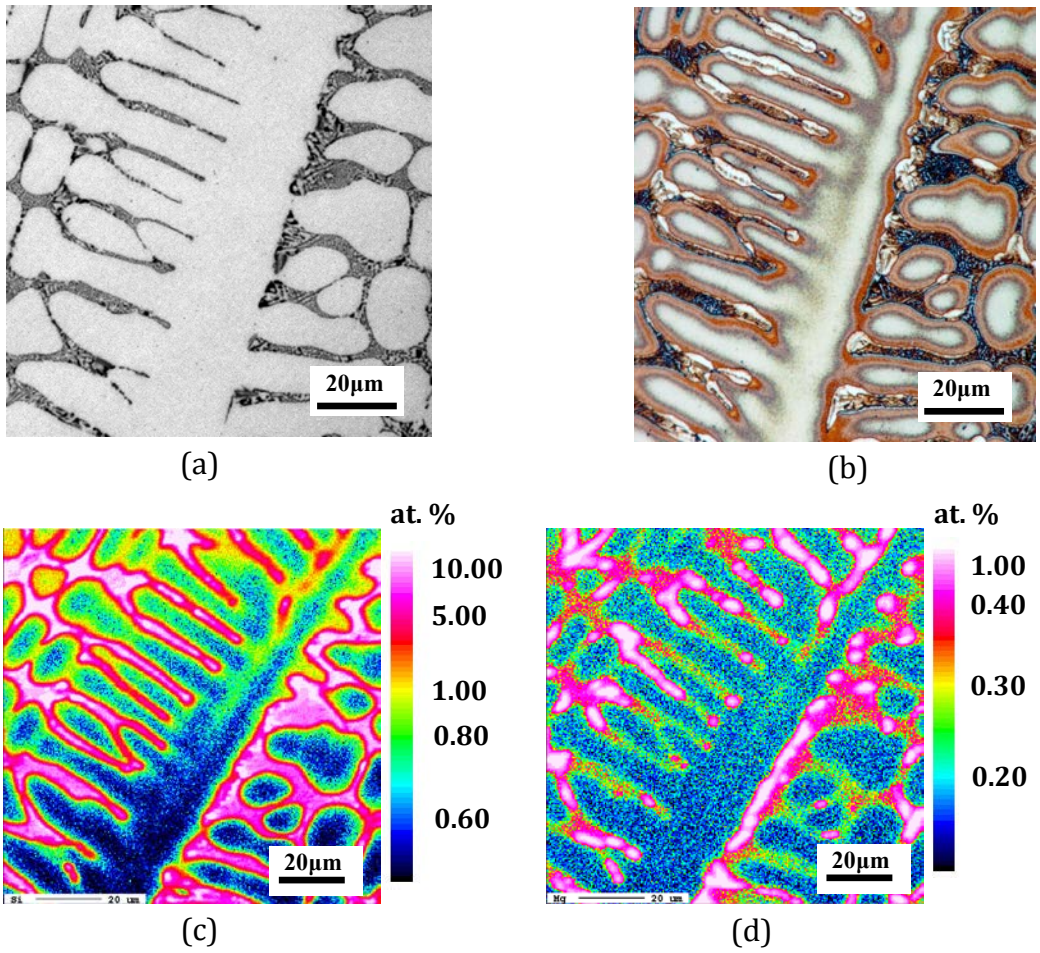

Fig. 2-7. Microstructures of Ti-free A356 Al alloy in dendritic shape before (a) and after (b) etching, as well as the distributions of Si (c) and Mg (d) detected by EPMA.

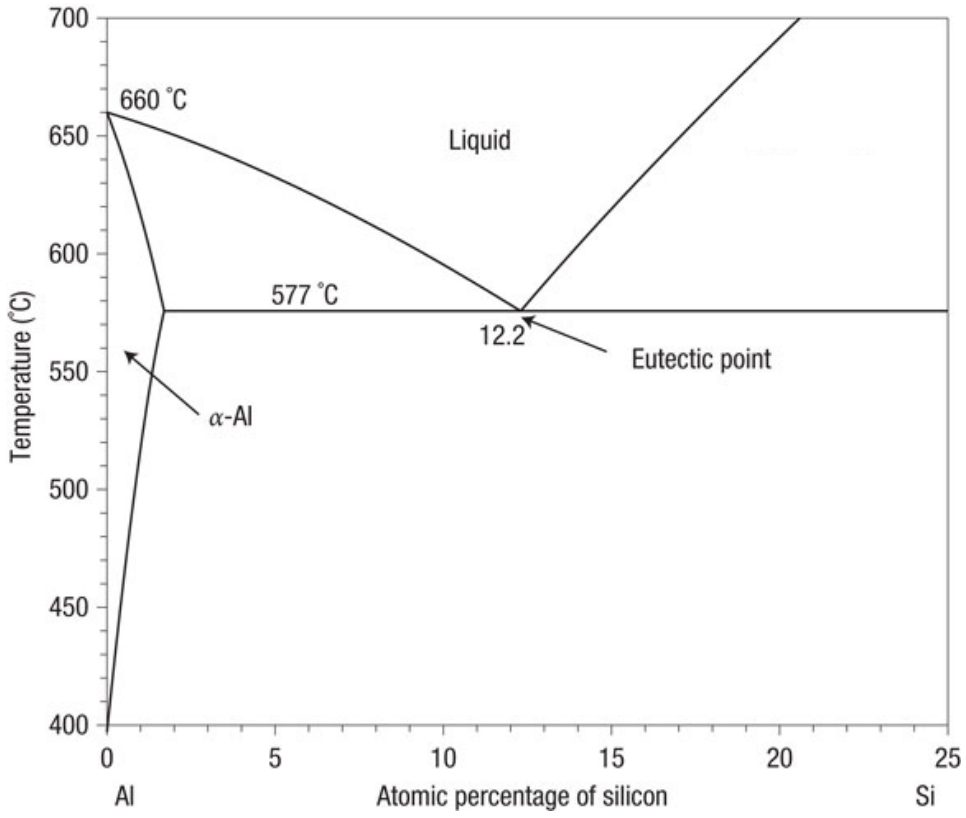

(a)

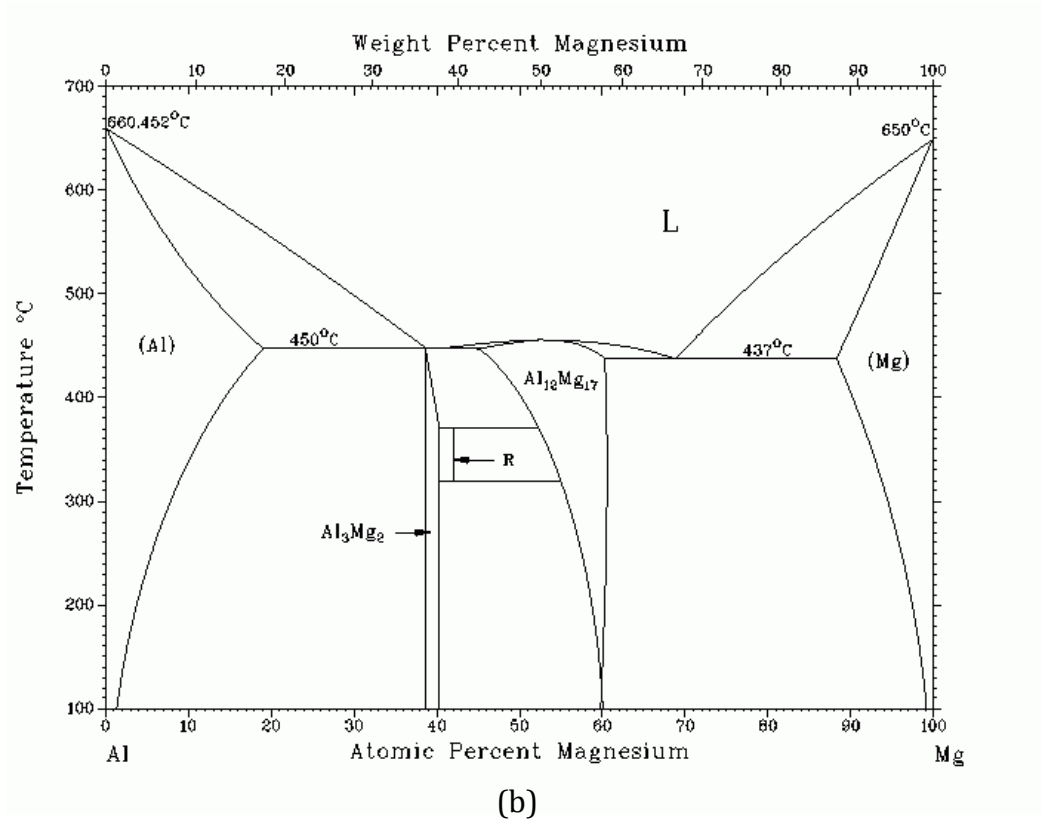

(b)

Fig. 2-8. Al-Si (a) and Al-Mg (b) phase diagrams

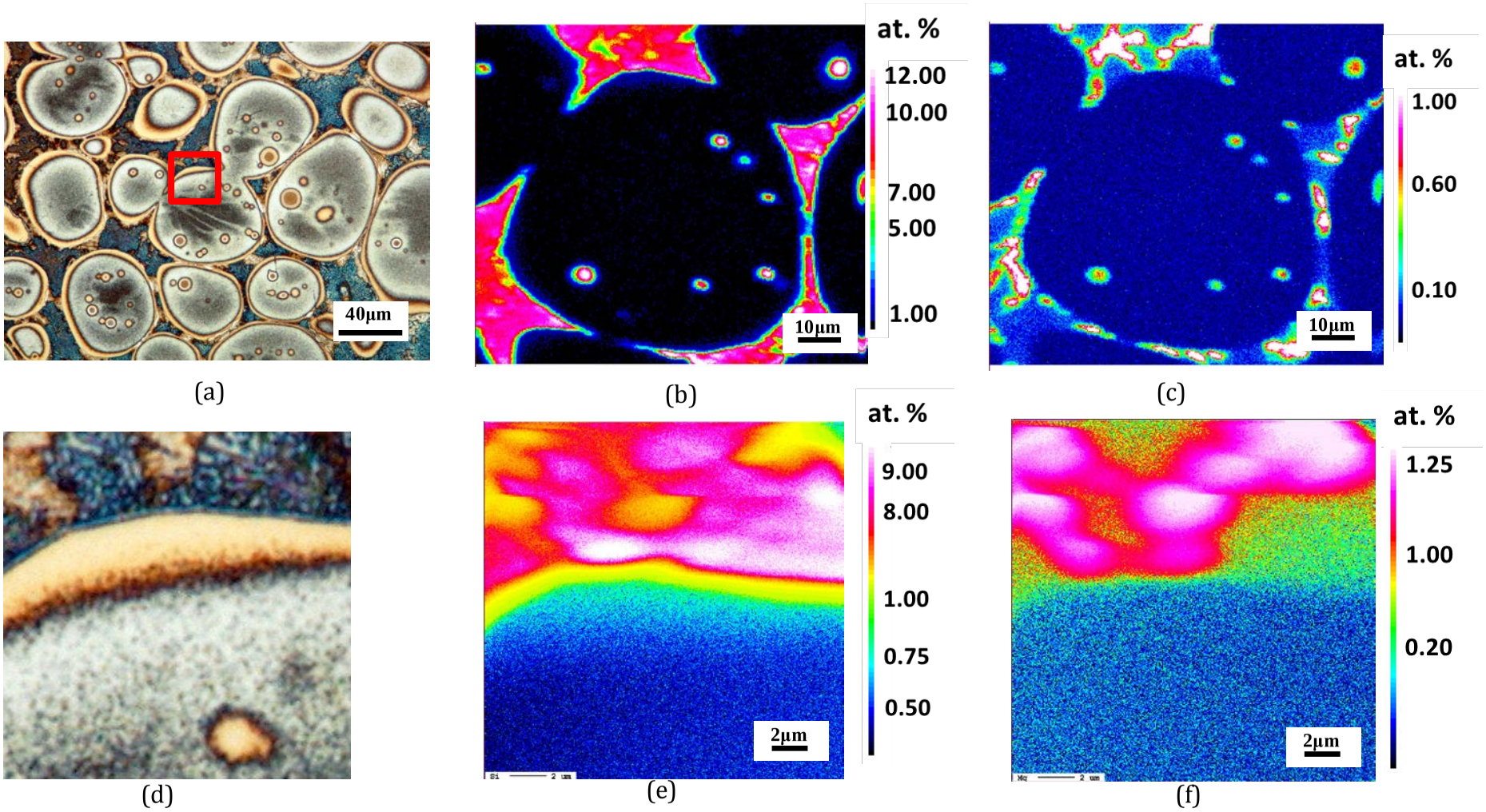

Fig. 2-9. Microstructures of Ti-free A356 Al alloy in spheroidal shape (a), Si (b) and Mg (c) distributions. Also the grain growth during water quenching (d), as well as Si (e) and Mg (f) distributions in this region.

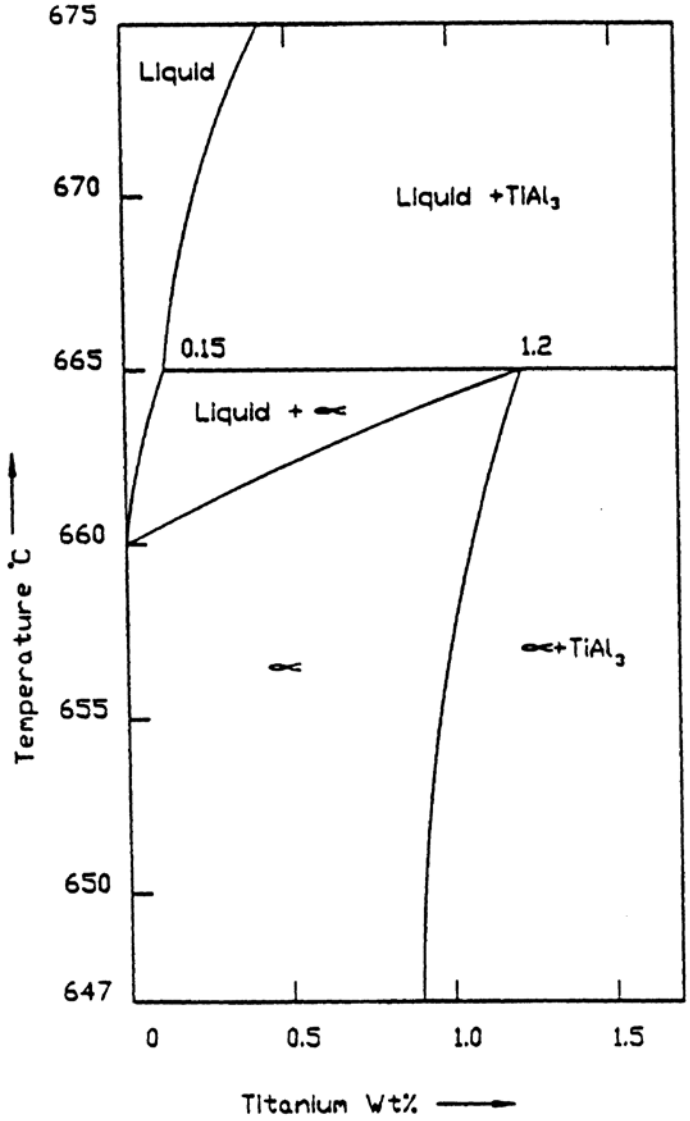

Fig. 2-10. Aluminum end of Al-Ti binary phase diagram provided by McCartney [13]

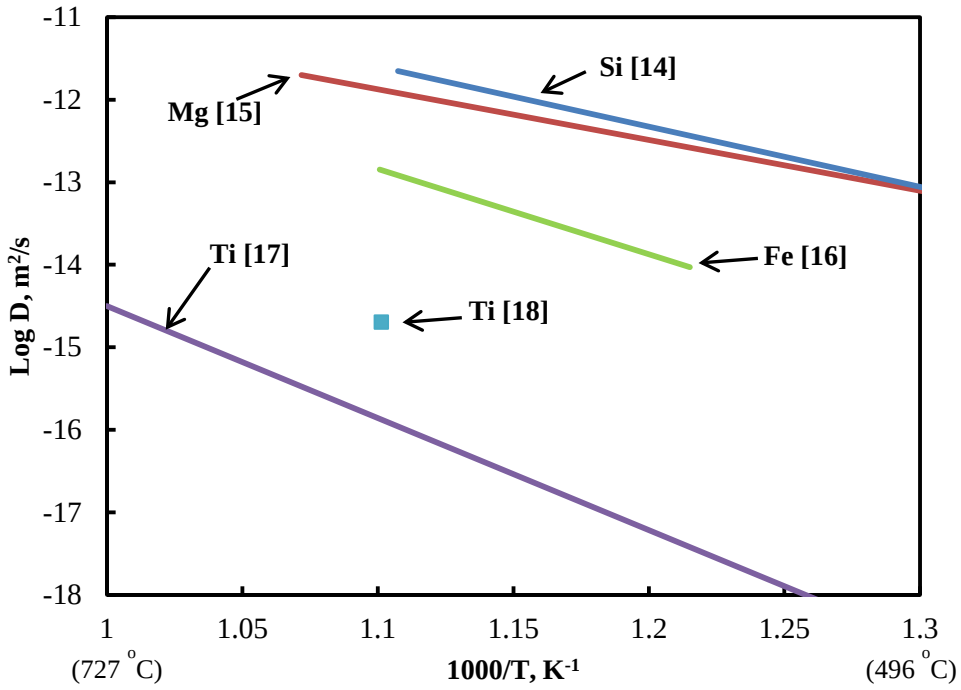

Fig. 2-11. Diffusion coefficients of Si, Mg, Fe and Ti summarized from published researches [14-18]

Chapter 3

Accurate solid fraction evaluation of Al alloy at semi-solid state by Weck's reagent

3.1. Introduction

As mentioned in Chapter 2, Weck's reagent can help to reveal the spheroidal grain growth during water quenching. This ability actually provides us with a possibility of accurately evaluating solid fraction from the optical micrograph.

Since solid fraction has a significant influence on the fluidity of semi-solid slurry which is directly related to mold-filling ability, the Pursuing of accurate solid fraction evaluation for a certain semi-solid temperature has been persisted since semi-solid process was brought to researchers' sight. Several routes are being used to measure or calculate the solid fraction. The most essential one is Scheil's model [1], where four assumptions are required: (1) the interface is at equilibrium; (2) there is no diffusion in the solid phase; (3) the compositions are homogeneous through the entire liquid phase; (4) densities of the solid and liquid phase are equal. More practically used methods are thermal analysis, thermodynamic simulation and quantitative metallography. Chen et al. [2], Nafisi et al. [3] and Tzimas et al. [4] compared the results from different

methods and commented on each method. However, in their studies, disagreement of results yielded from different solid fraction measuring methods is inevitable. Birol [5] focused on differential scanning calorimetry (DSC) experiment. Results show that measured solid fraction is influenced greatly by the scan (heating and cooling) rate. In situ optical measurement of solid fraction was carried out by Steinbach and Ratke [6]. The result is in agreement with Scheil's model. But the experimental set-up is complicate and scatter of result can be caused due to the scatter of intensity measured from the sample's surface by a CCD camera.

In Chapter 2 of this thesis, after etching the spheroidal structure, a ring-shaped structure was visualized in the peripheral part of every spheroidal grain. The specimen was water quenched from semi-solid state to room temperature. The ring-shaped structure is considered to be the grain growth during the water quenching process. In traditional observations of semi-solid microstructure, the grain growth which occurred during quenching is always ignored due to difficulty in distinguishing it from the original solid phase at semi-solid state. This brings overestimation to solid fraction when measured by the area fraction of solid phase in a 2-D micrograph. If the ring-shaped structure can be excluded in the image analysis, a more accurate value for the solid fraction can be expected. In this chapter, color micrographs obtained by using Weck's reagent are used to evaluate solid fractions and the results

are compared with those obtained by other methods.

3.2. Experimental

The material used in the chapter is the Ti-contained A356 Al alloy whose chemical composition is given in Table 3-1. The reason for choosing this alloy is that A356 Al alloy is the most frequently used alloy in semi-solid industry and Ti is also usually added to commercial Al alloys to refine the grain size.

As shown in Fig. 3-1, the cold compression of the billet was done in Nissan Motor Co., Ltd's factory. To avoid buckling, the billet was cut into small ones (Φ105×150mm). Compression was carried out axially by a 500 ton compressing machine. The compressing rate is 0.2mm/sec. The billet's temperature was increased to about 44 ^{o}C when the target height (100mm, 33% reduction) was reached. After compression, small specimens were cut from the billet and heated to semi-solid temperature ranging from 575 ^{o}C to 615 ^{o}C with an interval of 5 ^{o}C. When the target semi-solid temperature was reached, the specimen was isothermally held for at least 5 minutes in order to make sure that the specimen was heated homogeneously. After isothermal holding, the specimen was water quenched quickly.

Specimens were polished via standard metallographic techniques,

finished using Struers OPS colloidal silica. Subsequently, specimens were immersed in Weck's reagent for approximately 12 s at room temperature. Then the microstructure was observed by optical microscopy (OM) without any filters or analyzers.

For those specimens that were isothermally held at lower temperatures (with higher solid fraction), since the distribution of spheroidal Al grains is homogeneous even after being put into water, only one micrograph taken with 100X magnification (with an area about 1.35mm^2) was used for each specimen. On the contrary, specimens held at higher temperature changed their shape severely which leads to an inhomogeneous distribution of spheroidal Al grains. For these specimens, a broader area is needed for better representing the Al grains distribution. As shown in Fig. 3-2, a panoramic micrograph was made by merging several smaller micrographs. As indicated in the panoramic micrograph, solid particles were not homogeneously distributed. This is why the panoramic micrograph was needed. Then, the area representing the Al grain at semi-solid state was painted green. The solid faction is calculated by the ratio of green pixels to the whole image's pixels.

Besides this method, the solid fractions measured from the same specimen not etched, as well as the solid fractions calculated from Al-Si binary diagram were also obtained and compared. The reason for calculating solid fractions from Al-Si binary diagram is that A356 alloy's

composition is very close to Al-7%Si binary alloy so that level rule is frequently used to estimate A356 Al alloy's solid fraction at a certain temperature.

3.3. Results and discussion

3.3.1. Microstructures of specimens water quenched from different semi-solid temperature

According to Kliauga and Ferrante [7], the melting of A356 aluminum alloy starts at a temperature lower than the Al-Si eutectic melting temperature. Mg_2Si and Al-Mg-Fe-Si are firstly melted, resulting in Mg-rich liquid. After that, melting of Al-Si eutectic will take place. In the present research, we measured the solid fractions for temperatures equals to Al-Si eutectic temperature or higher, at which Al-Si eutectic will be completely melted if holding time is long enough.

Typical micrographs for both specimens heated to relatively lower semi-solid temperature and higher temperature are shown in Fig. 3-3. Comparing these two microstructures one can find several differences. First of all, the dendritic structure observed inside spheroidal grains in the specimen heated to lower temperature (Fig. 3-3 (a)) cannot be seen clearly in the specimen heated to higher temperature (Fig. 3-3 (b)). This is because after the specimen is heated to higher temperature and

isothermally held, the micro-segregation inside the grains becomes weaker due to diffusion of solute. Second, among the spheroidal grains shown in Fig. 3-3 (b), one observes small dendritic Al phase that do not exist in Fig. 3-3 (a). This phenomenon can be attributed to the higher temperature. At higher temperature, more Al phase is melted. Some compound acted as nucleation site can be released to liquid again once the Al phase wrapping it is melted. As a result, not only the grain growth from front of spheroidal grain, but also some new Al grains will be formed from the nucleation sites in the liquid phase. At last, it is obvious that the grain growth revealed in Fig. 3-3 (b) is unstable and there are some protrusions. This phenomenon is in accordance with the research done by Martinez et al. [8], which concludes that with a same cooling rate, lower solid fraction (higher temperature) tends to cause unstable growth.

It is also notable that thicker growth layers are formed in those specimens that quenched from higher temperature. Explanation for this phenomenon is as follows: as shown in Fig. 3-4, for the alloys with a partition coefficient $k<1$, such as Al-Si system, solute concentration profile in liquid can be expressed schematically in Fig. 3-4 (a). Such kind of profile can lead to the constitutional undercooling (Fig. 3-4 (b)). However, if the overlapping of solute field occurs as the grain growing from R_1 to R_2 (Fig. 3-4 (c)), the gradient of solute concentration in liquid phase is also reduced (changes from blue line to red line). As a result, the

curve of liquidus temperature ($T_{liquidus}$) will also change which leads to the weakening of undercooling exhibited by the shades in Fig. 3-4 (d). The theoretical model for Al-4.5wt%Cu described in [8] indicates a sharp decrease of grain growth velocity due to the decrease of undercooling caused by solute fields overlapping. That means the growth of grain during quenching is probably stopped by solute field overlapping in our case, too. For specimens heated at higher temperature, the lower solid fraction causes the larger average distance between two grains compared with it at lower temperature. Therefore, thicker growth layer can be formed before the onset of solute fields overlapping. This explanation can be further evidenced by the different thickness of growth layer of the grain located at the center of the Fig. 3-3 (a), where the thickness of growth layer changes coherently with the change of distance to the neighbor grains. However, such discipline is weakened in Fig. 3-3 (b), due to the interference of newly formed α-Al grains.

From the microstructural observation, it is clear that Weck's reagent has the ability to visualize the grain growth formed during water quenching. This is of great importance because until now, in order to obtain the real microstructural information at semi-solid state, one has to carry out in-situ observation using complicate and expensive devices such as synchrotron and CCD camera. With the help of Weck's reagent, the shape and size of the solid phase at semi-solid state can be re-produced again

after being cooled to room temperature.

3.3.2. Solid fractions evaluated with Weck's reagent and the comparison with other methods

As mentioned in detail in the experimental part, the solid fraction can be evaluated with a better accuracy if the grain growth can be distinguished from the original solid phase at semi-solid state. The result obtained with the help of Weck's reagent is exhibited in Fig. 3-5. Also in this figure, the solid fraction evaluated without the exclusion of the grain growth during water quenching and the results calculated from the Al-Si binary phase diagram are given.

Deviation between experimental results by image analyses with and without using Weck's reagent exists. Since in both cases, fine dendritic α-Al grains are excluded from the solid phase, such deviation should be caused by growth layer formed during water quenching. The deviation for high temperatures is more serious. This is not surprising because thicker growth layer is formed at high temperature as mentioned in Section 3.3.1. It is also clear that the results obtained using Weck's reagent is very close to the results calculated by level rule from Al-Si binary phase diagram. Considering the fact that A356 Al alloy has the chemical composition (Al-7%Si-0.4%Mg) near to Al-7%Si binary composition, such agreement in the solid fraction means the reliability of the results obtained using

Weck’s reagent.

The solid fraction evaluation by using Weck’s reagent is an improved image analysis. The most important step in this method is the area selection. Since a good contrast between original Al grain and growth layer is obtained after etching, the error resulted from area selection is thought to be suppressed.

How to deal with the entrapped liquid inside the spheroidal grains is worth to be discussed. In this study, the entrapped droplets are treated as solid phase when evaluating the solid fraction. The reason is as follows. Valer et al. [9] classified the entrapped liquid into two types. One is not totally entrapped by ripening dendrite but still connected with the intergranular liquid. During quenching, it is solidified in a similar manner with the intergranular liquid. The other one is completely entrapped by ripening dendrite and solidified into a very fine microstructure (finer than intergranular eutectic). In our research, most of the intragranular eutectic has a very fine microstructure which indicates the completely entrapping of the liquid. In semi-solid state, the volume fraction of intergranular liquid has a considerable influence on the viscosity, but those entrapped droplets are isolated from intergranular liquid, thus it is rational to treat the entrapped liquid as a part of the spheroidal grains when measuring the solid fraction.

3.4. Conclusions

This chapter focuses on the accurate evaluation of solid fractions for the commercial A356 Al alloy, using Weck's reagent to visualize the grain growth during water quenching.

When evaluating the solid fraction, the grain growth revealed by Weck's reagent was excluded and the area fraction of the original solid phase was calculated as the solid fraction. The solid fractions were measured for the entire semi-solid temperature ranging from 575 ^{o}C to 615 ^{o}C. The results obtained by excluding the grain growth using Weck's reagent agreed well with the values calculated from Al-Si binary phase diagram. The overestimation of those values obtained without excluding the grain growth was also exhibited. It was found that the overestimation was larger in the higher temperature side because at higher temperature, the grain growth during water quenching was also thicker, so without excluding the growth layer, more overestimation will be caused.

Solid fraction evaluation by using Weck's reagent is an improved image analysis. Comparing with in-situ observation technique, the present method is time saving and economical. Furthermore, this color etching method can be applied to both equilibrium and unequilibrium state without influence of the experiment conditions.

Reference

[1] M.C. Flemings, Solidification Processing. McGraw-Hill, New York, 2004.

[2] S.W. Chen, C.C. Huang, Solidification curves of Al-Cu, Al-Mg and Al-Cu-Mg alloys, Acta Mater. 44(1996) 1955-1965.

[3] S. Nafisi, D. Emadi, R. Ghomashchi, Semi solid metal processing: The fraction solid dilemma, Mater. Sci. Eng. A 507(2009) 87-92.

[4] E. Tzimas, A. Zavaliangos, Evaluation of volume fraction of solid in alloys formed by semisolid processing, J. Mater. Sci. 35 (2000) 5319-5329.

[5] Y. Birol, Solid fraction analysis with DSC in semi-solid metal processing, J. Alloys Compd. 486(2009) 173-177.

[6] S. Steinbach, L. Ratke, In situ optical determination of fraction solid, Scripta Mater. 50(2004) 1135-1138.

[7] A.M. Kliauga and M. Ferrante, Liquid formation and microstructural evolution during re-heating and partial melting of an extruded A356 aluminium alloy, Acta Mater. 53 (2005) 345-356.

[8] R. A. Martinez, A. Karma, M. C. Flemings, Spheroidal particle stability in semisolid processing, Metall. Mater. Trans. A 37 (2006) 2807-2815.

[9] J. Valer, P. Ménéses, F. Saint-Antonin, M. Suéry, Microstructural and mechanical characterisation of an Al-21.8 wt.% Ge brazing alloy with

a globular morphology of the primary Al-rich phase, Mater. Sci. Eng. A 272 (1999) 342-350.

Table 3-1. Main chemical compositions of the materials used in this chapter (wt.%)

Alloy	Si	Mg	Fe	Ti	Sr	Mn	Al
Ti-contained A356	6.90	0.39	0.10	0.14	0.025	<0.10	Bal.

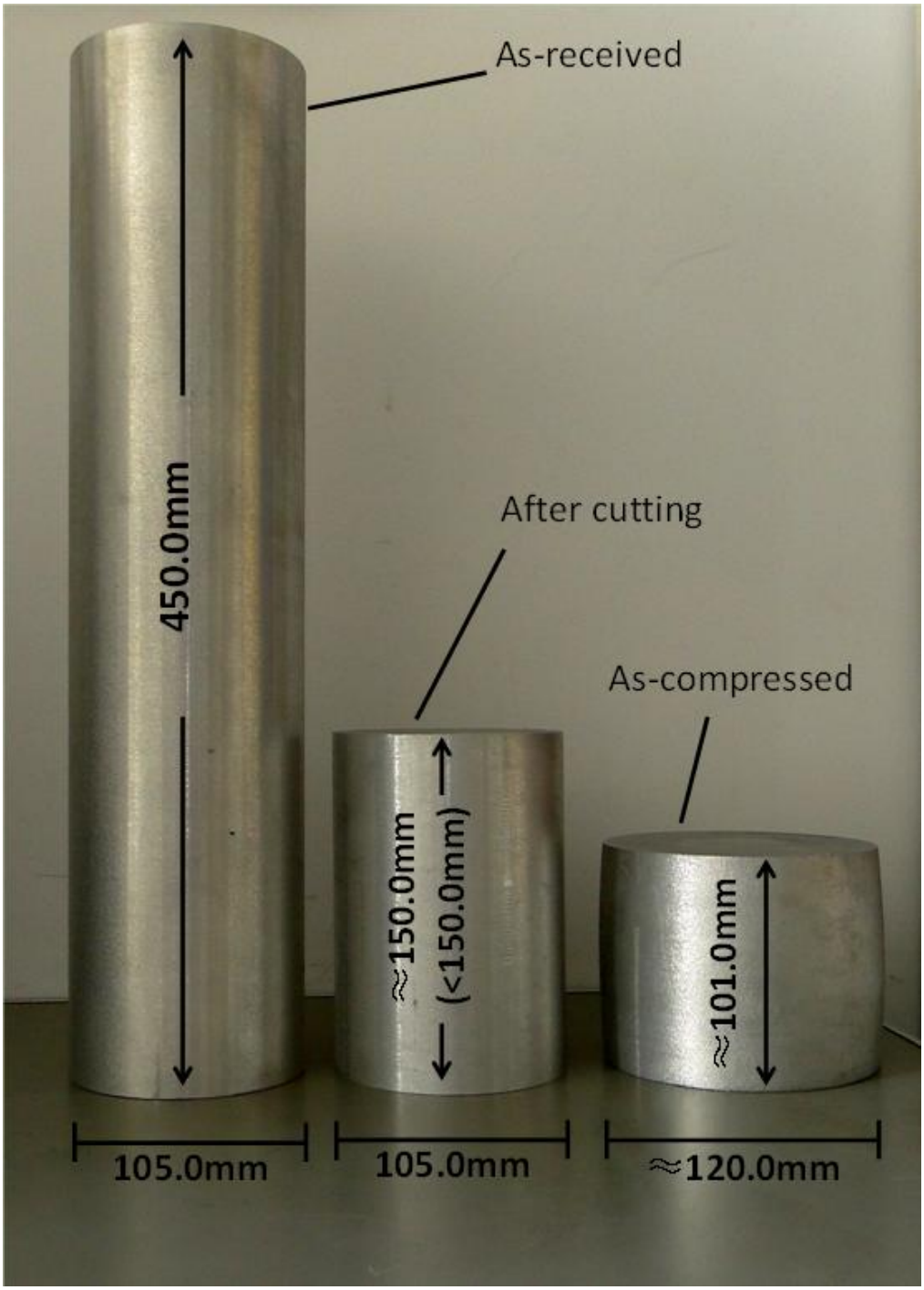

Fig. 3-1. Picture of the A356 aluminum billets used in this chapter, the as received billet was cut before compression in order to avoid buckling.

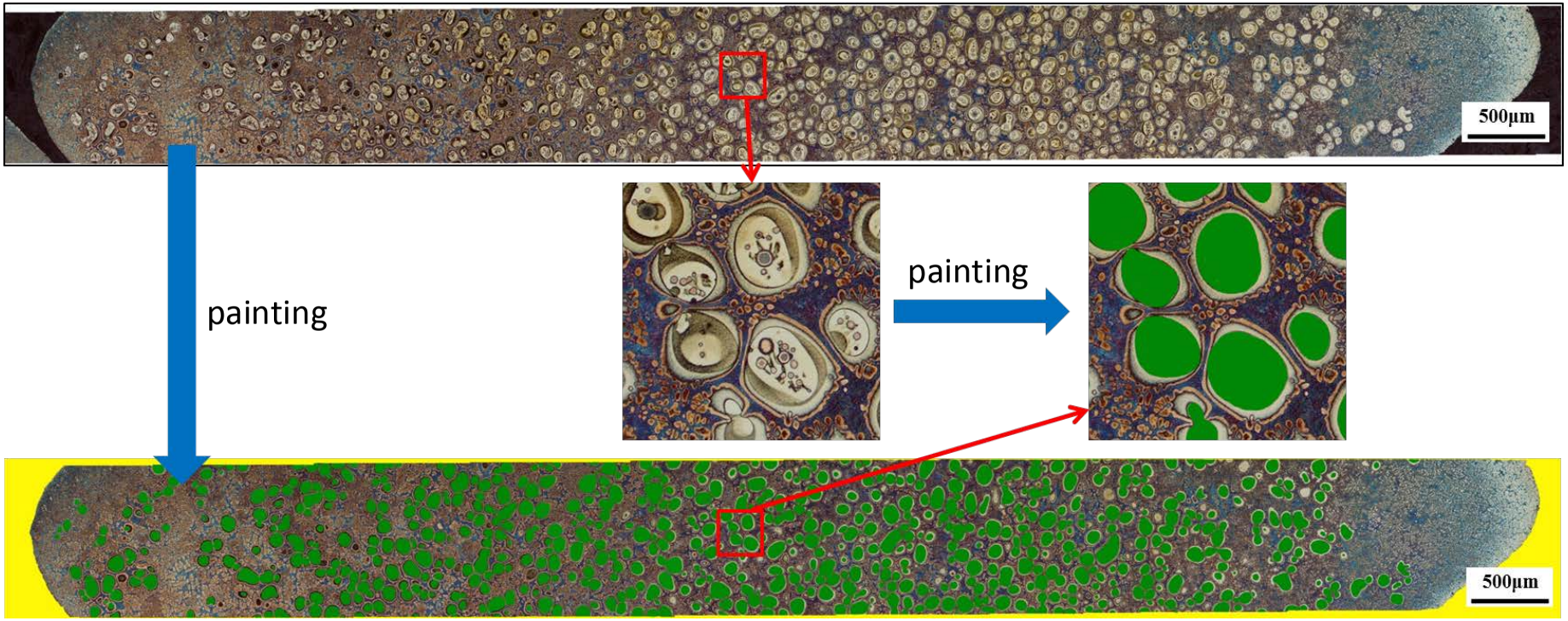

Fig. 3-2. Measuring solid fraction after etching by Weck's reagent

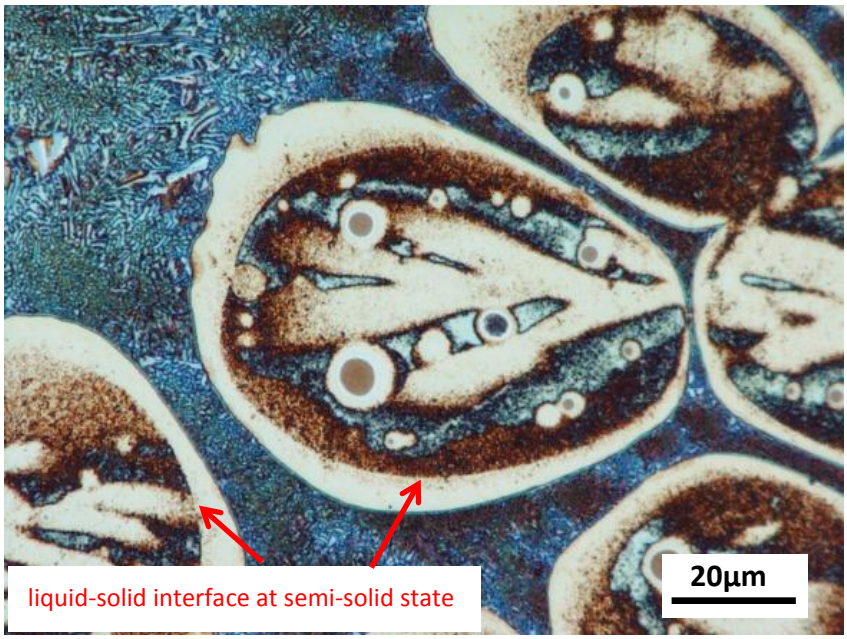

(a)

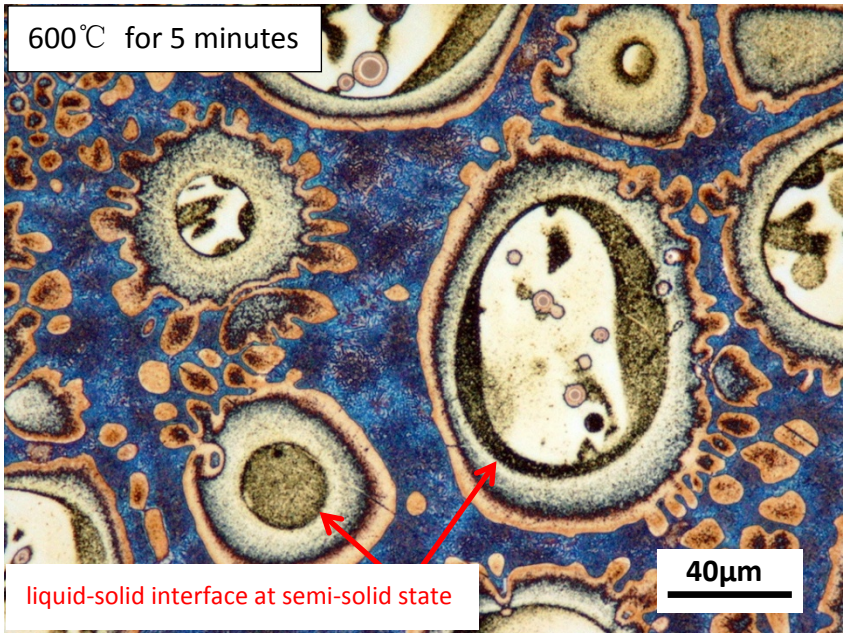

(b)

Fig. 3-3. Microstructures of specimens heated to different semi-solid temperatures. (a) 581 ^{o}C, (b) 600 ^{o}C. The original solid-liquid interface is indicated by red line or arrows in the figure.

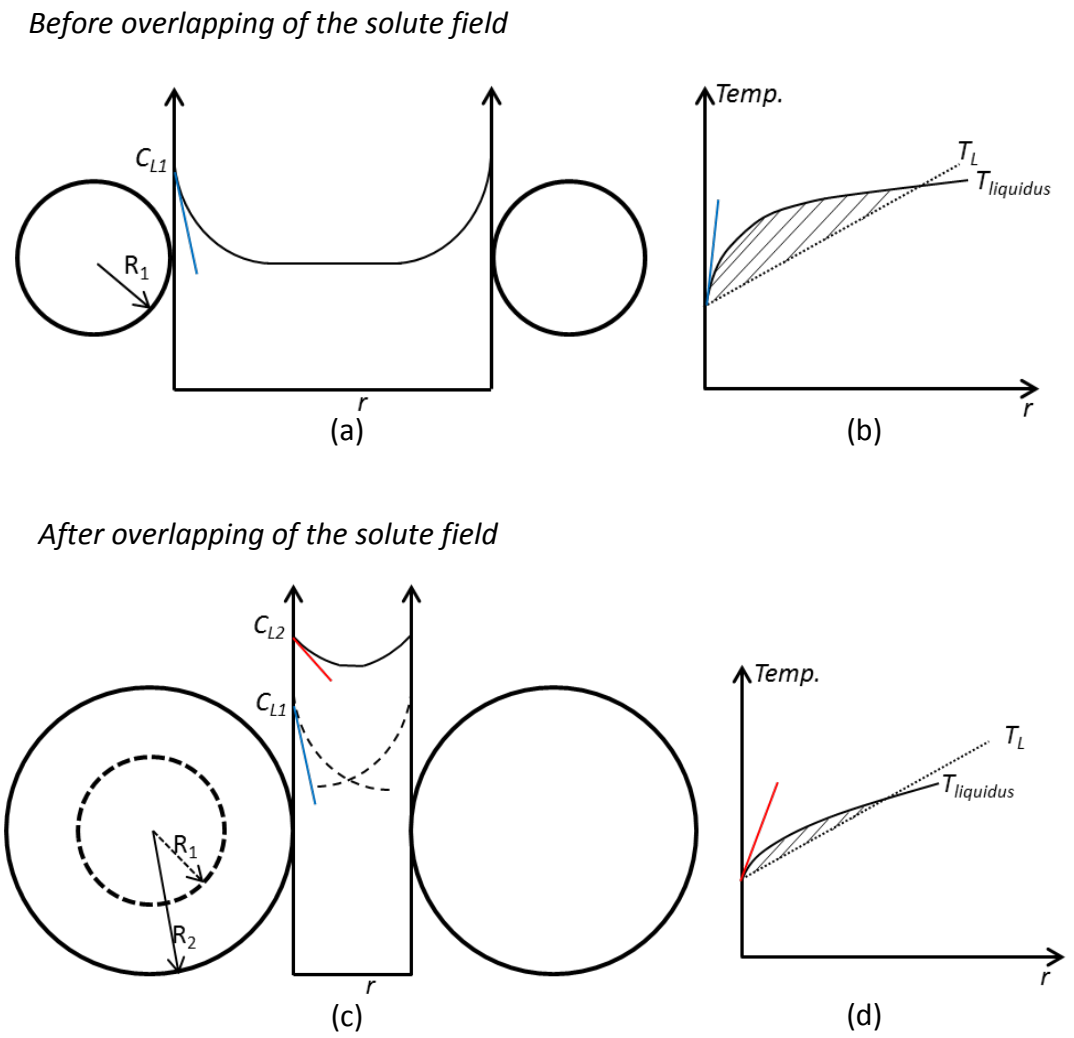

Fig. 3-4. Solute concentration profile in liquid (a, c) and constitutional undercooling (b, d) before and after overlapping of the solute field.

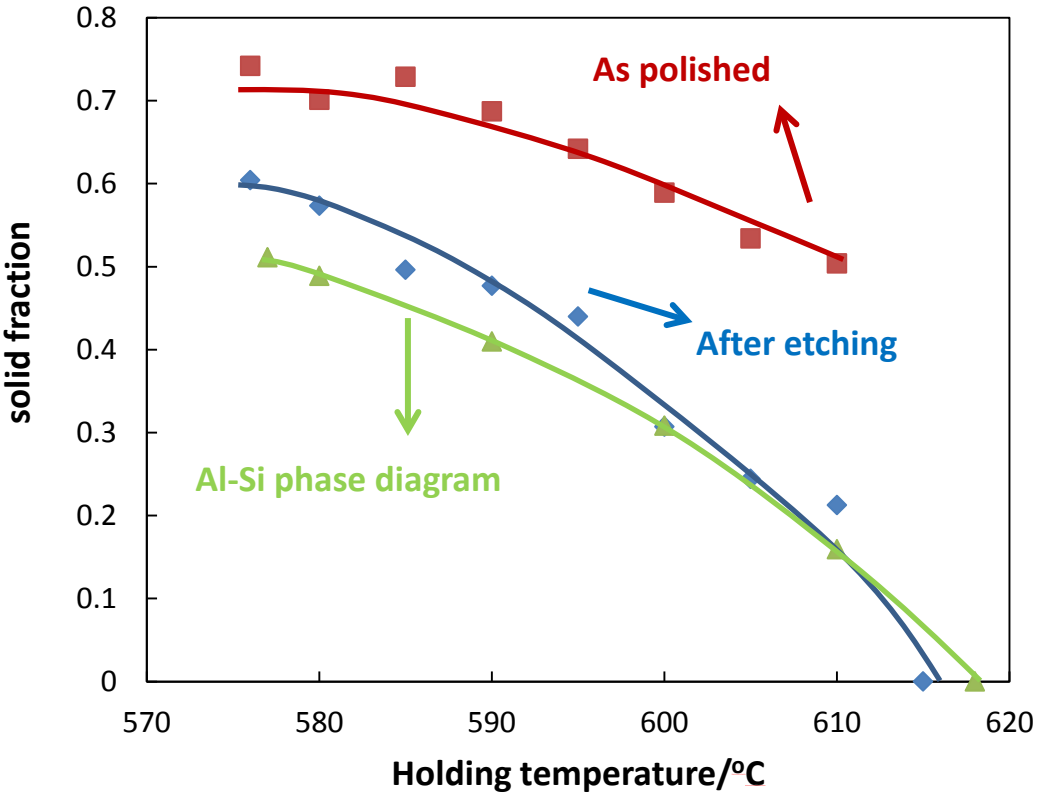

Fig. 3-5. Solid fractions of Ti-contained A356 Al alloy measured from as polished and as etched specimens, as well as the calculation using Al-Si binary phase diagram.

Chapter 4

Spheroidization mechanism of Al phase at semi-solid state by compression and partial re-melting process

4.1. Introduction

In the last three chapters, Weck's reagent has been used to characterize both the dendritic and spheroidal microstructures. In this chapter however, microstructural evolution from dendritic to spheroidal structure is focused. Weck's reagent is also used to characterize the microstructure that undergoing spheroidization.

In aluminum alloy SSP, the existence of spheroidal Al grains is required. Besides the partial re-melting of spray formed materials [1], generally speaking, the methods of making semi-solid slurry containing spheroidal Al grains can be mainly classified into two categories. One is agitation either mechanically or electromagnetically [2] including SEED process [3] and bubbling process [4]. The other one includes strain induced melt activation (SIMA) [5] and recrystallization and partial melting (RAP) route [6], which can be used to get spheroidal grains via partially re-melting of previously deformed (rolling, extrusion, etc.) billet. The difference between SIMA and RAP is that SIMA process requires hot working above recrystallization temperature and cold working

subsequently, while RAP process is simpler and only needs to deform the material to a critical extent by “warm working” between room temperature and recrystallization temperature. For some alloys supplied in worked state, both SIMA and RAP processes have an advantage over the agitating of the alloy in liquid state because they are simpler and need less equipment[7].

Recrystallization is thought to be the key mechanism contributing to the grain refinement and spheroidization in both the SIMA process and RAP process by their inventors [5, 6], which is also widely considered by other researchers [8-13]. Needless to say, understanding of recrystallization behavior during SIMA process or RAP process is of great significance. However, most of the recognitions of recrystallization phenomenon in SIMA or RAP processes are obtained without visualization of deformed dendrites, which is commonly used as the starting material in the above two processes. Consequently, recrystallization behavior in previously deformed dendritic microstructure during heating and partial re-melting is still not clear.

4.2. Experimental

The material used in the chapter is the Ti-contained A356 Al alloy whose chemical composition is given in Table 4-1. As shown in Fig. 4-1,

the cold compression of the billet was done in Nissan Motor Co., Ltd's factory. To avoid buckling, the billet was cut into small ones (Φ105×150mm). Compression was carried out axially by a 500 ton compressing machine. The compressing rate is 0.2mm/sec. The billet's temperature was increased to about 44 ^{o}C when the target height (100mm, 33% reduction) was reached. After compression, small specimens were cut from the billet and heated and partially re-melted. The set-up inside electric furnace is exhibited in Fig. 4-2 (a). Two thermocouples (A and B) were installed to the furnace, thermocouple A is used to inspect the air temperature near the specimen while thermocouple B is inserted to the specimen, which was machined in the shape shown in Fig. 4-2 (b). The shape of the specimen was specially designed in order to make the inserting and withdrawing of the specimen easier.

The temperature measured by thermocouple A (define as T_A) was always adjusted to 600^{o}C before putting the specimen in. So if the holding time is long enough, the temperature of specimen (defined as T_B) will be equal to T_A=600 ^{o}C. Heating was interrupted at various stages when T_B is on the way to 600 ^{o}C and specimens were withdrawn from the furnace and quickly water quenched. T_B was recorded during heating and partial re-melting.

Fig. 4-3 shows the heating curves of the seven specimens used in this chapter. All the specimens had a similar approach to the target

temperature (600 ^{o}C) so their microstructures can represent the microstructure evolution during heating and partial re-melting. Three regions are labeled for the heating process. Specimens are named from Specimen 1 to Specimen 7 corresponding to points from left to right in Fig. 4-3. A specimen that was not compressed (Specimen 6) was also heated to 600 ^{o}C to compare with the specimen that was compressed before heating.

Specimens were polished via standard metallographic techniques, finished using Struers OPS colloidal silica. Subsequently, specimens were immersed in Weck's reagent for approximately 12 s at room temperature. Then the microstructure was observed by optical microscopy (OM) without any filters or analyzers.

In order to study the recrystallization behavior, Electron Backscatter Diffraction analysis was done for a recrystallized A356 Al alloy specimens. The detector used was a NordlysNano EBSD detector produced by Oxford Instruments. The accelerating voltage was set at 20 kV. The EBSD mapping was made to compare with the optical micrograph of the same specimen in order to confirm whether Weck's reagent can be used to detect grain boundaries or not.

4.3. Results and discussion

4.3.1. Microstructures of as-received and as-compressed billets

Fig. 4-4 shows both the microstructures observed after polishing and etching by Weck's reagent. As shown in Fig. 4-4 (a), the as received billet has a typical dendritic microstructure. After being etched by Weck's reagent, shown in Fig. 4-4 (b), the different colors inside dendrites can be seen. Fig. 4-4 (c) shows the microstructure after compression. α-Al grains are deformed and elongated. After being etched by Weck's reagent, seen in Fig. 4-4 (d), similar information with what is shown in Fig. 4-4 (b) can be obtained. Internal fracture was not found after compression.

4.3.2. Comparison of semi-solid microstructure between strain-induced specimen and strain-free specimen

Semi-solid microstructures of Specimen 6 and Specimen 7 are shown in Fig. 4-5. As indicated in Fig. 4-3, they have similar heating curves. Fig. 4-5 (a) and (b) are corresponding to different regions of Specimen 6 which was strain free before heating. While Fig. 4-5 (c) and (d) are corresponding to different regions of Specimen 7 which was compressed before heating. It is obvious that either Specimen 6 or Specimen 7 has an inhomogeneous distribution of Al grains and the region containing fewer Al grains tend to form more Al dendritic grains during quenching. Comparing Specimen 6 with Specimen 7, one observes that the specimen which was compressed before heating forms finer and spheroidal Al

grains when partially re-melted. On the contrary, spheroidization cannot be realized in strain-free specimen. Moreover, less amount of liquid is entrapped in the previously compressed specimen.

Additionally, because of the high temperature and long heating time (about 1400 s indicated in Fig. 4-3), solid state diffusion enhances homogenization inside Al grains. That is why in both figures, original dendrites cannot be seen as clearly as discussed in last chapter.

4.3.3. Microstructure evolution of strain-induced specimens during partial re-melting.

Fig. 4-6 shows the as polished microstructure evolution of previously compressed specimens during partial re-melting. The six micrographs are corresponding to Specimen 1-5 and Specimen 7 in Fig. 4-3, respectively. One observes that Al dendrites evolve gradually into spheroidal grains. The Al dendrites coarsening behavior is similar to the “ripening” of dendrites in solidification processes. Therefore the terminology “ripening” will be used in this research to describe the coarsening behavior of Al grains. Microstructures with higher magnification are shown in Fig. 4-7, focusing on the intergranular morphological change. In accordance with Loué and Suéry’s research [14], during heating in Region A (indicated in Fig. 4-3), eutectic Si is coarsened which is corresponding to Fig. 4-7 (a) and (b). Through in-situ optical microstructure observation, Sato et al. [13]

confirmed that such Si particle coarsening phenomenon occurs during heating. After all the Si particles are coarsened, the eutectic structure begins to melt (Region B, indicated in Fig. 4-3) and the formed liquid penetrates along ripened grains' boundaries and finally solidifies into fine eutectic structure again during quenching, as shown in arrowed areas of Fig. 4-7 (c) and (d). At this stage (Region B), indicated in Fig. 4-3, the temperature is almost kept at a constant value, which is defined as $T_{eutectic}$. Temperature increases again when all the eutectic melts and at this very moment, as shown in Fig. 4-7 (e), as well as Fig. 4-6 (e), the desired fine spheroidal microstructure is obtained. The subsequent heating until 600℃ (Region C, indicated in Fig. 4-3) leads to coarsening of Al grains, as indicated by Fig. 4-6. (f).

Fig. 4-8 shows microstructures of Specimen 3 and 4 etched by Weck's reagent, which were quenched when partial re-melting is in progress. One can see that the ripening dendritic morphology takes up the most area of the micrograph. A limited number of smaller spheroidal grains are also observed as marked by red circles, which are thought to be peripheral cross sections of ripening dendrites. It is also possible that they are incipient grains formed due to recrystallization. Similar phenomenon has been reported for 7075 aluminum alloy [8]. But obviously in the present research, they don't have a considerable contribution to the refinement of Al grains.

Microstructures of Specimen 1-5 obtained after etching by Weck's reagent are shown in Fig. 4-9, the inner microstructures are visualized. The contrast of coarsened Si particles with their background (appear light blue, indicated by arrows) is reduced but they are still distinguishable. A new phenomenon was discovered that contributes to the refinement of Al grains. As mentioned already in Section 3.1, internal fracture was not found in as compressed specimen, as indicated by Fig. 4-5 (d). However, as shown in Fig. 4-9 (a) and (b), seemingly, when the temperature is increased, revealed by Weck's reagent, "separation" of dendrite's branches by many black lines is found. Fig. 4-9 (c), (d) and (e) show that such separation of dendrites produces more candidates with simpler shape for spheroidal Al grains thus decreases the average grain size. At the same time, liquid penetrates into the separating lines and further spheroidized the Al grains. This refining effect is somewhat similar to the refinement of primary Al grains caused by stirring during rheocasting described in [2]. With more and more liquid formed, it becomes easier for ripened grains to move so it is more difficult to find such phenomenon in specimens with lower solid fraction. But we still luckily captured one micrograph (Fig. 4-9 (f)) of Specimen 4 showing two Al grains totally separated by liquid.

Fragmentation of dendrites in solidification process by agitation is thought to be an important factor that leads to a refined and non-dendritic

microstructure [2]. Margarido and Robert also suggest that fractured dendrites are responsible for grain refinement and spheroidization in RAP process [16]. However, the micrograph (in black and white but the etching method was not mentioned) of “fragmented dendrite” given as the evidence in their paper is more like cross section cutting the parallel branches that are still connected to the main trunk of a dendrite, which is called pseudo-individual and isolated particles proposed by Nafisi et al. [17]. Furthermore, the present research has shown that in most cases, evidence of separated dendrites can only be found before the fragments are totally separated by liquid, namely, before the boundary is completely wetted by liquid (Fig. 4-9). Therefore, micrographs in Fig. 4-9 can be regard as the direct evidence of the theory that deformed dendrites separation during heating and partial re-melting contributes to refinement and spheroidization of Al grains at semi-solid state. As for the decreasing in the number of separating lines, two different explanations can be made. One is that as partial re-melting continues, sintering occurs. The other one is that those separation sites are actually migrating grain boundaries. The dendrites fracturing cannot be observed in as polished condition, which indicates a higher possibility that the separating lines are actually migrating grain boundaries.

Atkinson et al. [9] observed recrystallization in 7075 aluminum alloy characterized by new grains formed between deformed and elongated

grains. However, in our research, as well as some other researches using A356 aluminum alloy [18, 19], such phenomenon was not observed. Kliauga and Ferrante observed low angle grain boundaries (LAGB) in extruded (at 400℃) A356 aluminum alloy by using electron back scatter diffraction (EBSD) technique [18]. When the specimen was heated and partially re-melted to about 560℃, a decrease in the number of LAGB was found. A recently published research done by Moradi et al. observed the HAGB formation inside strain induced grain during heating [19]. The material processing is quite similar to ours. As cast A356 alloy was equal channel angular pressed (ECAP) at room temperature and heated, followed by quenching. The formation of HAGB was found inside coarsening Al grains quenched from 190℃ and 450℃. They also illustrated the formation mechanism of HAGB schematically. In order to confirm our hypothesis, EBSD analysis was carried out for the same specimen and the result is shown in Fig. 4-10. Of course the specimen was polished and again before EBSD analysis to remove the etching surface. After that, the electropolishing was carried out. During electropolishing, both the dendritic Al phase and eutectic Al were preferentially attacked simultaneously. Furthermore, during EBSD analysis the sample is usually tilted at approximately 70^{o} relative to normal incidence of electron beam. As a result, the Al phase's dendritic shape was not very clear. Even so, we confirmed that inside Al phase, the

HAGBs existed (Fig. 4-10 (b)). Although the EBSD mapping was not the same location with the OM micrograph, it is still strong evidence to prove that the lines in OM micrograph correspond to HAGBs formed during recrystallization.

From the discussion above, one can conclude that the separating lines in Fig. 4-9 are probably HAGBs formed during heating. When the dendrites are ripening, simultaneously those HAGBs are migrating inside dendrites and tend to link with each other to become longer, resulting in the decrease in the number of them.

4.4.Conclusions

A356 aluminum alloy was RAP processed to produce semi-solid slurry with spheroidal Al grains. Optical microstructure observation was carried out by using Weck's reagent to visualize the inner microstructure of ripening Al grains with attention paid on the microstructure evolution and ripening behavior of Al dendritic grains.

In contrast to the coarse grains which could not be spheroidized in the strain free specimen after partial re-melting, the strain induced specimen shows a much finer and spheroidal structure at semi-solid state. Microstructures before complete spheroidization showed that the dendritic Al grains were ripened gradually. At the same time, eutectic Si

particles were also coarsened at first and then melted when the temperature became higher than eutectic melting temperature. After that, liquid phase penetrated toward grain boundaries, which contributed to the spheroidization of Al phase.

By optical observation after etching using Weck’s reagent, Al dendrites were found separated during heating before liquid was formed, which contributed to the refinement and spheroidization of Al grains. This phenomenon was compared with EBSD observation, which leads to the conclusion that the separating lines are actually HAGBs. This comparison proves that Weck’s reagent can also be used to reveal grain boundaries in Al alloys. The EBSD analysis found that numbers of those HAGBs was decreasing during heating due to the connection of them resulted from migration inside dendrites.

Reference

[1] H-S. Kim, I.C. Stone, B. Cantor, Microstructural evolution in semi-solid AA7034, J. Mater. Sci. 43(2008) 1292-1304.

[2] M.C. Flemings, Behavior of metal alloys in the semisolid state, Metall. Trans. A 22A(1991) 957-981.

[3] D. Doutre, G. Hay, P. Wales (2002) United States Patent No. 6428636.

[4] J. Wannasin, R.A. Martinez, M.C. Flemings, Grain refinement of an aluminum alloy by introducing gas bubbles during solidification, Scripta Mater. 55(2006) 115-118.

[5] K.P. Young, C.P. Kyonka, J.A. Courtois (1983) United States Patent No. 4415374.

[6] D.H. Kirkwood, C.M. Sellars, L.G. Elias-Boyed (1992) European Patent No. 0305375 B1.

[7] Bolouri Amir, Shahmiri Mohammad, C.G. Kang, Coarsening of equiaxed microstructure in the semisolid state of aluminum 7075 alloy through SIMA processing, J Mater Sci. 47(2011) 3544-3553.

[8] H.V. Atkinson, K. Burke, G. Vaneetveld, Recrystallisation in the semi-solid state in 7075 aluminium alloy, Mater. Sci. Eng. A 490(2008) 266-276.

[9] K. Nakagawa, K. Hoshino, T. Otani, Microstructural Changes of Strained AC4C and Al-17mass%Si Alloys at Semi-Solid

Temperatures, J. Jpn. Foundry Eng. Soc. (in Japanese) 76(2004) 9-14.

[10] Bolouri Amir, Shahmiri Mohammad, C.G. Kang, Study on the effects of the compression ratio and mushy zone heating on the thixotropic microstructure of AA 7075 aluminum alloy via SIMA process, J. Alloys Compd. 509(2011) 402-408.

[11] B.J. Jung, S. Ichihata, T. Sato, H. Tezuka, A. Kamio, Saikawa S, Nakai K, Semi-solid solidification microstructures of a strain-induced Al–7%Si–0.5%Mg alloy, J. Jpn Inst. of Light Met. (in Japanese) 47(1997) 626-631.

[12] W. Lapkowski, Some studies regarding thixoforming of metal alloys, J. Mater. Proc. Technol. 80-81(1998) 463-468.

[13] T. Sato, H. Ueno, H. Tezuka, Microstructure Control and Improved Mechanical Properties of Al-Si-Cu-Fe Alloy by Deformation-Semi-Solid Casting Process, J. of Jpn. Foundry Eng. Soc. (in Japanese) 77(2005) 547-553.

[14] W.R. Loué, M. Suéry, Microstructural evolution during partial remelting of Al-Si7Mg alloys, Mater. Sci. Eng. A 203(1995) 1-13.

[15] M.C. Flemings, Solidification Processing. McGraw-Hill, New York, 1974.

[16] M. Margarido, M.H. Robert, Influence of thermomechanical treatments on the production of rheocast slurries by partial melting, J. Proc. Technol. 133(2003) 149-157.

[17] S. Nafisi, R. Ghomashchi, The microstructural characterization of semi-solid slurries, JOM 58(2006) 24-30.

[18] A.M. Kliauga and M. Ferrante, Liquid formation and microstructural evolution during re-heating and partial melting of an extruded A356 aluminium alloy, Acta Mater. 53 (2005) 345-356.

[19] M. Moradi, M. Nili-Ahmadabadi, B. Poorganji, B. Heidarian, M.H. Parsa, T. Furuhara, Recrystallization behavior of ECAPed A356 alloy at semi-solid reheating temperature. Mater. Sci. Eng. A 527 (2010) 4113-4121.

Table 4-1. Main chemical compositions of the materials used in this chapter (wt.%)

Alloy	**Si**	**Mg**	**Fe**	**Ti**	**Sr**	**Mn**	**Al**
Ti-contained A356	6.90	0.39	0.10	0.14	0.025	<0.10	Bal.

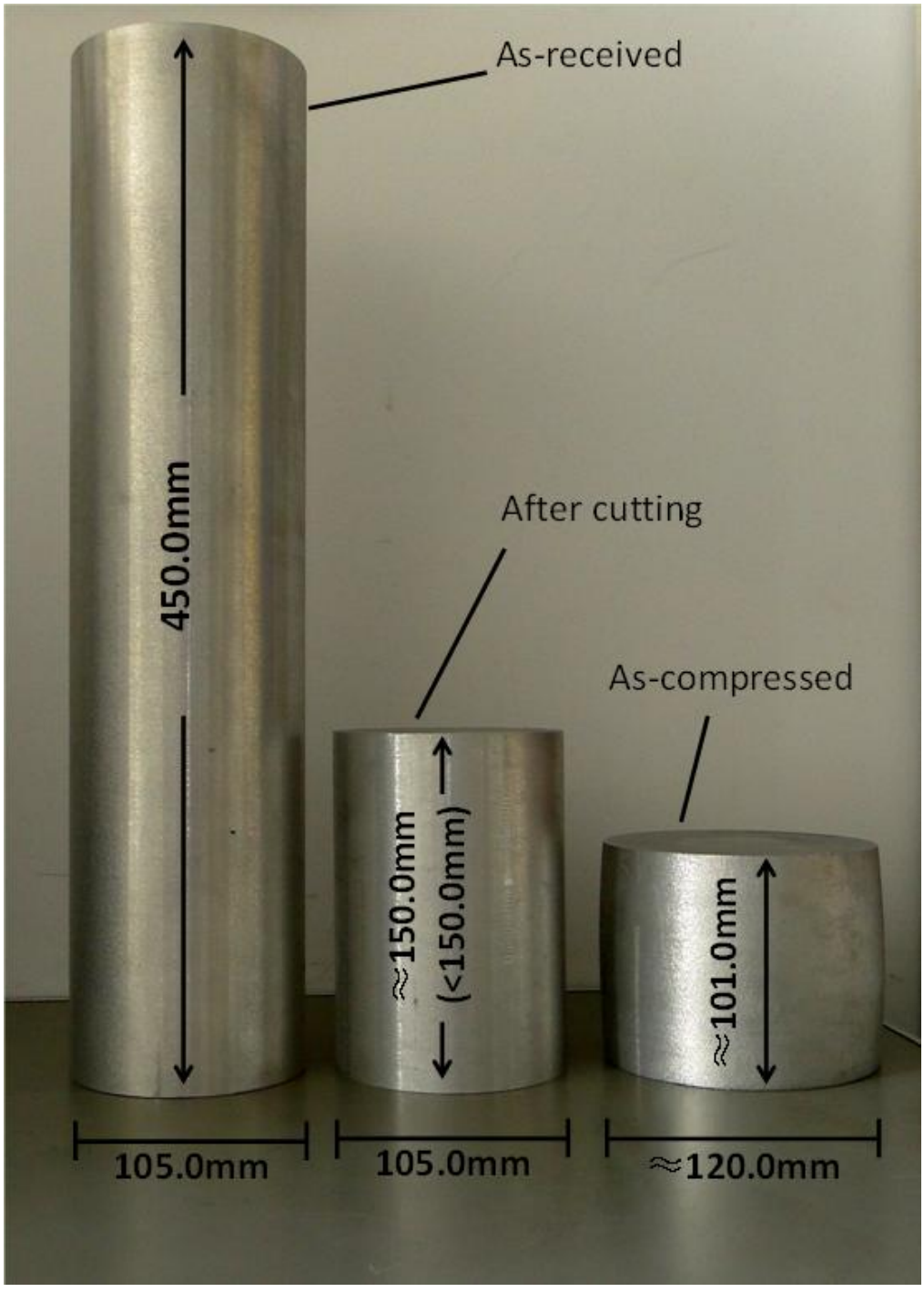

Fig. 4-1. Picture of the A356 aluminum billets used in this chapter, the as received billet was cut before compression in order to avoid buckling.

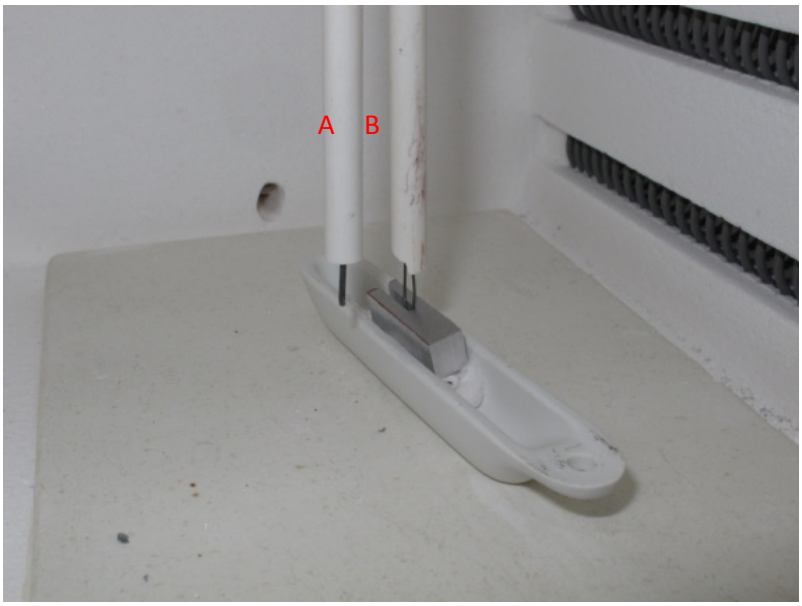

(a)

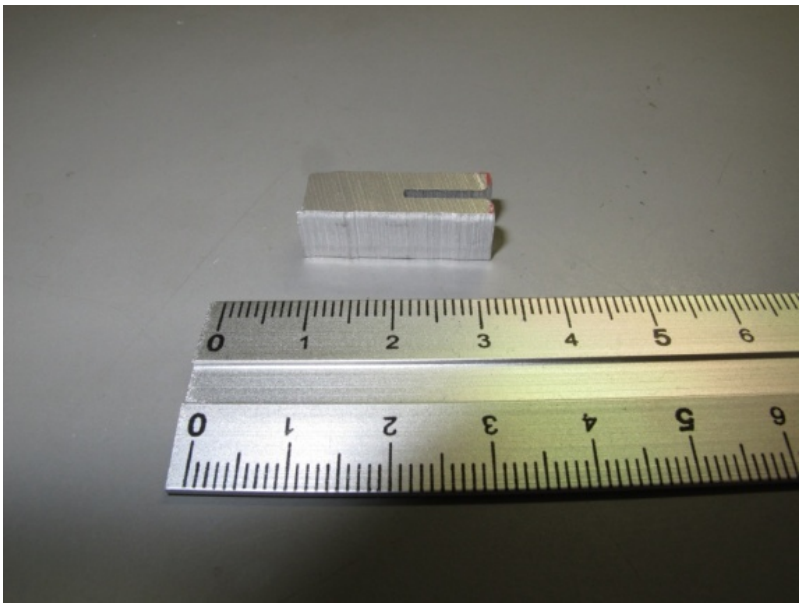

(b)

Fig. 4-2. (a) experimental set-up inside furnace (b) the specially designed specimen used for the partial re-melting experiment.

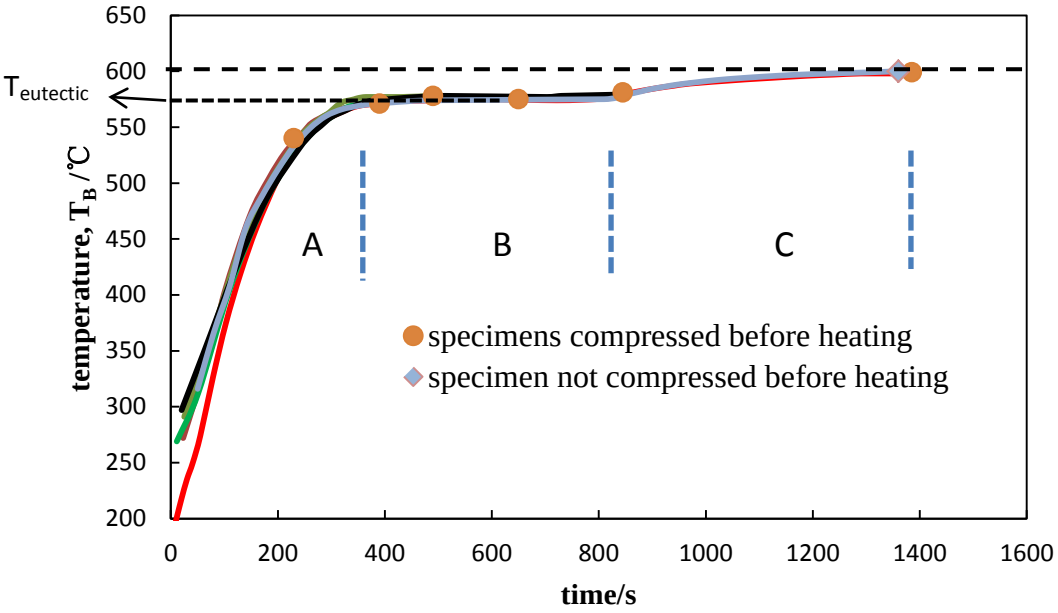

Fig. 4-3. Heating curves of specimens in this chapter.

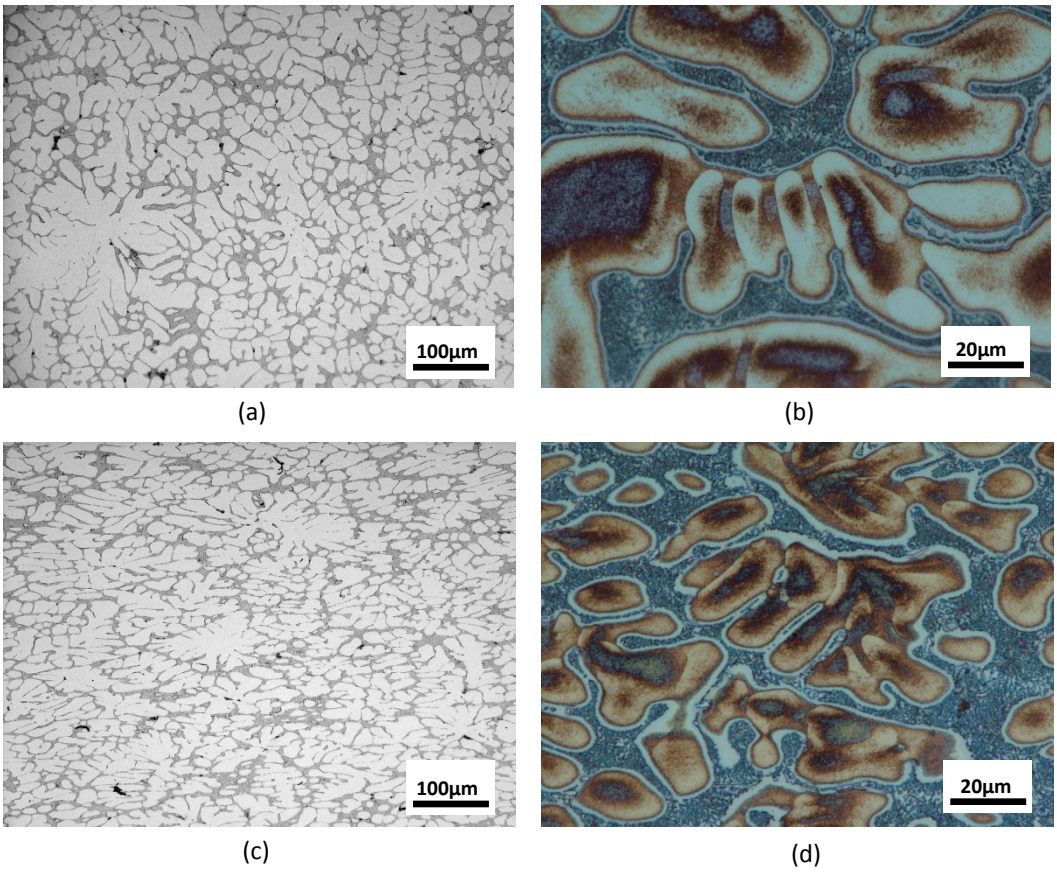

Fig. 4-4. Microstructures of as received specimen and as compressed specimen. (a) as received, as polished; (b) as received, etched by Weck's reagent; (c) as compressed, as polished; (d) as compressed, etched by Weck's reagent.

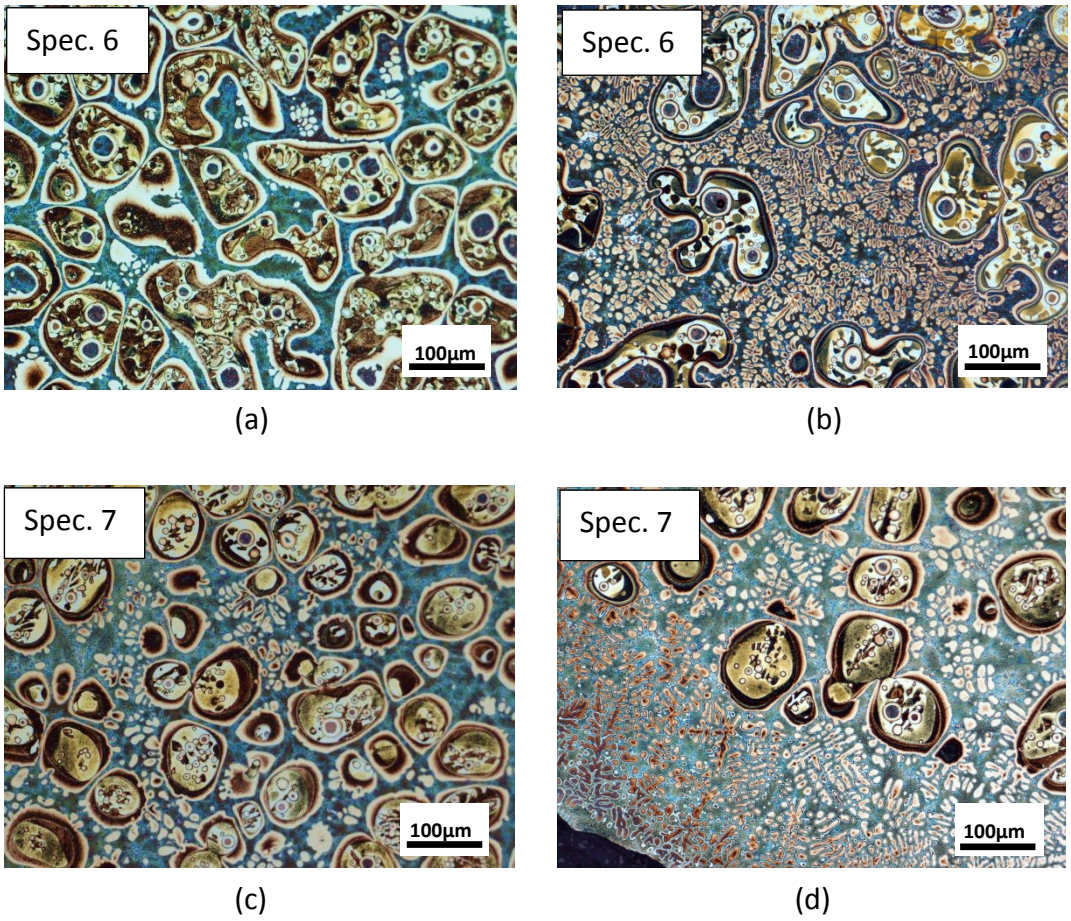

Fig. 4-5. Comparison of partial-remelted microstructure between strain-induced specimen and strain-free specimen. (a) (b) Specimen 6 in Fig. 2; (c) (d) Specimen 7 in Fig. 2.

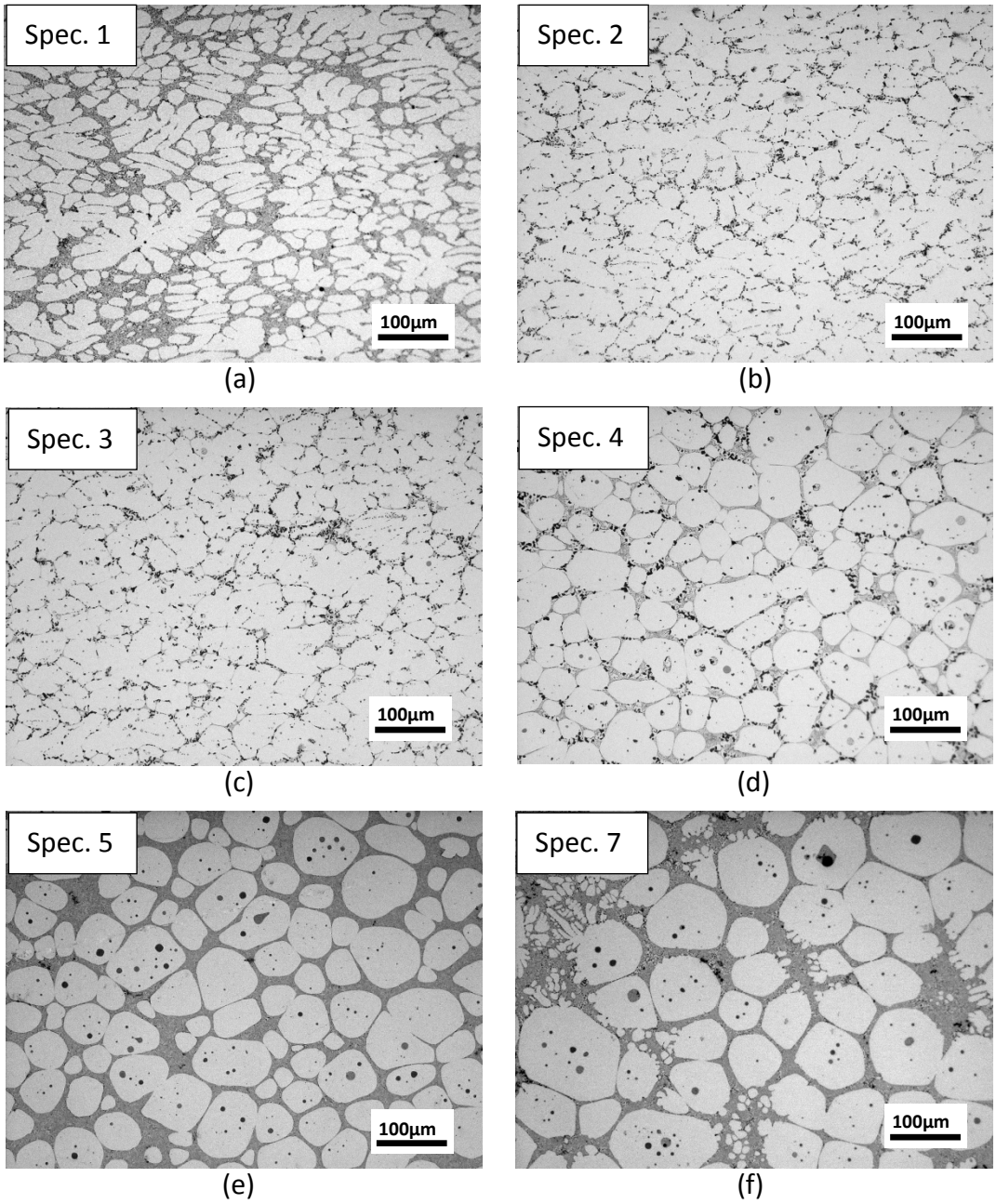

Fig. 4-6. Microstructure (as polished, 200x magnification) evolution during partial re-melting. (a)-(e) Specimen 1-5 in Fig. 2, respectively; (f) Specimen 7.

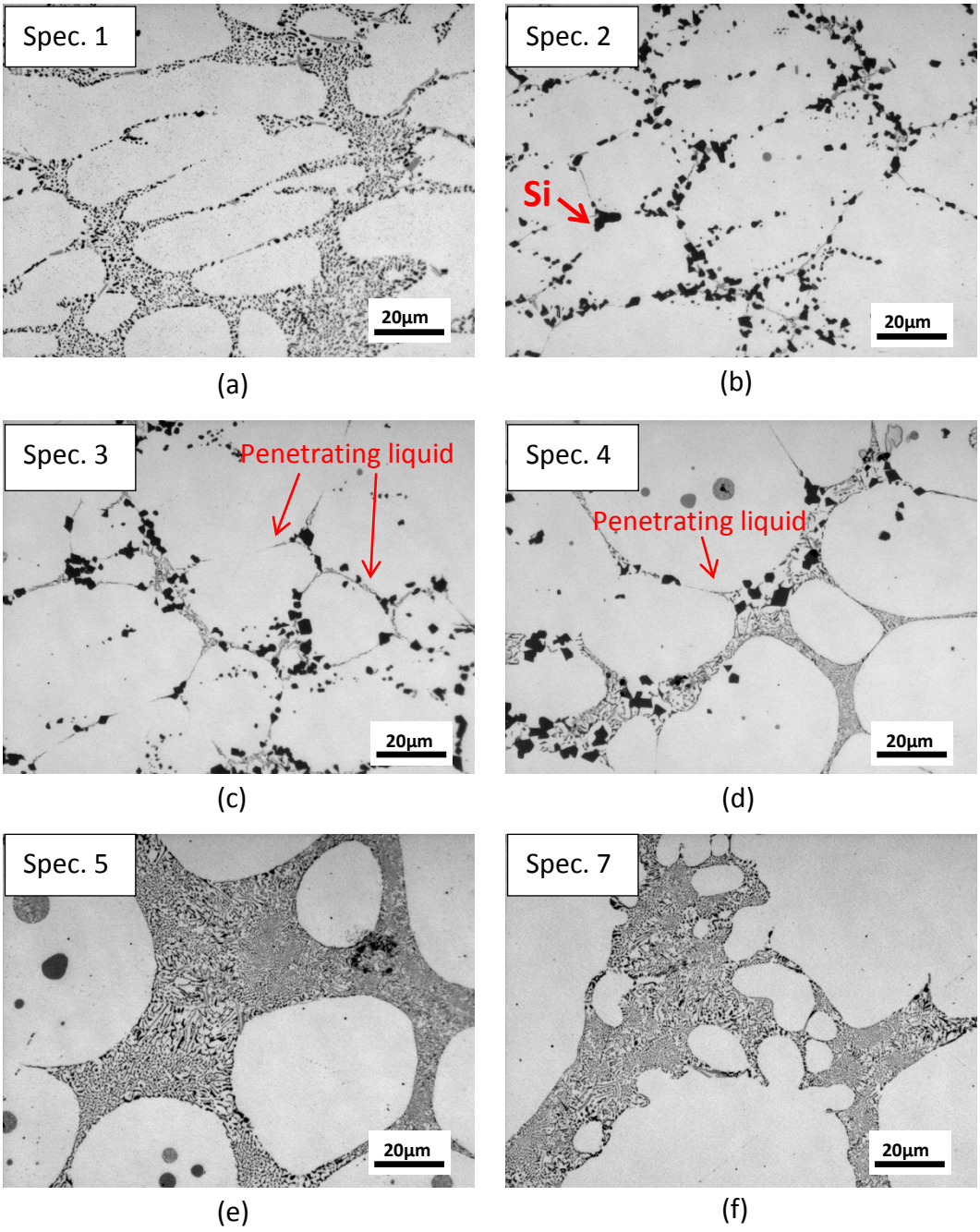

Fig. 4-7. Microstructure (as polished, 1000x magnification) evolution during partial re-melting. (a)-(e) Specimen 1-5 in Fig. 2, respectively; (f) Specimen 7.

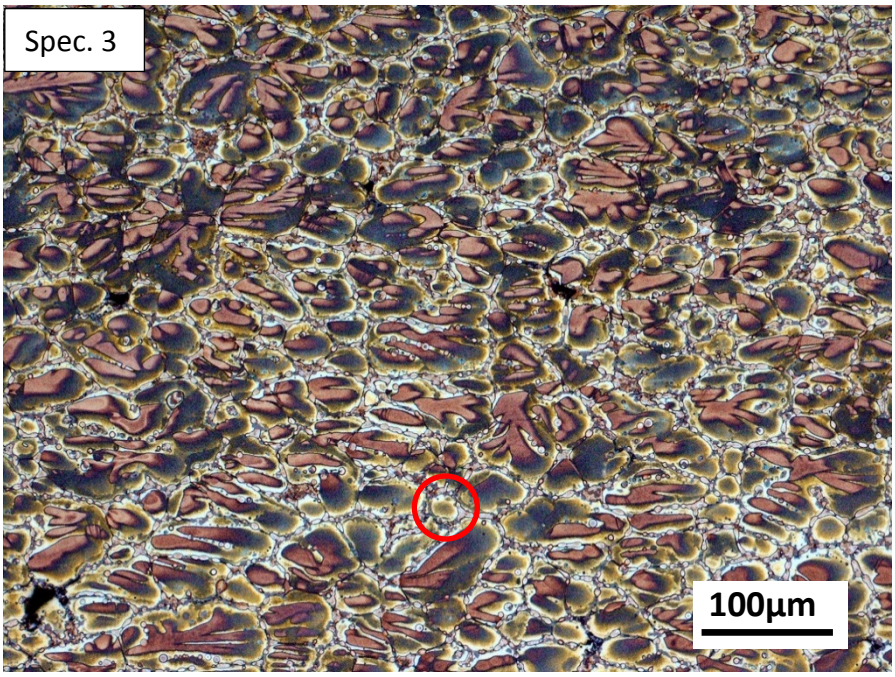

(a)

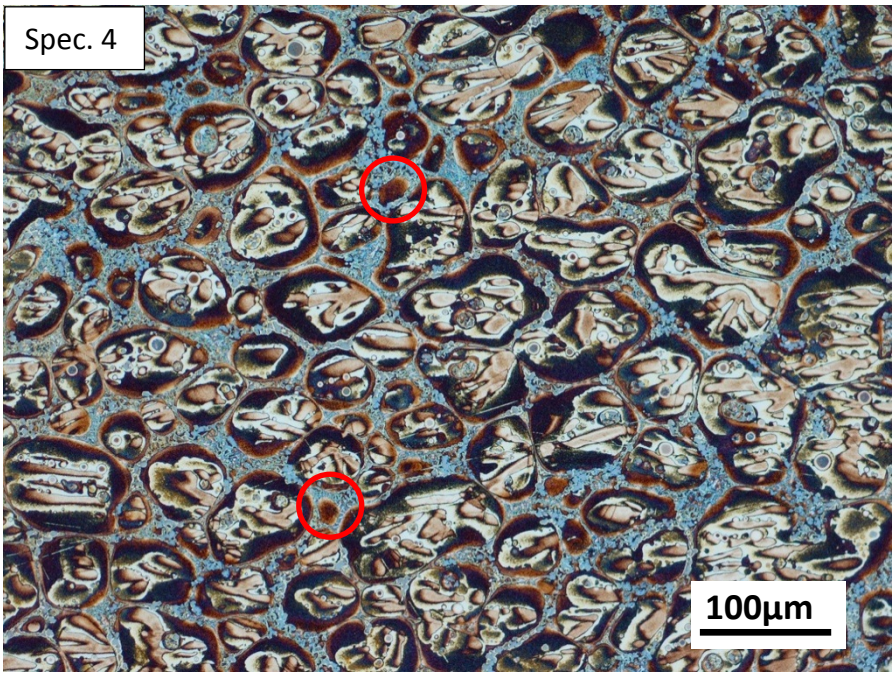

(b)

Fig. 4-8. Microstructure of Specimen 3 and 4 etched by Weck's reagent. The small grains marked by circles are thought to be peripheral cross sections of ripened dendrites, but also possible that they are newly formed grains due to recrystallization.

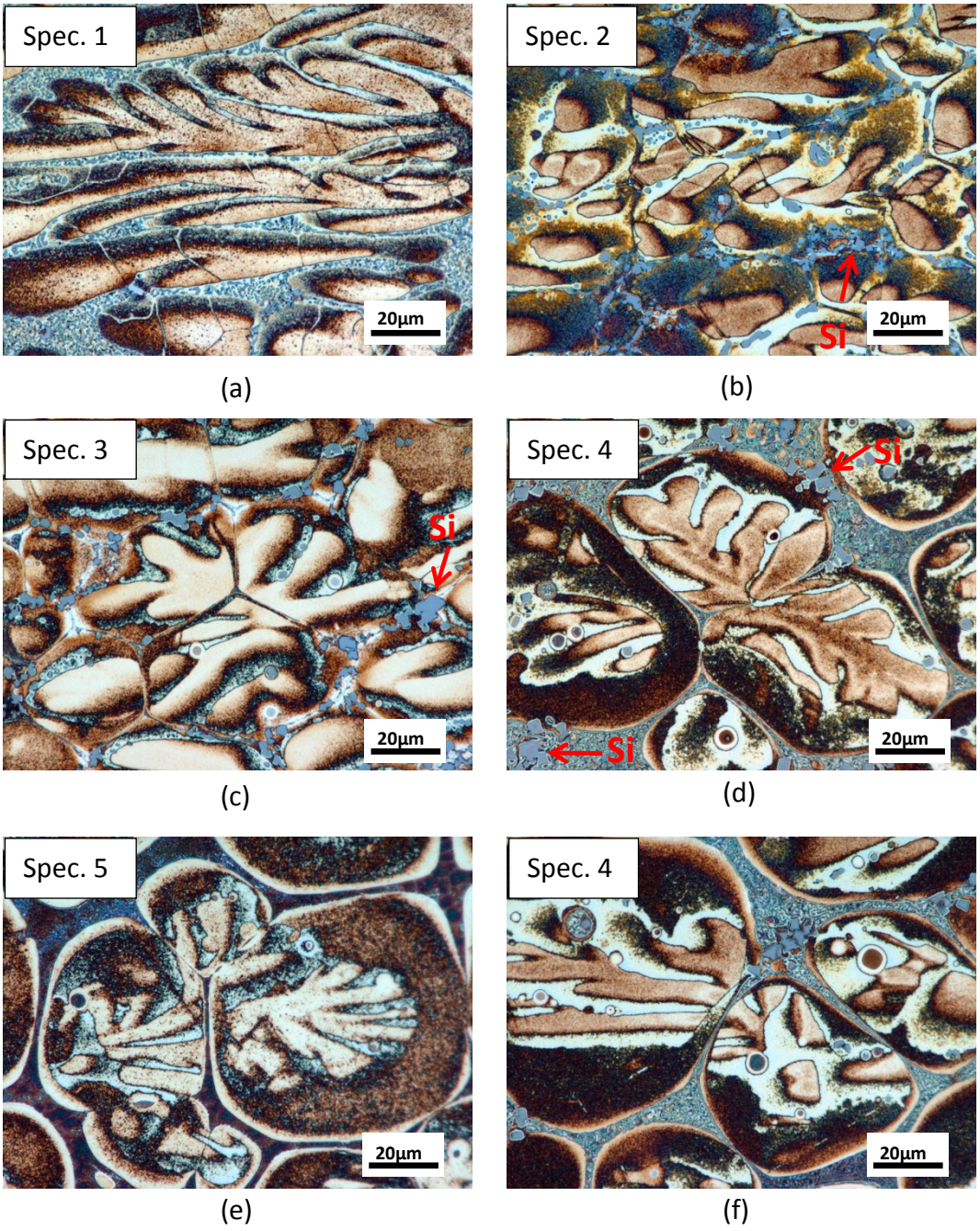

Fig. 4-9. "fractured" dendrites observed in (a)-(e) Specimen 1-5, respectively; (f) Specimen 4. Note that in (f), the spheroidal grains are completely separated.

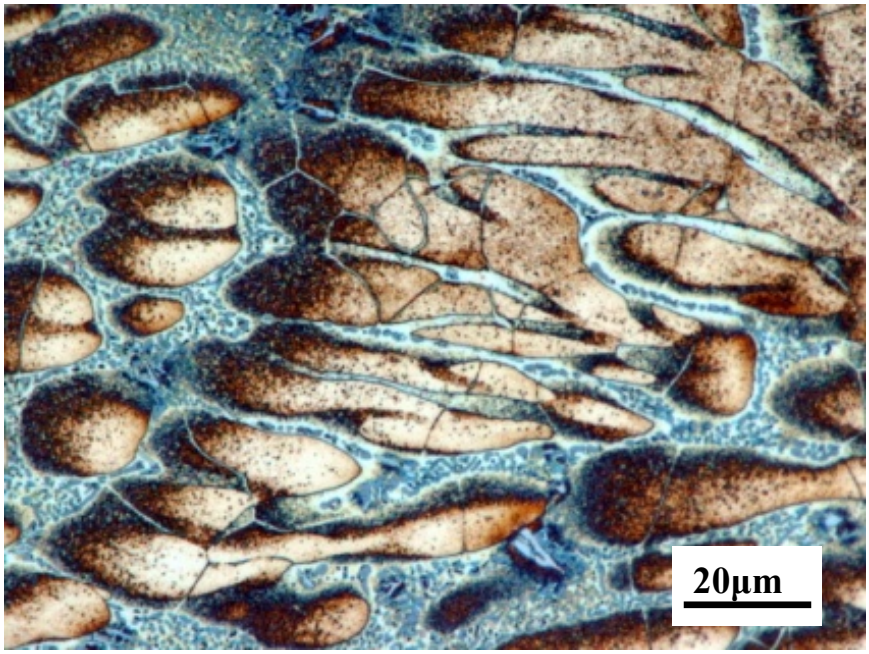

(a)

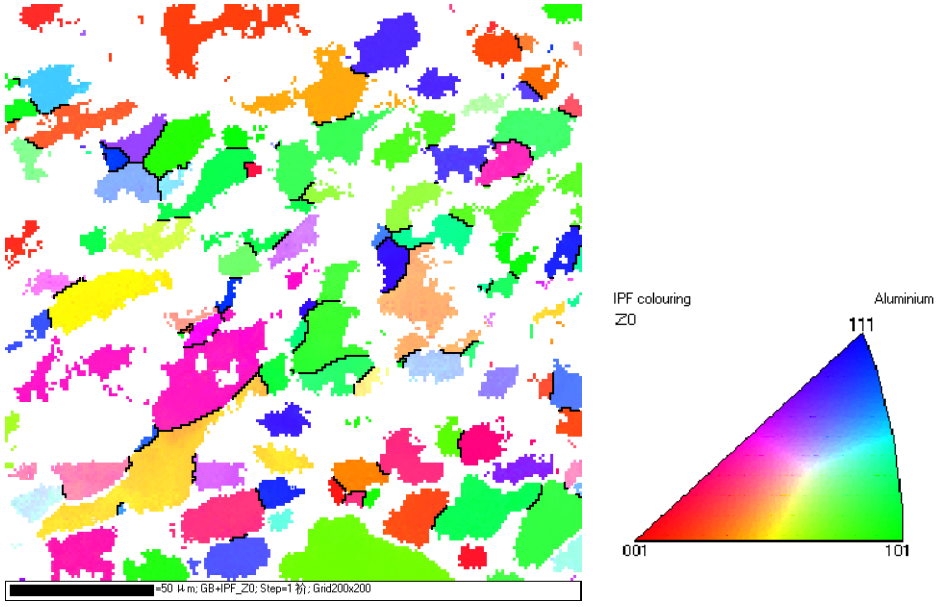

(b)

Fig. 4-10. (a) Micrograph showing the dendrites in recrystallization state with crack-like lines inside; (b) grain orientation map of the same specimen.

Chapter 5

Coloring mechanism of Weck's reagent studied by characterization of the etched surface

5.1. Introduction

In the last three chapters, three applications of Weck's reagent are introduced, which are 1. Detection of micro-segregation in Al phase, 2. Accurate evaluation of solid fractions and 3. Detection of grain boundaries. Many applications could be realized thanks to the coloration of Al phases by Weck's reagent. However, as mentioned in Chapter 1, understanding of coloring mechanism is difficult although there are already several mechanisms proposed and accepted [1]. In many cases of color etching, a thick film that leads to inference light is formed after etching. The difference in the thickness of film or optical properties generates different colors from grain to grain or inside one grain. Besides these kinds of coloring mechanism, etching pitting (anodizing of Al or Al alloys) and line etching [2] can also produce color under optical microscope by using polarized light.

Besides color etching, many objects and daily phenomena also interest us because of the beautiful color they have or produce. Examples can be given such as animals' (birds, butterflies, etc.) colorful appearance or

artificial objects (prints, CDs, etc.). Especially in the case of a CD disk, iridescent color is seen due to the small pits organized in a series of concentric circles as shown in Fig. 5-1 [3]. Light is diffracted and interfered on the surface because the gaps between those pits are a few times of the wavelength of visible light. This well-known phenomenon indicates that color can be produced without an interference film if the surface is micro structured in order. However, despite some well-studied cases, historically, people produce color generally based on experiences without deep understanding or studying of the coloring mechanisms. As a result, reports focusing on the coloring mechanism are limited.

According to Suárez-Peña et al. [4], when etching Al alloy by Weck's reagent, a manganese oxide film is formed via the following reaction:

$$Al + MnO_4^- + 2\ H_2O \rightarrow Al(OH)_4^- + MnO_2$$

However, since no experimental confirmation is done, whether MnO_2 exists or not is still not clear. In this chapter, the surface observation is firstly carried to confirm Suárez-Peña et al.'s hypothesis. Upon confirmation, attention is paid on the surface characterization in order to study the coloring mechanism in detail.

5.2. Experimental

5.2.1. Materials and process

There are two kinds of A356 aluminum alloy billets used in this research, one with 0.14 wt.% Ti included and the other free of Ti. Their chemical compositions are indicated in Table 5-1. The Ti-contained A356 billet was direct-chill cast and supplied by Kyushu Mitsui Aluminium Co., Ltd, while the Ti-free A356 billet was cast in a ship-shaped Cu-mold and provided by Nissan Motor Co., Ltd.

In order to induce plastic deformation to the billets, they were compressed without pre-heating. To avoid buckling, as shown in Fig. 5-1, the billet was cut into small ones (Φ105×150mm). Compression was carried out axially by a 500 ton compressing machine. The compressing rate is 0.2mm/sec. The billet's temperature was increased to about 44 ^{o}C when the target height (100mm, 33% reduction) was reached.

Small specimens were cut from the compressed billet and heated to semi-solid state. Once the temperature of specimen reaches 581 ^{o}C, specimen was quickly water quenched.

5.2.2.Etching and optical microstructure observation

Specimens were polished via standard metallographic techniques, finished using Struers OPS colloidal silica. Subsequently, specimens were immersed in Weck's reagent for approximately 12 s at room temperature.

Then the microstructure was observed by optical microscopy (OM) without any filters or analyzers. In order to prove the reproducibility of the color revealed by Weck's reagent, 12 s etching was repeated for 4 times and before each time's etching, slight polishing was carried out to remove the etching layer remained from previous etching. Four optical micrographs were taken for the same location. In order to study the influence of etching time, one specimen was etched for five times, for 4 s, 8 s, 12 s, 20 s and 28 s. Before each time of etching, slight polishing of the previous etched surface was done to remove the etching layer. The micrographs were taken for the same location in the specimen.

5.2.3. Scanning electron microscopy (SEM) and field emission scanning electron microscopy (FE-SEM)

Imaging with secondary electrons by both SEM and FE-SEM was applied to characterize the etched surface. SEM was used at first to conform if there was a film formed on the surface after etching. The accelerating voltage was set at 5 kV. FE-SEM (accelerating voltage is set at 12 kV) was used for observations with higher resolution at high magnifications. Different locations within one spheroidal Al grain were observed in terms of their surface topography.

5.2.4. Laser microscopy and atomic force microscopy

Both Keyence VX-200 laser microscope and Olympus OLS4500 Nano search microscope with cantilever were used to characterize the etched surface. Both of these two microscopes are able to accurately select a certain area to observe with the help of optical microscope equipped together. The surface average roughness (R_a) of a selected area can be measured by both these two microscopes and the results were compared with the color expressed in RGB values obtained by VX-200 laser microscope.

5.2.5. Transmission electron microscopy (TEM) and scanning transmission electron microscopy (STEM)

TEM observation was carried out with the observation angle vertical to the etched surface. The TEM specimen was made by first mechanically polishing the alloy side of the specimen to less than 100 μm and then electro polishing ($HClO_4$:C_2H_5OH=3:7, 13 V) until a tiny hole appeared on the surface. The accelerating voltage was set at 1020 kV. Diffraction pattern was also taken. In the case of STEM, in the beginning, carbon was deposited on the etched surface to protect the surface. Then, a focused ion beam (FIB) was used to slice a small specimen vertical to the surface, namely a cross section of film, with the thickness thin enough for the STEM observation. The observation was carried out for the cross section of film so that the thickness of the film can be seen directly. Energy

Dispersive X-ray Spectroscopy (EDS) was also used to measure the film composition qualitatively. Concentration mappings of Al, Mn, O, Si, Mg and Ti were obtained.

5.2.6. Time of Flight Secondary Ion Mass Spectrometry (TOF-SIMS)

Secondary ion mass spectrometry was carried out because it can characterize the film composition showing the concentration mapping of the film. Ti-contained A356 Al alloy with a spheroidal Al grain structure was used. The first iron was Bi^+ ion. Concentration mappings of Al, O, Si, Mn, MnO and MnO_2's ion (both positive and negative) were obtained with the image size of 128 x 128 pixels.

5.3. Results

5.3.1. Reproducibility of the color revealed by Weck's reagent

Experiments concerning this topic were carried out by repeating the etching for four times with 12 s constantly. Prior to each time of etching, the etching surface was removed by polishing. The result is shown in Fig. 5-3. It is clear that the re-producibility is quite good with all the characteristics (dendritic structure, grain growth during water quenching) visualized equally every time. There is some small change in the shape of dendritic structure. This is because of the polishing before etching each

time that the cross section went deeper into the grain. Through careful observation, we can see that there was a tiny color change especially in the intergranular region but overall, the color is invariable. The third time etching shown in Fig. 5-3 (c) exhibits a relatively low quality probably due to the problems of polishing before etching.

5.3.2. Surface observation after etching by SEM and FE-SEM.

Fig. 5-4 shows the optical microstructures of a spheroidized Al grain both before and after etching. The etching time was 12 s. Inside the spheroidal grain shown in Fig. 5-4 (b), different colors can be seen. Detailed explanation of this microstructure can be found in Chapter 2. SEM observation was carried out for this grain, as shown in Fig. 5-5. Comparing micrographs in Fig. 5-5 with Fig. 5-4 (b), one finds that the coloration brought by Weck's reagent has a strong correlation with the surface condition. In detail, as indicated more clearly in Fig. 5-5 (b) and (c), the film was not uniformly formed within one grain. Referring to Fig. 5-5 (e), it shows that in the dendritic region (marked as region 1 in Fig. 5-5 (b) and (c)) which has the highest Ti concentration, the film is densely formed. On the contrary, it seems that film is not at all formed in the region (marked as region 2) adjacent to the dendritic region, or poorly formed in other region (marked as region 3). It is surprising to see that the boundary of region 1 is so clear and sharp because there is a sudden

change of the film condition indicated by the red arrows in Fig. 5-5 (b) and (c). The film on the region corresponding to the grain growth during water quenching is well formed as indicated in Fig. 5-7 (d) (observed area corresponds to the red box in Fig. 5-5 (a)).

However, in the case of Ti-free alloy whose microstructures are shown in Fig. 5-6, the color contrast is decreased comparing with Fig. 5-4 (b). Furthermore, according to the SEM observation which is indicated in Fig. 5-7, lack of Ti results in a much poorer film formation throughout the spheroidal grain. Although the dendritic region is still visible in the SEM micrograph, its boundary can be hardly distinguished under high magnification (Fig. 5-7 (b) and Fig. 5-7 (c)). Comparing the etched surfaces between Ti-contained and Ti-free alloy, it suggests that Ti is an important factor that influences the film formation and coloring. However, in the region of grain growth during water quenching exhibited in Fig. 5-7 (d) (observed area is the same as the red box in Fig. 5-7 (a)), the film is densely formed similar to the Ti-contained case (Fig. 5-6 (d)).

SEM has successfully confirmed the existence of a film after etching. Also the local change of the surface topography is observed. In order to obtain more information about the topography change, FE-SEM was used since it has a better resolution than SEM. Results are shown in Fig. 5-8. Fig. 5-8 (a) located in the center exhibits optical microstructure of the grain observed. The specimen is the Ti-contained A356 Al alloy and

water quenched when the temperature reached 581 ^{o}C. Same characteristics with Fig. 5-4 (b) can be observed such as grain growth during water quenching, dendritic structure inside the spheroidal grain and the dark brown area surrounding the dendritic structure. FE-SEM micrographs are shown in Fig. 5-8 (b-e), with the observing locations indicated by red boxes and arrows. During the observation, the accelerating voltage was set at 12 kV. For observing surface topography, this voltage seems to be too high. However, with lower voltage such as 3 kV or 5 kV, satisfying image contrast could not be obtained. The reason for this will be discussed later.

From Fig. 5-8 (b-e), one sees more details of the surface topography compared with those shown in Fig. 5-5 (a-d). Fig. 5-8 (b) shows the micrograph corresponding to the grain growth formed during water quenching. It demonstrates that this part has a well formed (dense) film which is in line with the observation in Fig. 5-5 (d). But there are also some pores existing which could not be visualized by normal SEM. Fig. 5-8 (c) and (d) show the morphology of dendritic structure and the dark brown area surrounding it. In the previous observation by SEM, it was confirmed that the dendritic region has a film smoothly formed in contrast to the rough morphology in the dark brown area. Fig. 5-8 (c) and d exhibit a good agreement that the film in the dendritic region has a finer morphology than it in the dark brown region. Comparing Fig. 5-8 (c) with

Fig. 5-8 (b), one can clearly see that the morphologies are different in those two regions, despite the fact that they look the same in Fig. 5-5. It seems that there is no film or the film is thiner between two dendritic arms, which is shown in Fig. 5-8 (e).

SEM and FE-SEM observations have revealed the surface topography clearly and the correlation between the color and surface condition is also proved to be strong. In order to study the coloring mechanism at a quantitative level, laser microscopy and AFM were carried out. The following two sections will demonstrate the results obtained by these two methods.

5.3.3. Influence of the etching time on the specimen coloration

The material used is Ti-contained A356 Al alloy. The specimen was etched for 5 times with etching time 4 s, 8 s, 12 s, 20 s and 28 s. As already mentioned in the materials and methods part, prior to each time etching, the specimen surface was slightly polished to remove the etching layer remained from last time etching. After etching, micrographs were taken for the same location. As can be seen in Fig. 5-9, it is interesting that such small difference in etching time could cause a big change of color. In the dendritic structure region, we observe that on 4 s etching, the dendritic region became gray (Fig. 5-9 (a)). As the etching continues, it turned brown and the contrast decreased when etching time was over 12 s

(Fig. 5-9 (d) and (e)). As for the ring-shape grain growth formed during water quenching, it can be seen that this region became brown (Fig. 5-9 (a-c)) at first and finally turned white (Fig. 5-9 (d) and (e)). In addition, in the intergranular eutectic region, the color kept darkening from 4 s to 28 s. Among those different etching times, we can easily find that 12 s etching provided the result with the best color contrast. As mentioned before, a Mn oxide film is formed on the surface during etching.

SEI images in Fig. 5-10 show the surface topography corresponding to different etching time. Upon 4 s etching, one observes that the film starts to grow on the dendritic area. After that, the differences in the topography increases and 12 s etching yields to the best contrast in the micrograph, which is in accordance with the best color contrast obtained by 12 s etching shown in Fig. 5-9. After 12 s etching, the film still keeps growing but the difference in the topography is decreased. As a result, 20 s and 28 s etching do not show a good color contrast under optical microscope compared with 12 s etching.

5.3.4. Surface observation after etching by laser microscopy and AFM

Fig. 5-11 shows the three kinds of information directly obtained by laser microscopy, namely color, laser intensity and surface profile. The color information is obtained by optical microscope. Laser intensity is the intensity of reflected laser so the whiter it appears, the higher intensity of

laser is reflected. Surface profile is obtained by scanning the “height” on the surface. Later, the average roughness of a selected area can be calculated automatically. From these figures, it can be seen that after etching, the etched surface has a different reflection of laser from location to location. The surface profile also indicates that the surface has difference in height, with some places rough and some places flat. In order to observe the surface more clearly, three dimensional micrographs are made based on the surface profile data, which are shown in Fig. 5-12 (red boxes in Fig. 5-12 (b) and c indicate the area where average roughness is calculated). It should be note that Z axis was enlarged by 6 times in order to emphasize the surface roughness. The optical micrograph pasted to the upper right part indicates the location of the 3D profile and the corresponding color. Exhibited in Fig. 5-12 (b), the dark brown area shows a quite rough morphology compared with the dendritic area shown in Fig. 5-12 (c). The average roughness of these two regions is also calculated to be 56 nm and 10 nm, respectively. The region between two dendritic arms which seems to be free of film is also very flat. But careful observation can find that in the edge of dendritic arms which appears black or dark brown as shown in optical micrograph, the roughness is higher. Fig. 5-12 (e) shows the area containing the grain growth during water quenching and eutectic phase. It can be seen that the grain growth region formed during water quenching has a flat surface and

the eutectic region is bimodal with Si particles higher than Al phase.

As mentioned before, three kinds of quantitative information can be obtained by laser microscopy. They are laser intensity, color (in RGB mode) and average roughness (R_a). The data can be collected from a selected area. Thus the relationship between laser intensity and R_a, as well as the relationship between color and R_a, can be expressed quantitatively, which is demonstrated in Fig. 5-13 and Fig. 5-14, respectively. Eight areas are selected inside the spheroidal grain which cover all the colors appear. Laser intensity, RGB values and R_a are obtained for every selected area.

In Fig. 5-13, one sees that the reflected laser intensity decreases as the surface roughness increases. Especially on the low roughness side, the decrease is dramatic. Relationship of R_a and RGB values is shown in Fig. 5-14. The trend of the color change from 0 to 255 is expressed in Fig. 5-14 (a) first. The higher the value is, the brighter the color looks. In Fig. 5-14 (b), two points should be mentioned. First, the value of red, green and blue decreases as the surface roughness increases, which is similar to the trend of laser intensity. Second, among those 8 areas where data were collected, most of them has a sequence of value red > green > blue. This is because this kind of combination yields to the color looks brown or close to brown, which takes most of the area inside spheroidal grain as indicated in Fig. 5-11 (a).

Besides laser microscopy, AFM is also an effective method of characterizing surface topography quantitatively. The spheroidal grain selected for AFM observation is shown in Fig. 5-15 (optical micrograph). Where three regions (2 μm×2 μm) are scanned, which correspond to dendritic structure (region 1), dark brown area (region 2) and grain growth during water quenching (region 3). The surface topography in both 2D and 3D is displayed in Fig. 5-16. According to the above laser microscopy results, the dark brown area has the roughest surface (region 1, $R_a \approx 50$ nm) while the other two regions are flat ($R_a < 10$ nm). However, it is quite surprising that AFM measurements show that all the three regions are flat and have the average roughness about 3 or 4 nm. This conflict in the result of R_a between laser microscopy and AFM will be discussed later.

5.3.5. Microstructural observation and compositional analysis of the film by TEM and STEM

Fig. 5-17 is a TEM micrograph taken at relatively low magnification (X20,000). The diffraction pattern is also shown in the upper left of the micrograph. The micrograph was taken with the observation vertical to the film. At this magnification, the difference in the topography of the film can be seen clearly. Also, the halo pattern also suggests that the film is amorphous. The Four more TEM micrographs with higher

magnification are shown in Fig. 5-18. The black shades observed in Fig. 5-18 (a-c) are corresponding to remained Al substrate during electro polishing. In Fig. 5-18 (a) and (b), one observes numerous tiny structures which look like “bubbles”. The density of those structures is higher in Fig. 5-18 (a) than it in Fig. 5-18 (b). It is difficult to know which region inside spheroidal grain those TEM micrographs represent. But comparing with the FE-SEM observation shown in Fig. 5-8, Fig. 5-18 (a) and (b) might correspond to the dendritic and dark brown regions, respectively because those “bubbles” have the corresponding size with the asperity and similar density difference shown in Fig. 5-8 (c) and (d). The morphologies shown in Fig. 5-18 (c) and (d) are different from Fig. 5-18 (a) and (b), where the bubble like structure cannot be observed. Instead, they look somewhat close to the FE-SEM observation results of the area between two dendritic arms (Fig. 5-8 (d)) and grain growth during water quenching (Fig. 5-8 (b)).

The cross section of the film was observed by STEM, whose micrographs are shown in Fig. 5-19. From the observation, film’s thickness is confirmed to be around 100 nm and in some regions, it is near 200 nm. In Fig. 5-19 (a), there is a large particle appears black, which is actually a eutectic Si particle. Therefore, the film on the left of the Si particle is probably the film on the grain growth during water quenching. Fig. 5-19 (b) is a magnification of that area, it can be noticed

that the morphology indicated in Fig. 5-19 (b) is different Fig. 5-19 (c), which is probably corresponding to the morphology difference observed by both TEM (between Fig. 5-18 (c), (d) and Fig. 5-18 (a), (b)) and FE-SEM (between Fig. 5-8 (b) and Fig. 5-8 (c), (d)). Also from Fig. 5-19, the surface of the film is flat. In contrast, the interface between the film and the substrate is rough.

The results of composition analysis by EDS are shown in Fig. 5-20. The analysis was carried out for two locations with different morphologies but the composition seems to be the same. The results indicate that the film is free of Al and Mg, while concentrated with Mn, O and Si. The concentration of Mn and O infer that the existence of manganese oxide is reliable, but if it is MnO_2 is not clear. The mapping of Si shows that the Si's concentration is even higher than it in the Al substrate. This can be explained by the cost of Al during reaction with reagent which results in as increase of Si's concentration relatively.

5.3.6. Further analysis of the film composition by SIMS

The results of SIMS analysis are shown in Fig. 5-21 and Fig. 5-22. Fig. 5-21 shows the compositional image together with negative ion mappings. Among those mappings, O^-, Si^-, MnO^- and MnO_2^- ions have clear contrast which means that the difference in contraction is large from location to location. O^- ion mapping probably indicates that the concentration of

manganese oxide differs in different locations. Mappings of MnO^- and MnO_2^- also support this result: higher concentration of both MnO^- and MnO_2^- can be found in the dendritic regions. Si^- mapping indicates that SI concentrates in eutectic region. The existence of MnO_2^- ion has proved that the film has the composition of MnO_2. MnO^- ions may come from ionized MnO_2, so it is not clear if MnO exists in the film.

Positive ion mappings are shown in Fig. 5-22. Al has been proved not exist in the film. But its positive ion appears in the mapping. This is due to the fact that the surface was sputtered deeply so that after the film is completely ionized, Al substrate will be sputtered and ionized. Mn^+ ion mapping again proved that the manganese oxide has different concentration in different parts of the film. It was found that the Mn^+ ions also come from the eutectic part. This is due to the reaction between eutectic Al with the Weck's reagent, which also produces manganese oxides in the eutectic region.

5.4.**Discussion**

5.4.1. Surface topography characterized by SEM, FE-SEM, laser microscopy and AFM

In this chapter, topography of etched surface are characterized both qualitatively and quantitatively. The SEM and FE-SEM microscopy

confirmed the existence of a film formed after etching with Weck's reagent. Moreover, inside one spheroidal grain, both flat area and rough area exist. Comparing SEI images with optical micrographs (same observing location) shows clearly the surface topography is in strong correlation with color difference revealed by Weck's reagent. Such correlation is furthermore confirmed quantitatively by using laser microscope. Fig. 5-13 and Fig. 5-14 exhibit the relationship of laser intensity vs. roughness and RGB value vs. roughness. However, AFM analysis found that the surface roughness dose not differ that much, which conflicts with the laser microscopy analysis. This conflict can be explained as follows.

In the characterization of a thin film by laser microscopy, as shown in Fig. 5-23, both the surface and interface between substrate and film can reflect incident laser (Fig. 5-23 (a)), which results in two peaks of laser intensity as shown in Fig. 5-23 (b). Ordinary laser microscope only identify the higher peak. If the roughness of the interface between substrate and film is larger than the film surface, it will result in a wrong 3D profile which corresponds to the interface of substrate and film, not the surface of film. Therefore, the rough surface morphology observed by laser microscope in the present study maybe the interface of the Al alloy substrate and the film. Evidence can be found in the results of cross section observation by STEM (Fig. 5-19), which indicates that the surface

of the film is relatively smooth while the interface between the substrate and film is rough.

Recently, some manufacturers of laser microscope have added the function which can identify those two peaks caused by analyzing a transparent film. However, this function usually requires the thickness of the film to be large enough so that the two peaks can be distinguished [5]. In the present study, the film is very thin (less than 200 nm). Therefore, two peaks merge into a single one or the peak 2 is not clear enough to be distinguished, resulting in the difficulty to use this function.

5.4.2. Film formation and its relationship with the micro-segregation in spheroidal grain

As mention in the introduction section, during etching with Weck's reagent, Al reacts with MnO_4^- ions, producing a film consists of manganese oxide. The existence of MnO_2 in the film has been confirmed in the composition analysis by STEM. Such kind of film formation is called "conversion coating" in coating industry, which means the substrate is reacted and produces a film. In the case of Al alloy, chromate conversion coating (CCC) is the most popular conversion coating used as a corrosion inhibitor. The influence of substrate chemical composition on the film formation during CCC was studied by Liu et al. [6]. The research has shown that with addition of alloying elements, such as 2.3at.%Cu,

1.9at.%Au or 20at.%Au, growth rate of the coating and also the consumption of the metal can be reduced. However, due to the toxicity of hexavalent chrome, the substitute of CCC is also being studied nowadays. One of the possible solutions is permanganate conversion coating (PCC), which consumes Al to produce a manganese oxide film on the substrate. This process is very close to the etching process with Weck's reagent. However, research on PCC is very limited and the alloying influence on the coating has not been studied yet.

In the present study, the film formation is closely related to the micro-segregations in spheroidal grains. Inside the spheroidal grain, the dendritic region possesses the highest concentration of Ti, as indicated in Fig. 5-5 (e). Film in the region is well formed as shown in Fig. 5-5 (b). On the contrary, the area surrounding the dendritic area has the lowest Ti concentration. In this area, film is poorly formed or not formed as can be seen in the area indicated by number 2 in Fig. 5-5 (b). The dark brown area has the Ti with concentration between dendritic region and the region surrounding it. In this area, the film is formed roughly. The above description indicates the trend that the addition of Ti actually promotes the chemical reaction thus film can be better formed. This is different from the CCC process where addition of elements suppresses the coating speed. In the area corresponding to the grain growth during water quenching, the morphology of the film formed during etching is different

from others as demonstrated in Fig. 5-8 (b), which is smooth but different from the smooth film in the dendritic region. In this region, according to EPMA analysis, both Si and Ti segregate, making the composition different from the inside of spheroidal grain. Maybe this is the reason for the special morphology of the film in this region.

Using Ti-free A356 Al alloy, the color contrast is reduced after etching due to the poor formation of film as indicated in Fig. 5-7. But when the grain started to grow during water quenching, micro-segregation of Si increases the concentration of Si in this region (Fig. 5-7 (e)), leading to a better formation of film as shown in Fig. 5-7 (d).

5.4.3. Proposed coloring mechanism

Several coloring mechanisms of color etching have been mentioned in the introduction section. Although the existence of the film has been confirmed, it seems the coloring mechanism cannot be explained by only light interference. First of all, the laser microscopy has clearly revealed the strong correlation between surface roughness and color, which means that the surface roughness is an important factor to the coloring. Besides, the interface between film and substrate is not flat thus even if light can be interfered by the film, the color will be unstable due to the different thickness of the film. Moreover, manganese oxide itself has color of black or blackish brown in powder state, namely the absorption of the

complementary color. Although it is not clear how the color will change in thin film state, such contribution to the color revealed by optical microscope should not be neglected.

There are a few published studies focusing on the coloring mechanism of nature species such as morpho butterflies and Japanese jewel beetles [7]. An example from [7] is given in Fig. 5-24, the special surface structure of the morpho butterfly's wing produces beautiful blue color. Such ordered structure leads to multilayer interference, diffraction and incoherence. The combination of these three effects results in the blue color we see.

According to the previous discussion that the film surface is flat while the interface between film and substrate is probably rough, the schematic graph of the cross section of the specimen after etching with Weck's reagent is shown in Fig. 5-25. Three different coloring mechanisms are considered. As a hypothesis, the color revealed by Weck's reagent should be the combination of the above three factors, or any two of them:

1. Interference of reflected lights. As discussed in before, the film probably has a flat surface but a rough interface with substrate. This kind of structure provides three different positions for the incident light to reflect, which is indicated by x, y and z in the figure. Since the structure asperity as well as the film thickness is in the order from tens nanometers to 200 nanometers, light traveling distance can differ in

the same order which can cause interference.

2. Diffraction. In the case of morpho butterfly, it was suggested that diffraction of light can also occur. The case of a CD disk as shown in Fig. 5-1 also suggests a high possibility of diffraction produced by the rough interface between film and substrate.
3. The absorption of a certain wavelength of manganese oxide itself. The absorption of light should not be forgotten because most of the colors we see from objects in daily life are produced by this effect. The color of manganese oxide is black or dark green in bulk and sometimes brown in powder state. Therefore, it is reasonable to consider that the film itself can absorb the light with a certain wavelength, producing the complementary color as a result.

Comparing the result of surface observation by SEM (Fig. 5-5 (a)) with the Ti distribution obtained by EPMA analysis (Fig. 5-5 (e)), one notices that the concentration of Ti in Al phase had a strong influence on the film's morphology. This phenomenon will be further discussed as follows.

Fig. 5-26 demonstrates the schematic graph showing the cross section of the specimen after 12 etching with respect to the change of Ti concentration. In the case of spheroidal grain, it can be divided into three parts according to the increase of Ti concentration namely the area between dendritic arms, the dark brown area (observed by OM) and the

dendritic area. The Ti's concentration was the lowest in the area between dendritic arms as proved in Fig. 5-5 (e). From the results obtained by laser microscopy (Fig. 5-11, 5-12) and AFM (Fig. 5-16), in this area, the film was considered to be very thin with a thickness about tens of nanometers. It was shown that the film surface and interface between film and substrate were flat and the RGB values were also the highest. In contrast to this, film formation was much promoted in the dark brown area (optical micrograph, 12 s) and the dendritic area with a thickness about 200 to 300 nanometers indicated by both laser microscopy (Fig. 5-11) and cross sectional observation using STEM (Fig. 5-19). In the dark brown area where the RGB values were the lowest, the roughness of the interface between film and substrate was the highest indicated by laser microscopy. In the dendritic area, the roughness of the interface between film and substrate was lower than the dark brown area but higher than the area between dendritic arms. From the above discussion, it is obvious that the roughness has a strong effect on the coloring mechanism. However, the roughness change seems not to be monotonic to the change of Ti concentration. This could be explained from the results concerning the influence of etching time (Fig. 5-9, 5-10).

The schematic graph showing the change of film morphology with the increase of etching is given in Fig. 5-27. In the beginning of etching, film started to grow preferentially on the dendritic region due to the higher

concentration of Ti, as indicated in Fig. 5-10. But at this time, the color is still light (Fig. 5-9) so it can be inferred that the roughness of the interface between film and substrate should be low. As the etching time increases to 8 s, the color in the dendritic area becomes darker which is probably due to the increase of interface roughness. The color in the other area is also different from the micrograph of 4 s etching, which indicates that the film formation in those areas is also in progress. When the etching time increases to 12 s, which shows the best color contrast, as discussed in the last paragraph, the film thickness as well as the interface roughness is different from location to location with respect to the change of Ti concentration. But after 12 s, which can be seen in the micrographs of 20 s and 28 s etching, there is a trend that the color of dendritic area stops to change and the rest region also changes into brown later. This probably indicates that the growth of film will be slowed down first in the dendritic area, and then in the rest region. This can be proved by the disappearance of dark brown area in the Al grain after 28 s etching, which suppose that the interface between film and substrate changes from rough to flat if the etching time is long enough.

From the discussion above, it can be summarized that the film's color is basically brown. But the brightness of brown is strongly influence by the roughness of the interface between film and substrate. The film grows preferentially in the area with higher concentration of Ti compared with

the late growth in the area with lower concentration of Ti. But if the etching time is long enough, the film morphology will be the same due to the limit of film growth. As a result, the color will be similar in spite of the difference in the Ti concentration. The 12 s etching yields to the best color contrast due to the biggest difference in the film thickness and morphology among different locations.

5.5.Conclusions

In this chapter, coloring mechanism of Weck's reagent was focused. Various characterization methods were applied to understand more about the film in terms of surface topography, cross section observation and chemical composition.

In the beginning of this chapter, the reproducibility of the color revealed by Weck's reagent was tested first by repeating the 12 s etching for four times in total. The results showed that the reproducibility of the color revealed by Weck's reagent was quite good, with stable color microstructure obtained every time.

The etched (12 s) surface topography of Ti-contained and Ti-free A356 Al alloy was observed by both SEM and FE-SEM. In the case of Ti-contained A356 Al alloy, the surface topography changed from location to location inside the spheroidal Al grain. Comparing the

topography with color optical micrograph, it can be seen that the topography was in strong correlation with the color difference revealed by Weck's reagent. Furthermore, the topography was also in correlation with Ti micro-segregation inside Al grain. Higher concentration of Ti in Al phase resulted in the formation of smooth film. On the contrary, lower concentration of Ti led to a rough surface. The Ti-free A356 Al alloy showed a low color contrast after etching with Weck's reagent. However, in the region corresponding to the grain growth during water quenching, due to the simultaneous segregation of Si and Ti, the film was smooth and well formed. But the morphology was different from the smooth film in the dendritic region in Ti-contained Al alloy. Color micrographs obtained with other etching times were also shown. Compared with 12 s etching, their color contrast was decreased. According to surface observation by SEM, 12 s etching showed the best contrast in topography.

The relationship between surface condition and color was investigated quantitatively by laser microscopy. The results showed that the reflected laser intensity and RGB values decreased as the average surface roughness increases. However, AFM analysis conflicted with laser microscopy by which the surface roughness seems to be low and constant. Considering the fact that the film is probably transparent, the rough surface detected by laser microscopy might be actually the interface of film and substrate, which was in agreement with cross section

observation of STEM.

TEM observation of film also detected difference in the film morphology from location to location. The halo pattern indicated that the film is amorphous. Some locations containing “bubble” like structure with different density were found, which might be in accordance with the SEM observations at dendritic and dark brown areas.

Cross section observation by STEM revealed that the film thickness ranged from tens of nanometers to 200 nm. It was also interesting that the interface between film and substrate was rougher than the surface of film, which supported the viewpoint that the rough surface observed by laser microscopy was actually the interface of film and substrate. Composition analysis carried by EDS equipped showed that the film was rich in Mn, O and Si in spite of the difference in morphology. This result proved that the film was actually manganese oxide. Si had higher concentration in the film than the substrate probably due to the consumption of Al reacted with Weck’s reagent.

SIMS analysis further helped to understand the chemical composition of the film. The existence of MnO_2 was confirmed. MnO^- ions were also detected that probably come from MnO_2 due to the ionization. The ion mapping also indicated that the concentration of manganese oxide differed in different location, which could also have an influence on the color observed by optical microscope.

Coloring mechanism was proposed with consideration of the structure of the film formed during etching with Weck's reagent. The surface of the film and the rough interface between film and substrate could both reflect incident light, which led to the interference of light. Diffraction can also happen but it was not confirmed. At the same time, the absorption of light with a certain wavelength by manganese oxide can also contribute to the coloration. The color observed by optical microscope should be the combination of those effects. The film's morphology can be influenced by both the concentration of Ti in Al and the etching time. Higher concentration of Ti can promote the film growth. 12 s showed the best color contrast because that the difference of film thickness and morphology among difference locations in the Al grain is the biggest. Film's thickness and roughness keep changing during etching, which produces different colors for different etching time. But as the etching time increases, in spite of the location or Ti concentration, the color tends to be brown and the morphology of film also becomes homogeneous.

The coloring mechanism can be finally concluded that as follows. The color after etching with Weck's reagent is produced by a Mn oxide film. The color is basically brown, which can be influenced by film's morphology (thickness and roughness), especially the brightness that is controlled by the roughness of the interface between film and substrate.

Reference

[1] A. Maltais, D. Dubé, F. Roy, M. Fiset, Optical anisotropy of a color-etched AZ91 magnesium alloy, Mater. Charact. 54 (2005) 315-326.

[2] A. Maltais, M. Fiset, G. Laroche, S. Turgeon, D. Dubé, Improvement in metallography of As-Cast AZ91 alloy, Mater. Charact., 52 (2004) 103–119.

[3] http://www.thenakedscientists.com/HTML/content/kitchenscience/exp/colours-in-cds/

[4] B. Suárez-Peña, J. Asensio-Lozano, G.F. Vander-Voort, Colour metallography in commercial Al-Si alloys. Optimization of the microstructural characterization techniques in light optical microscopy. Rev. Metal 46(2010) 469-476.

[5] Private communication with experts at laser microscopy from Olympus Corporation.

[6] Y. Liu, P. Skeldon, G.E. Thompson, H. Habazaki, K. Shimizu, Chromate conversion coatings on aluminium: influences of alloying. Corro. Sci. 46 (2004) 297-312.

[7] S. Kinoshita and S. Yoshioka, Structural Colors in Nature: The Role of Regularity and Irregularity in the Structure, ChemPhysChem. 6 (2005) 1442-1459.

Table 5-1. Main chemical compositions of the materials used in this chapter (wt.%)

Alloy	Si	Mg	Fe	Ti	Sr	Mn	Al
Ti-contained A356	6.90	0.39	0.10	0.14	0.025	<0.10	Bal.
Ti-free A356	7.04	0.43	0.13	0.0006	0.0024	0.006	Bal.

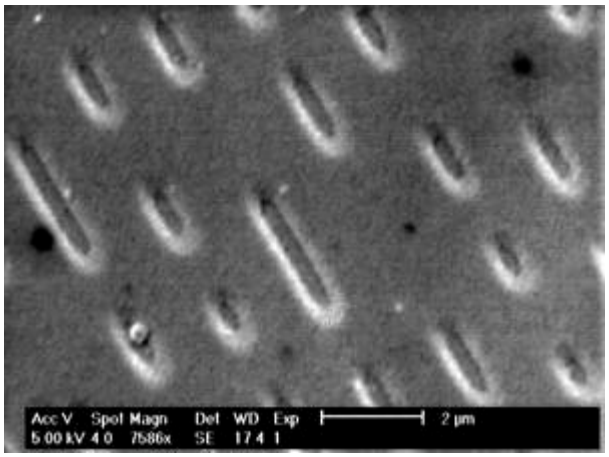

Fig. 5-1. An SEM micrograph showing the pits on a CD disk's surface [3].

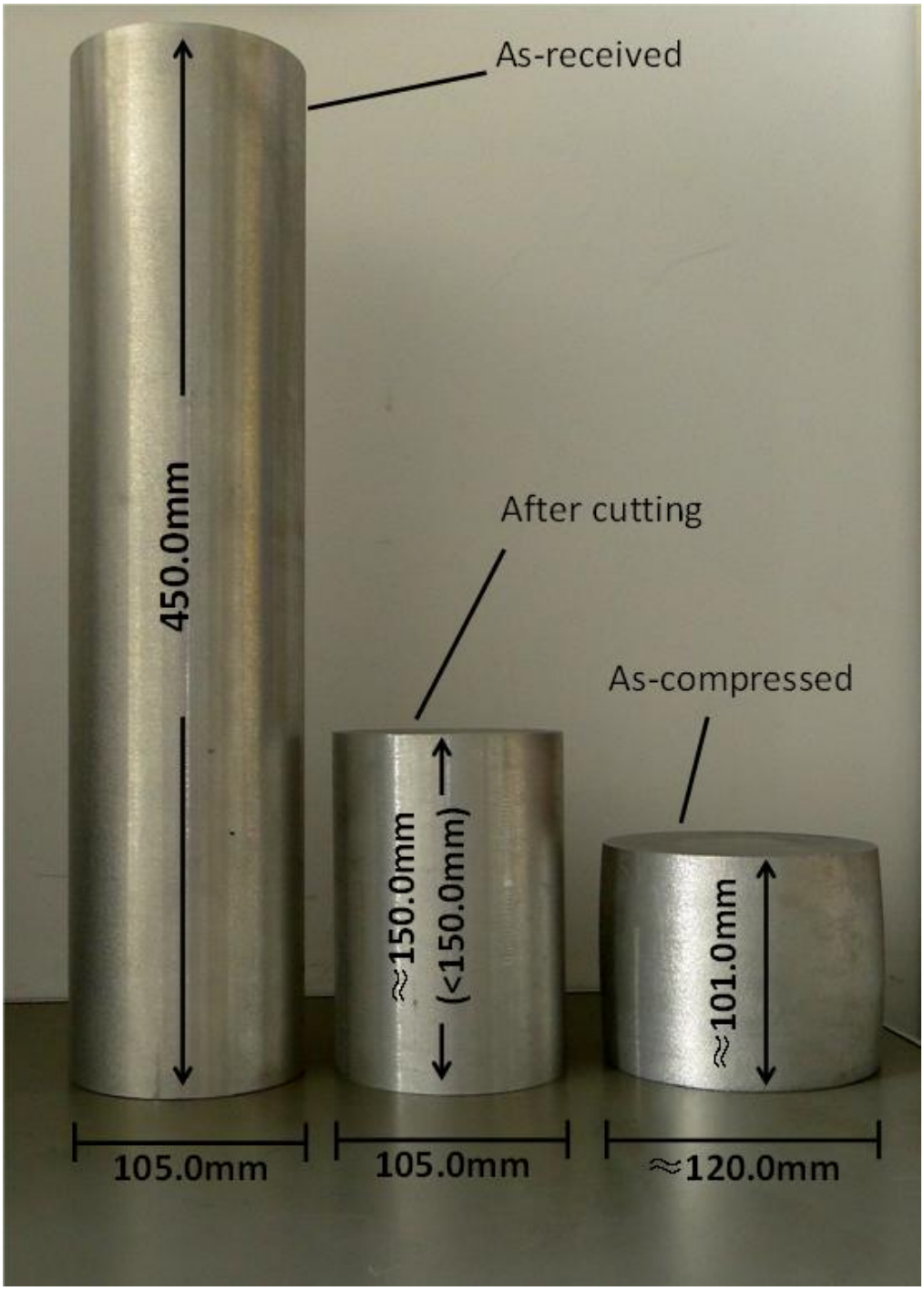

Fig. 5-2. Picture of the A356 aluminum billets used in this chapter, the as received billet was cut before compression in order to avoid buckling.

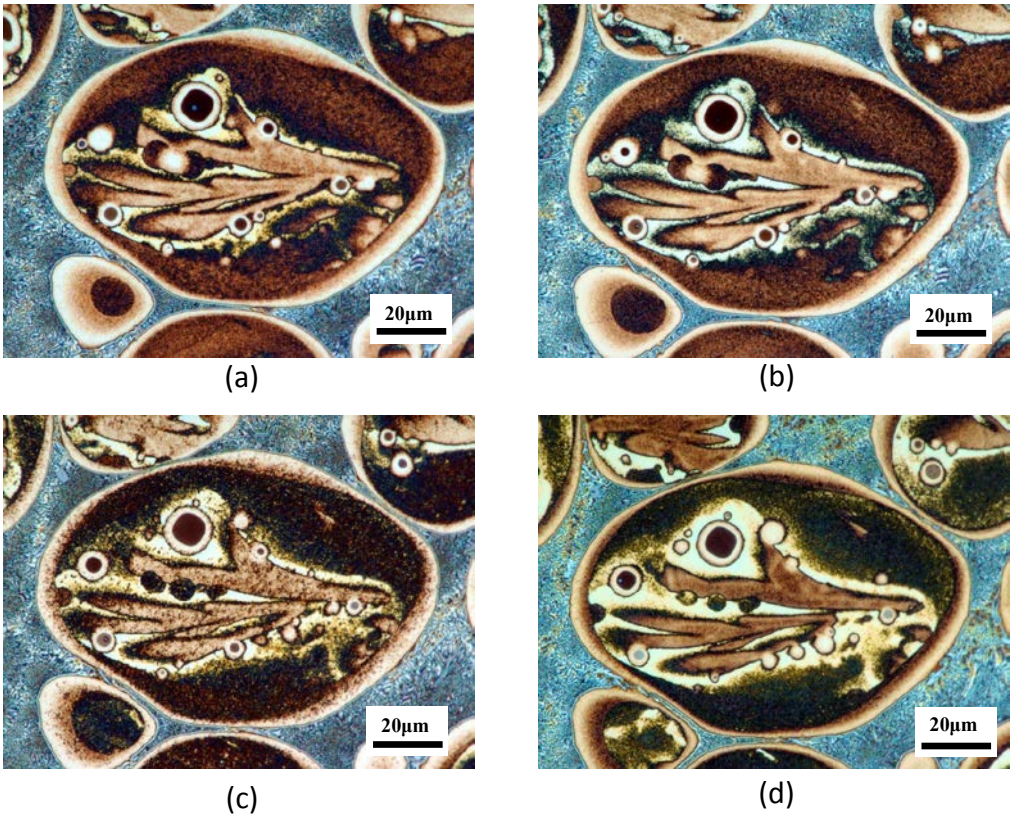

Fig. 5-3. Repeating etching using Weck's reagent for four times with the same etching time of 12 s.

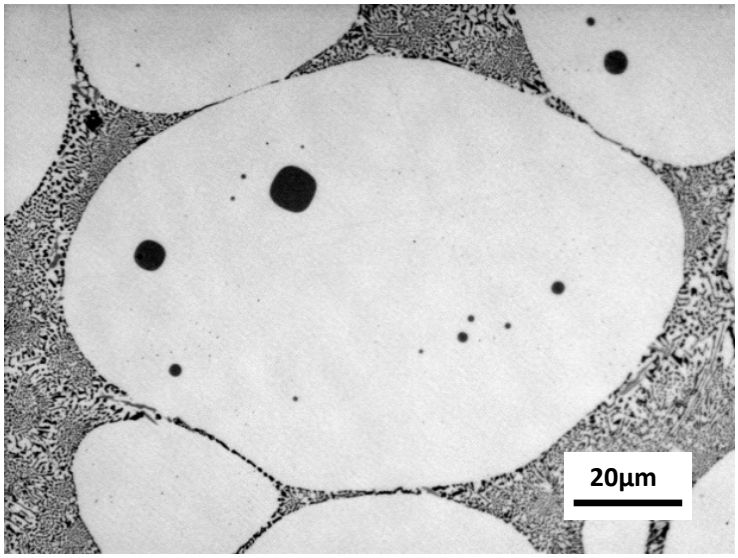

(a)

(b)

Fig. 5-4. A spheroidal Al grain in Ti-contained A356 Al alloy observed by optical microstructure before (a) and after (b) etching with Weck's reagent.

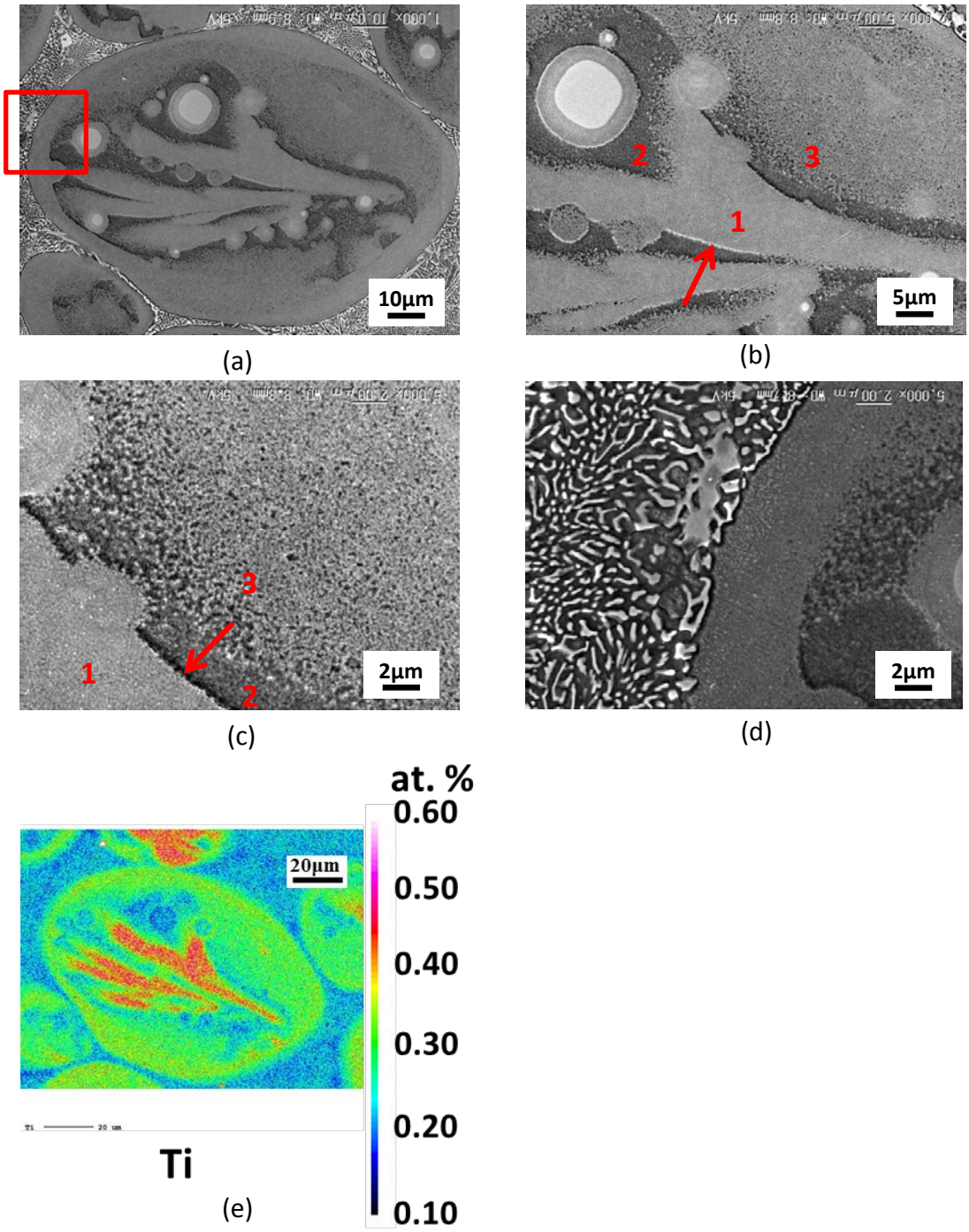

Fig. 5-5. SEM observation (a-d) of the etched surface whose optical microstructure is shown in Fig. 1 b, as well as the Ti distribution (e) in the Al grain obtained by EPMA analysis after etched surface is removed.

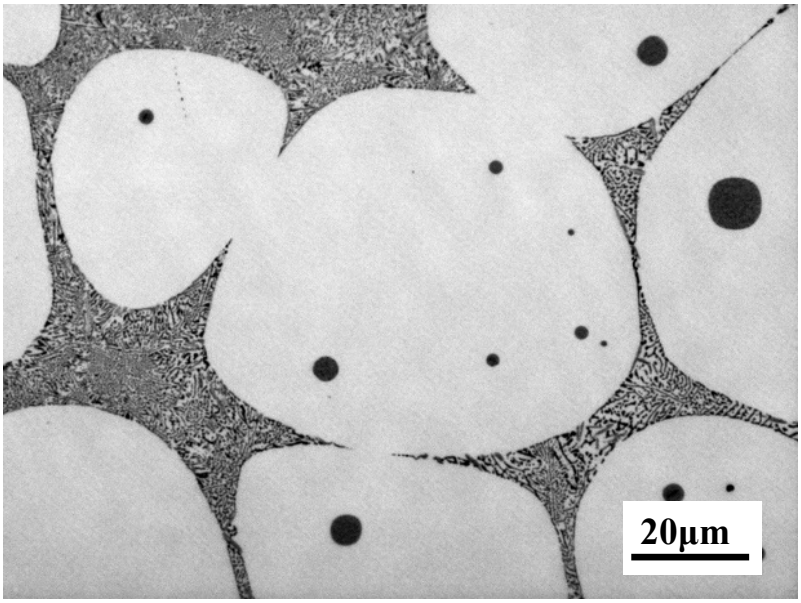

(a)

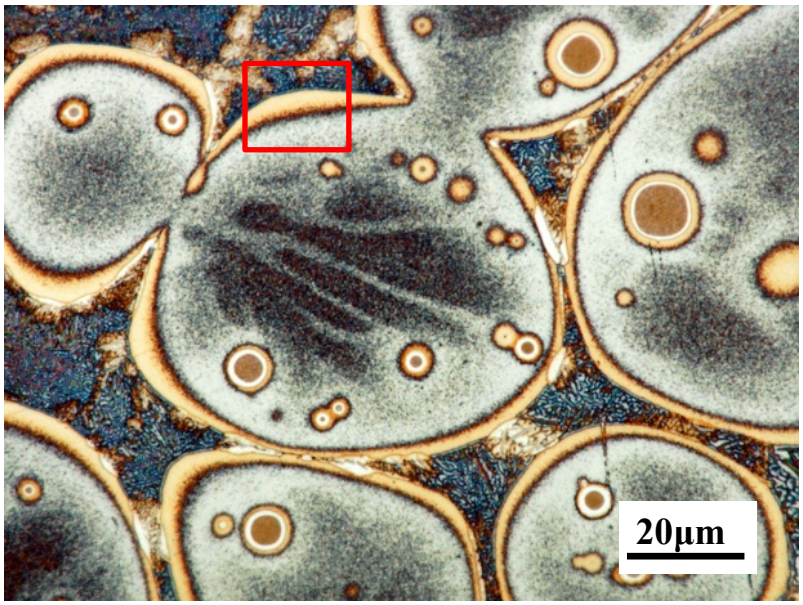

(b)

Fig. 5-6. A spheroidal Al grain in Ti-free A356 Al alloy observed by optical microstructure before (a) and after (b) etching with Weck's reagent.

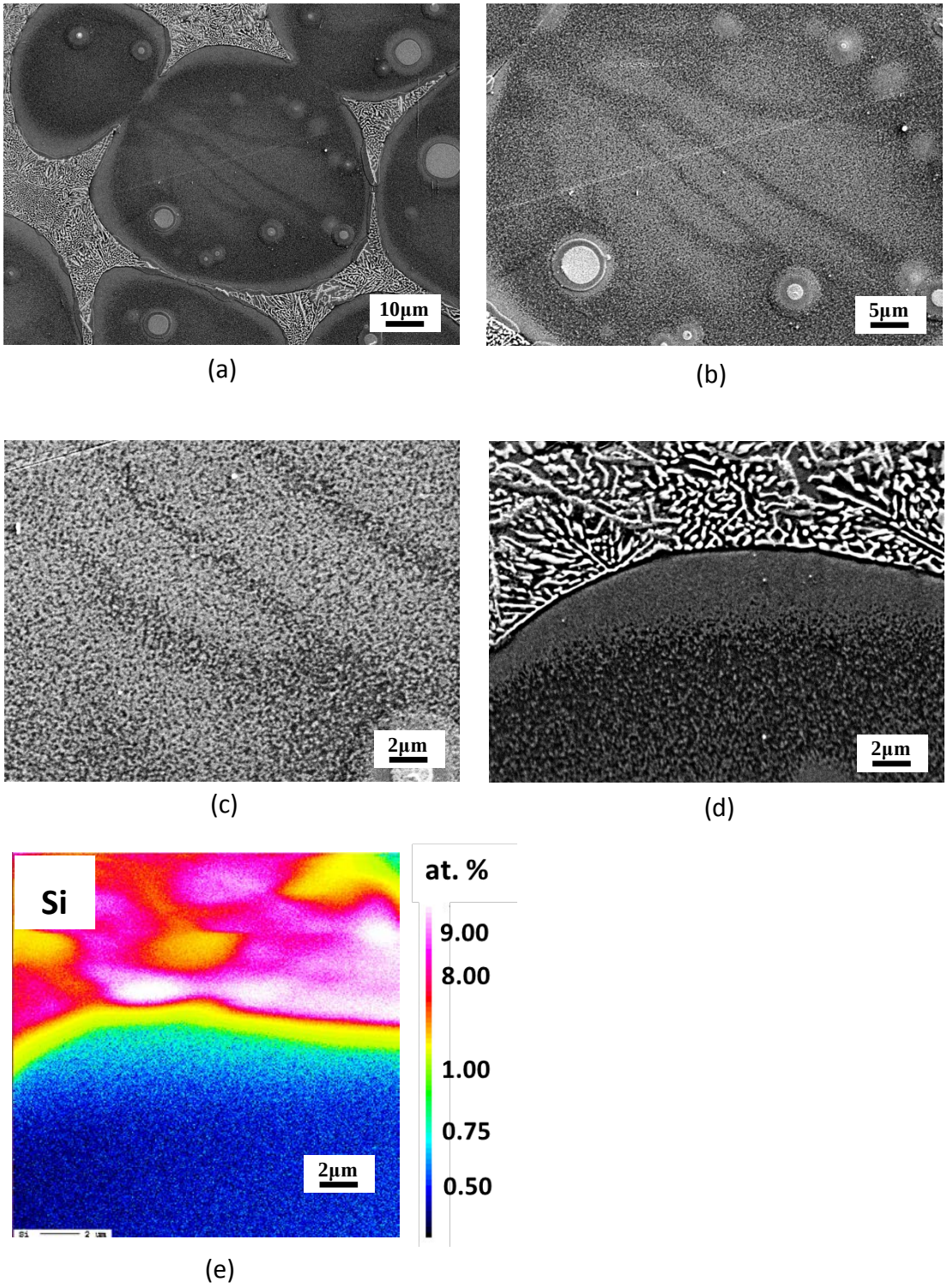

Fig. 5-7. SEM observation (a-d) of the etched surface whose optical microstructure is shown in Fig. 4 b, and the Si concentration (e) in the area corresponding to (d)

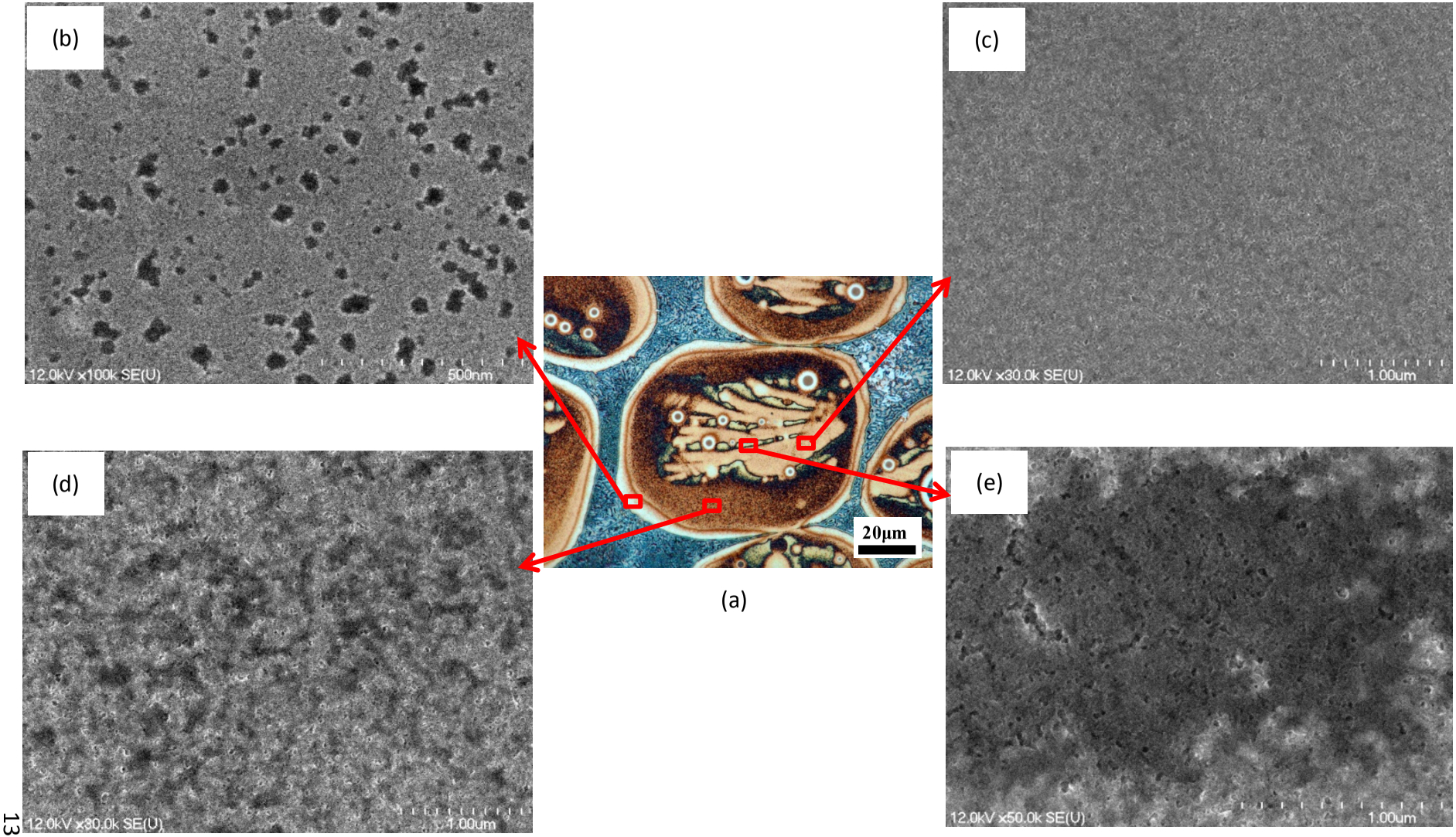

Fig. 5-8. FE-SEM observation of the etched surface .

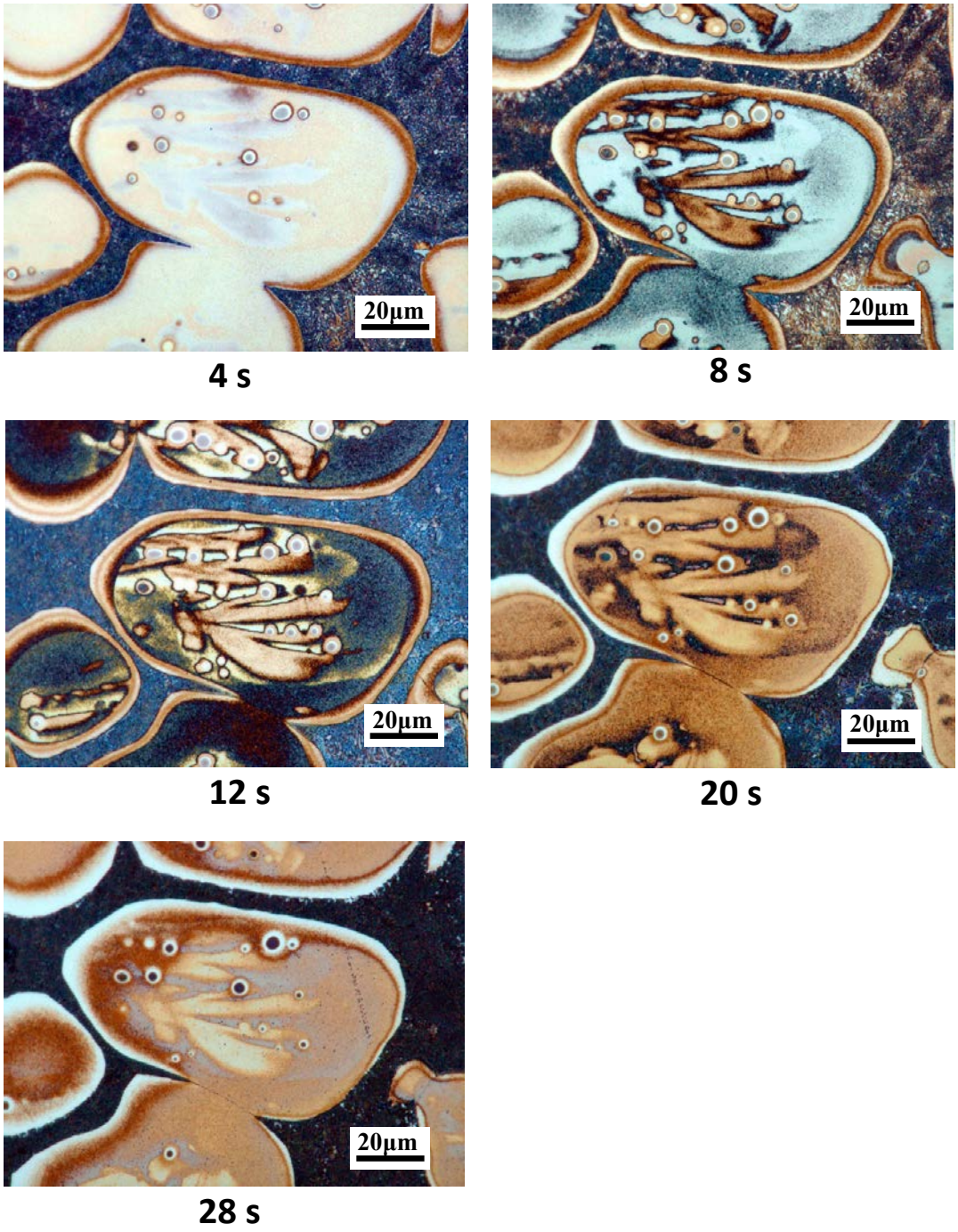

Fig. 5-9. Microstructures of Ti-contained A356 Al alloy obtained after different times of etching using Weck's reagent.

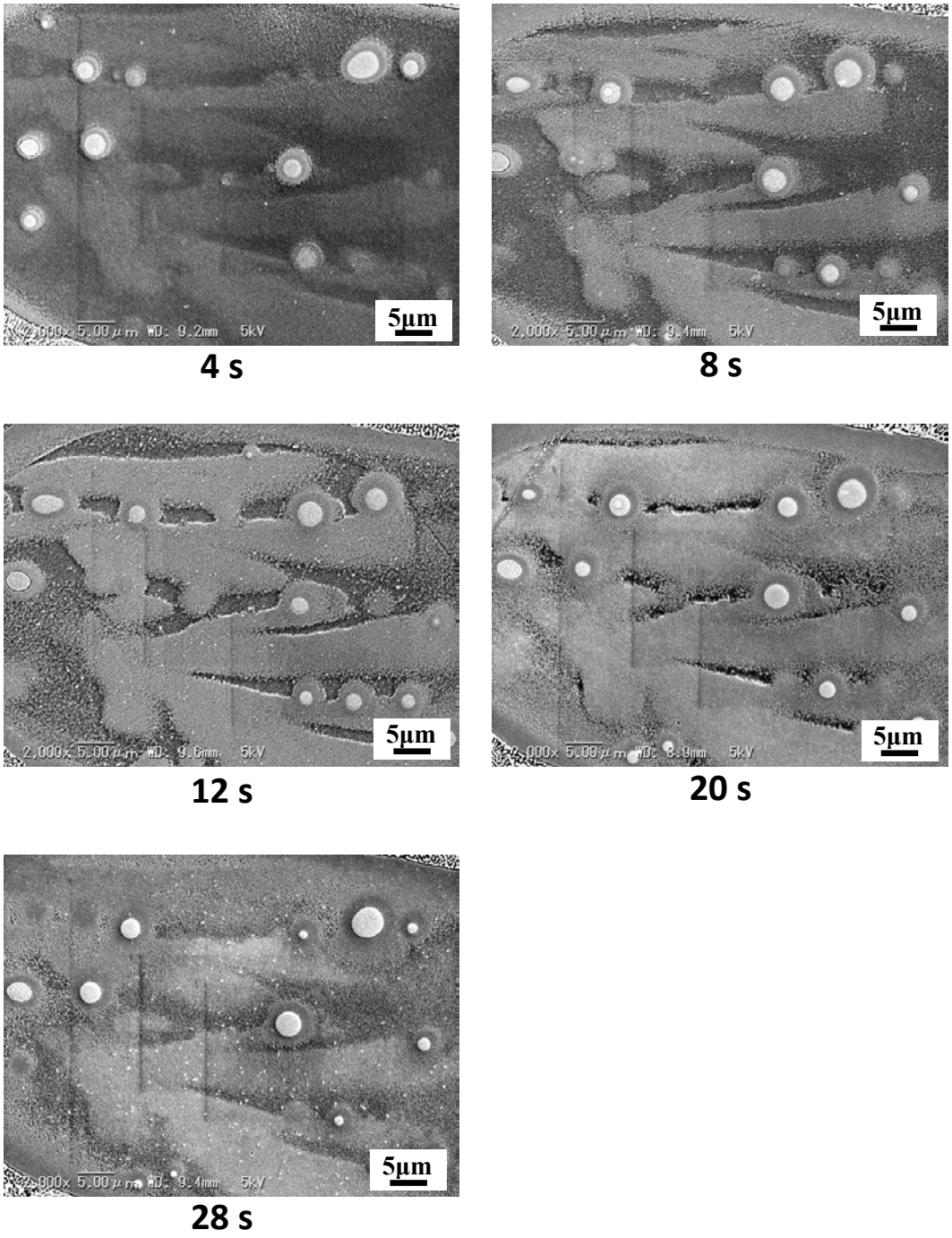

Fig. 5-10. SEM observation of the etched surface at different etching time.

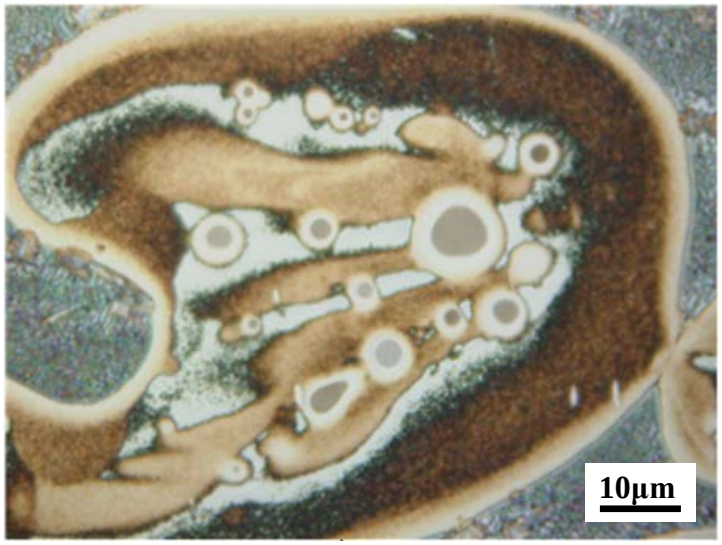

(a)

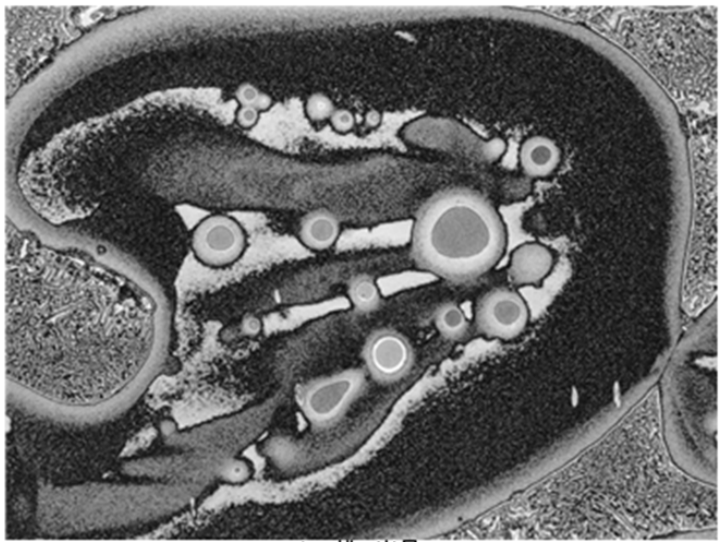

(b)

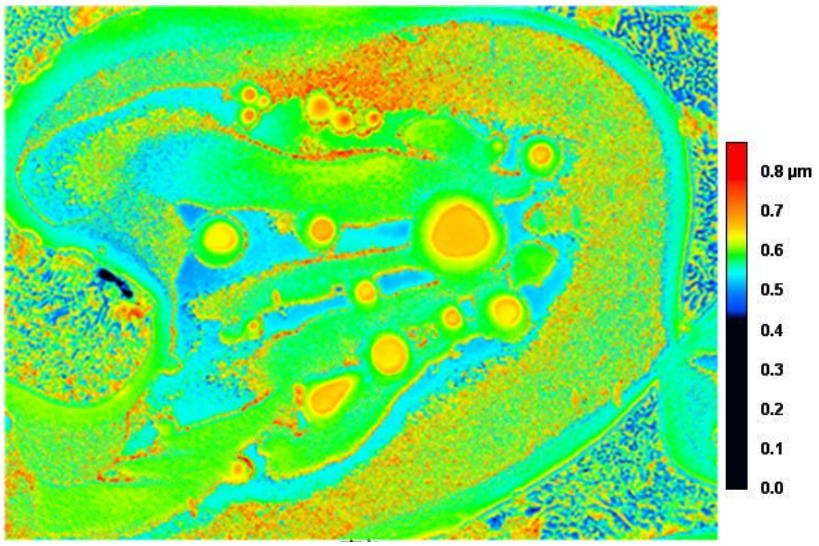

(c)

Fig. 5-11. Results obtained by Laser microscopy: (a) color, (b) laser intensity and (c) surface profile

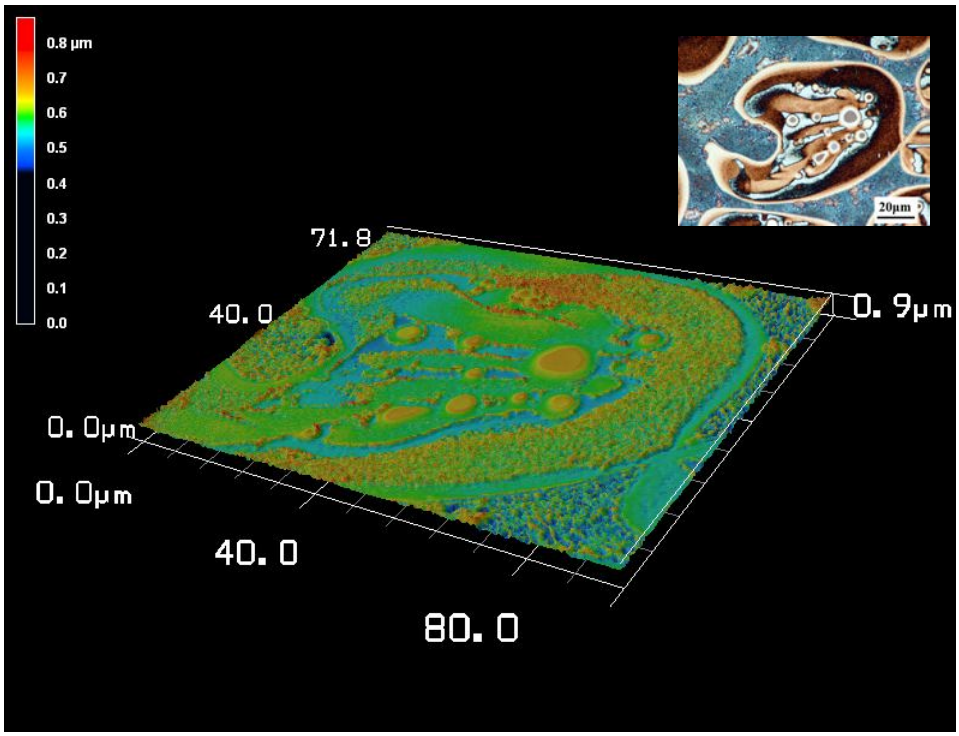

(a)

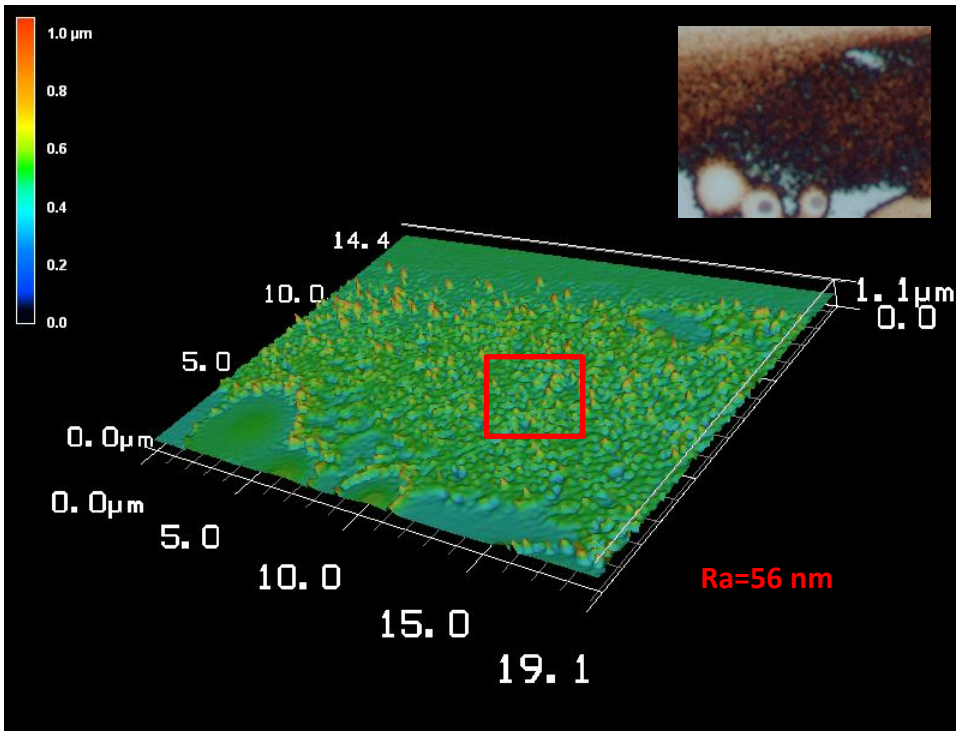

(b)

Fig. 5-12. 3D surface profile made by laser microscopy. Optical micrograph of the same location is shown on the upper right of every 3D profile.

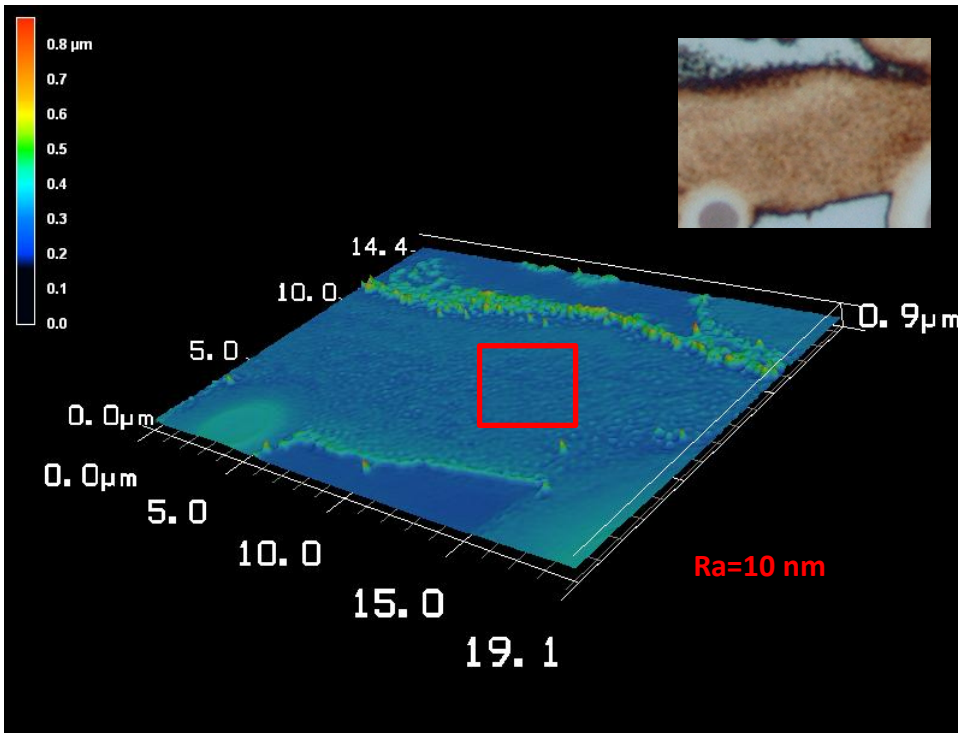

(c)

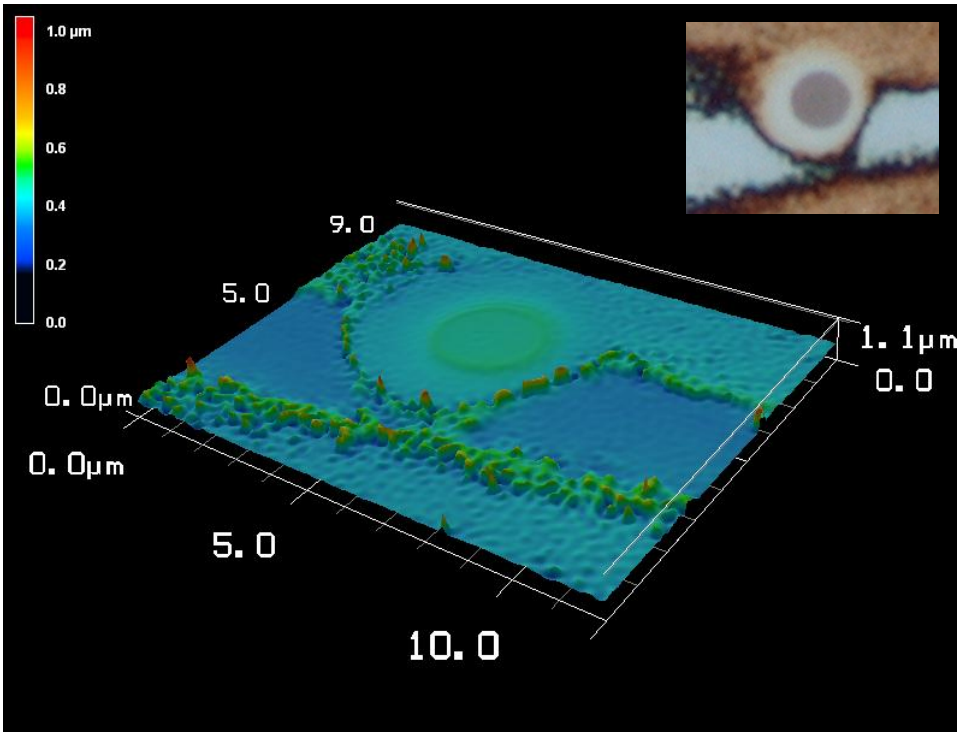

(d)

Continued

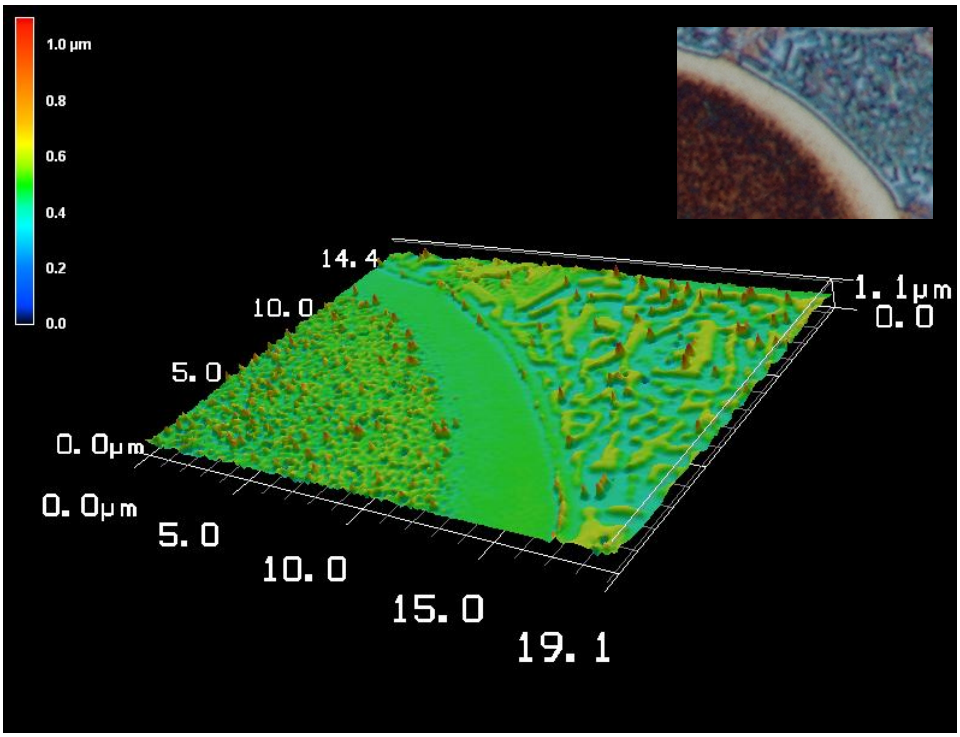

(e)

Continued

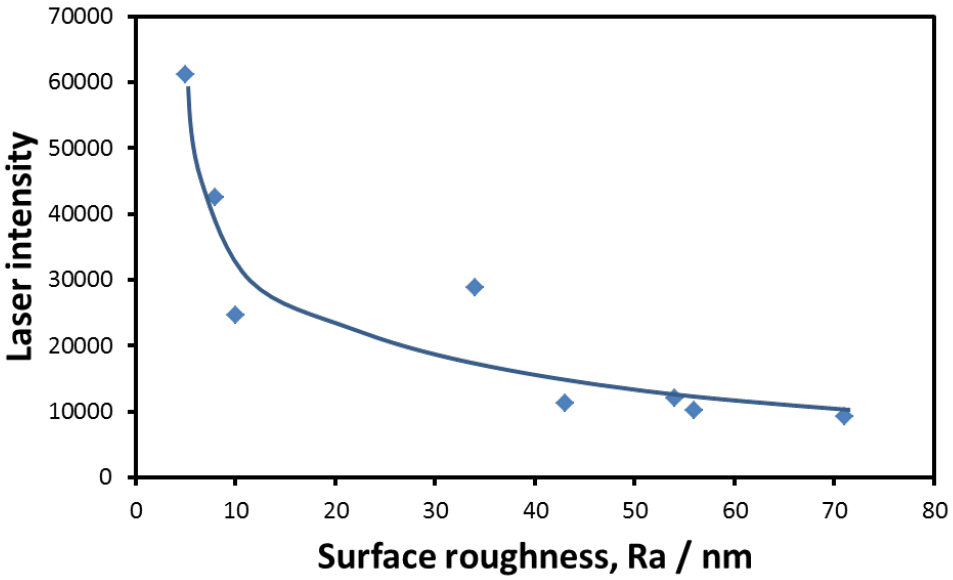

Fig. 5-13. Relationship between laser intensity and surface roughness

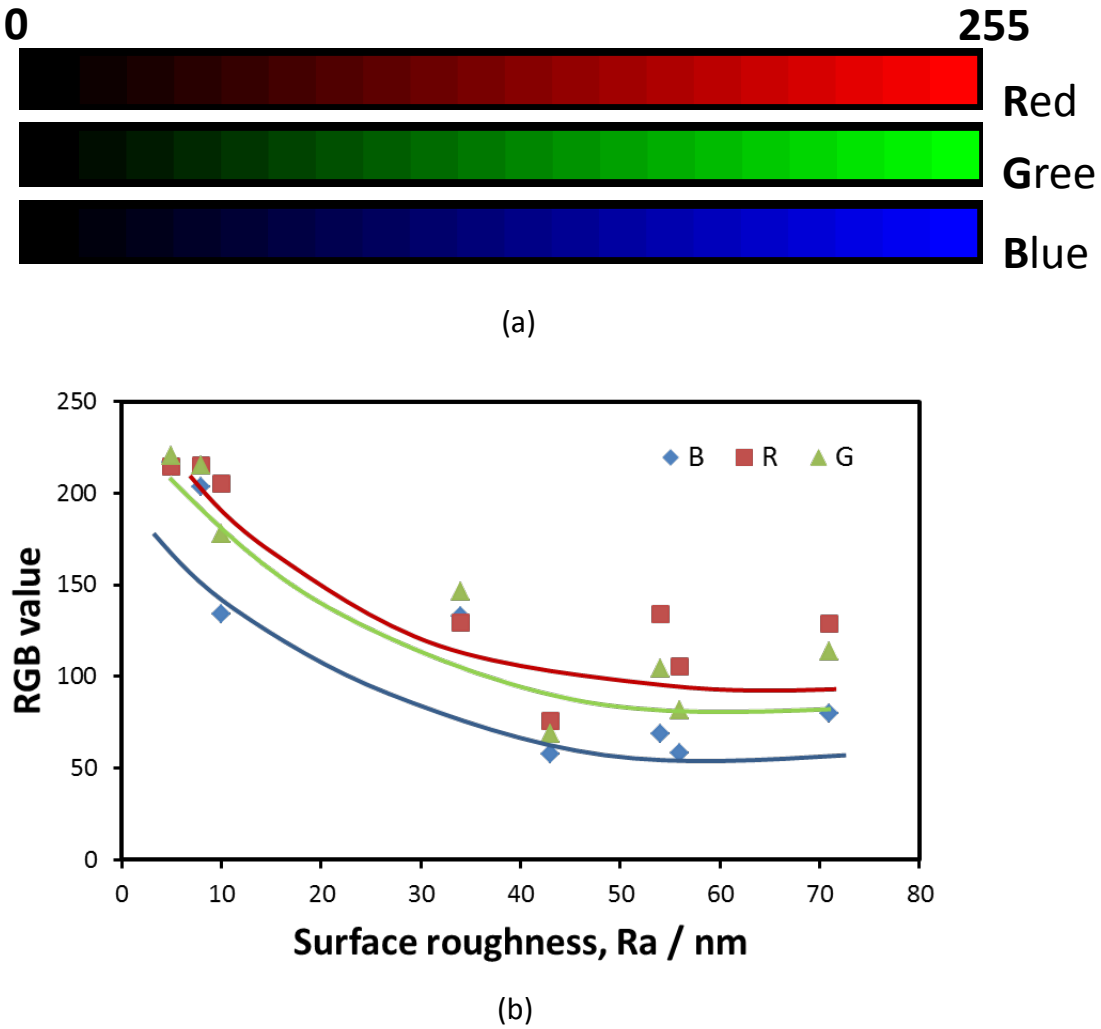

Fig. 5-14. (a) Red, green and blue with different RGB mode value, (b) relationship between RGB value and surface roughness.

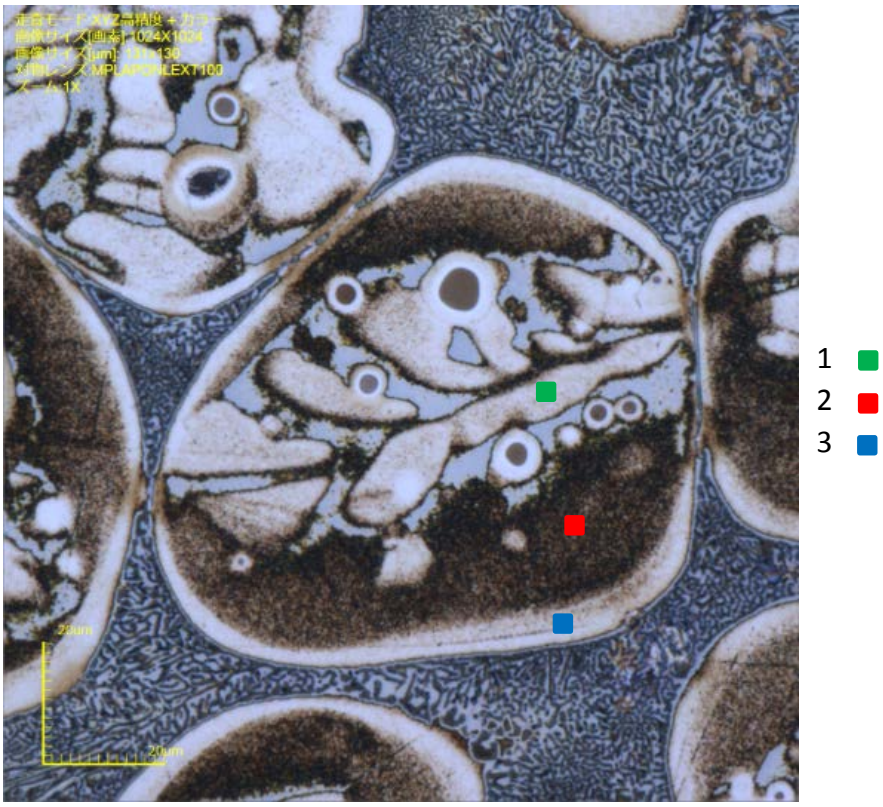

Fig. 5-15. Optical micrograph of the spheroidal grain which was characterized by AFM. The three analysis locations are indicated by three points.

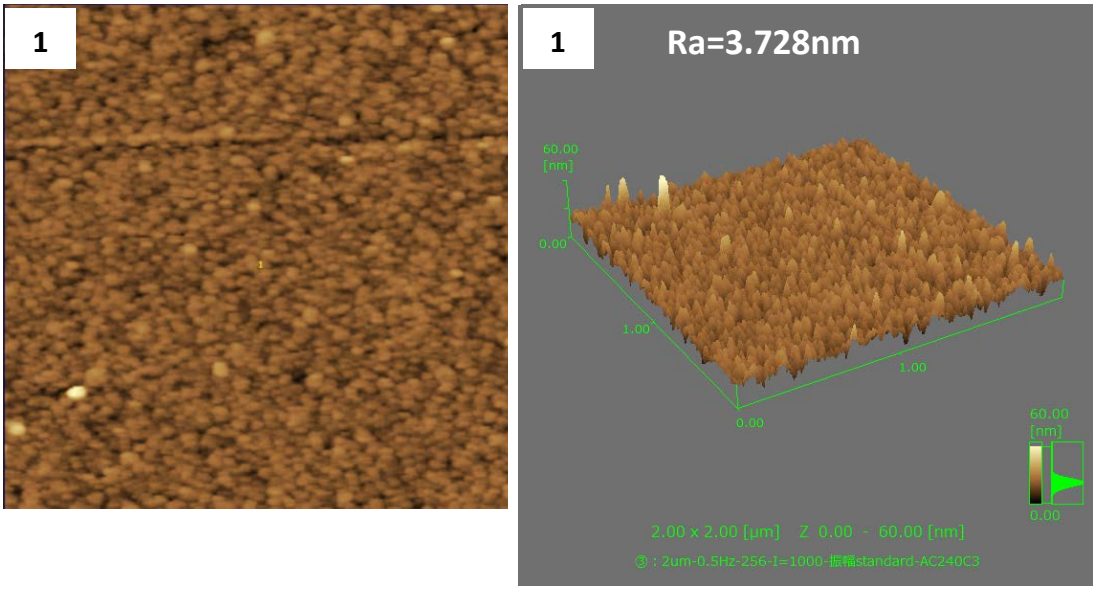

(a)

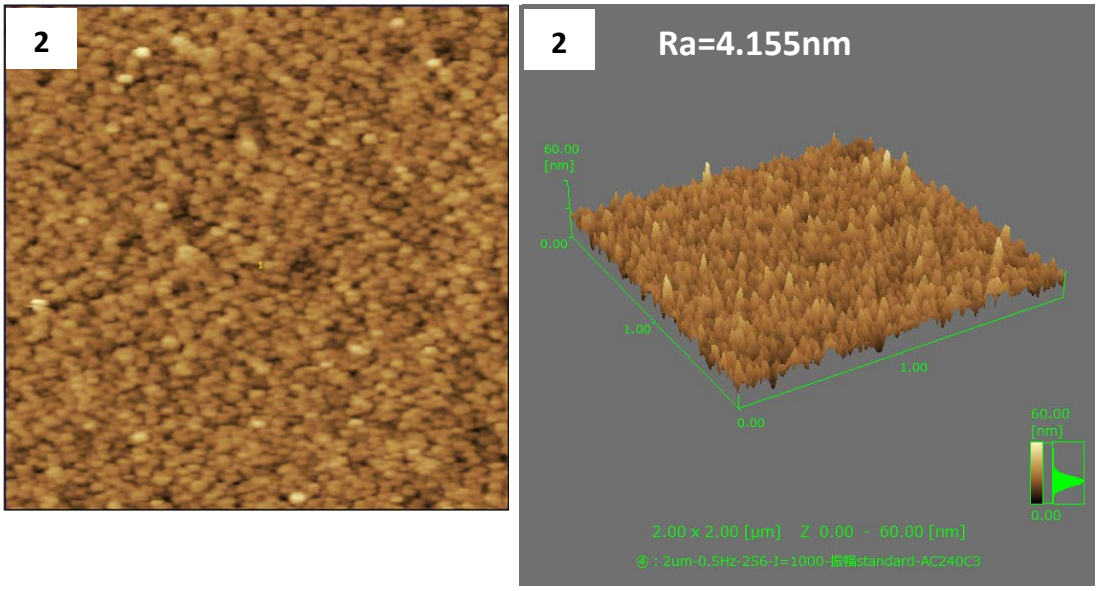

(b)

Fig. 5-16. Both 2D and 3D surface profile made by AFM, the number indicates the analyzed location in Fig. 11.

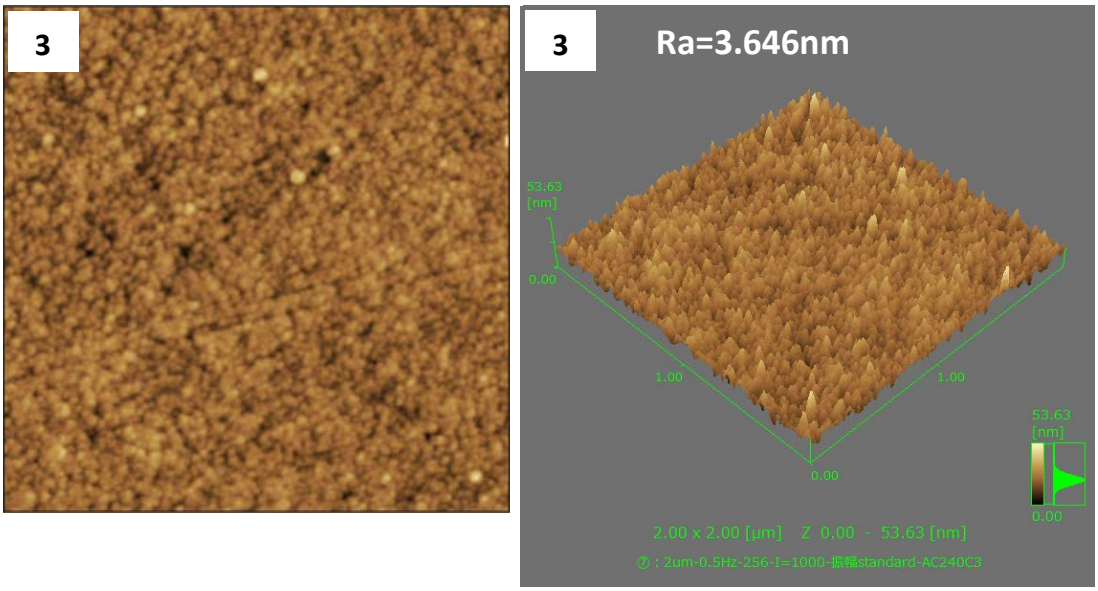
3
3
Ra=3.646nm
53.63
[nm]
0.00
1.00
1.00
0.00
53.63
[nm]
0.00
2.00 x 2.00 [µm] Z 0.00 - 53.63 [nm]
: 2um-0.5Hz-256-I=1000-振幅standard-AC240C3

(c)

Continued

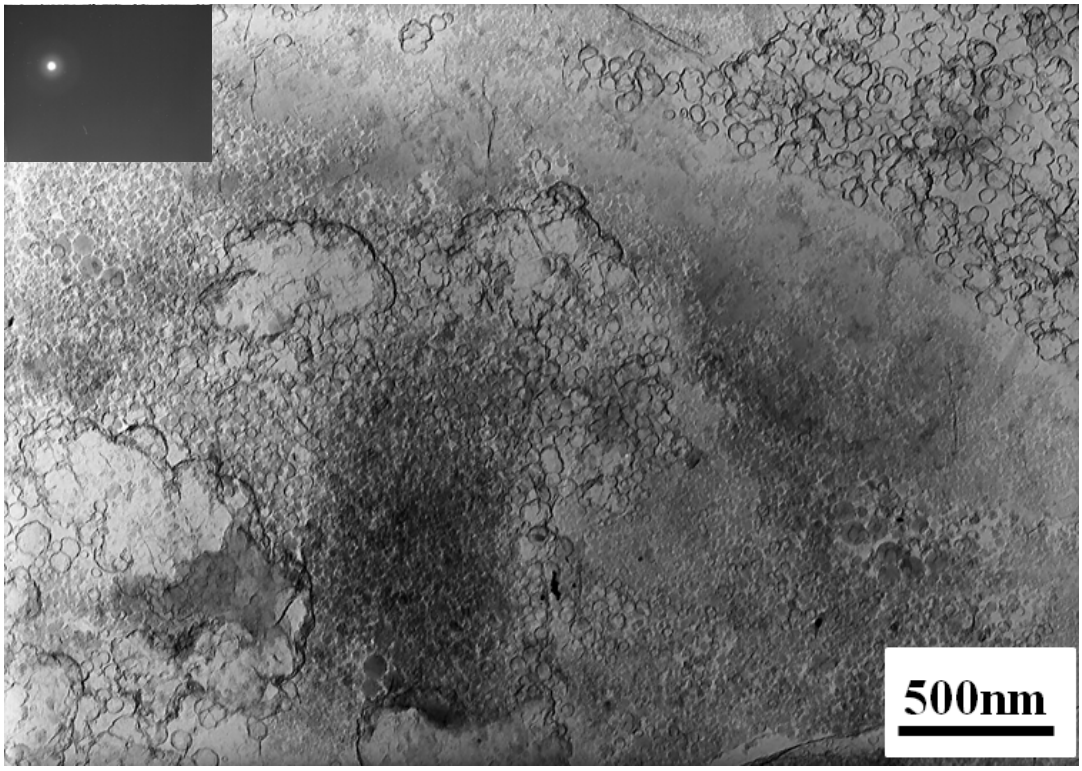

Fig. 5-17. A TEM micrograph at relatively low magnification.

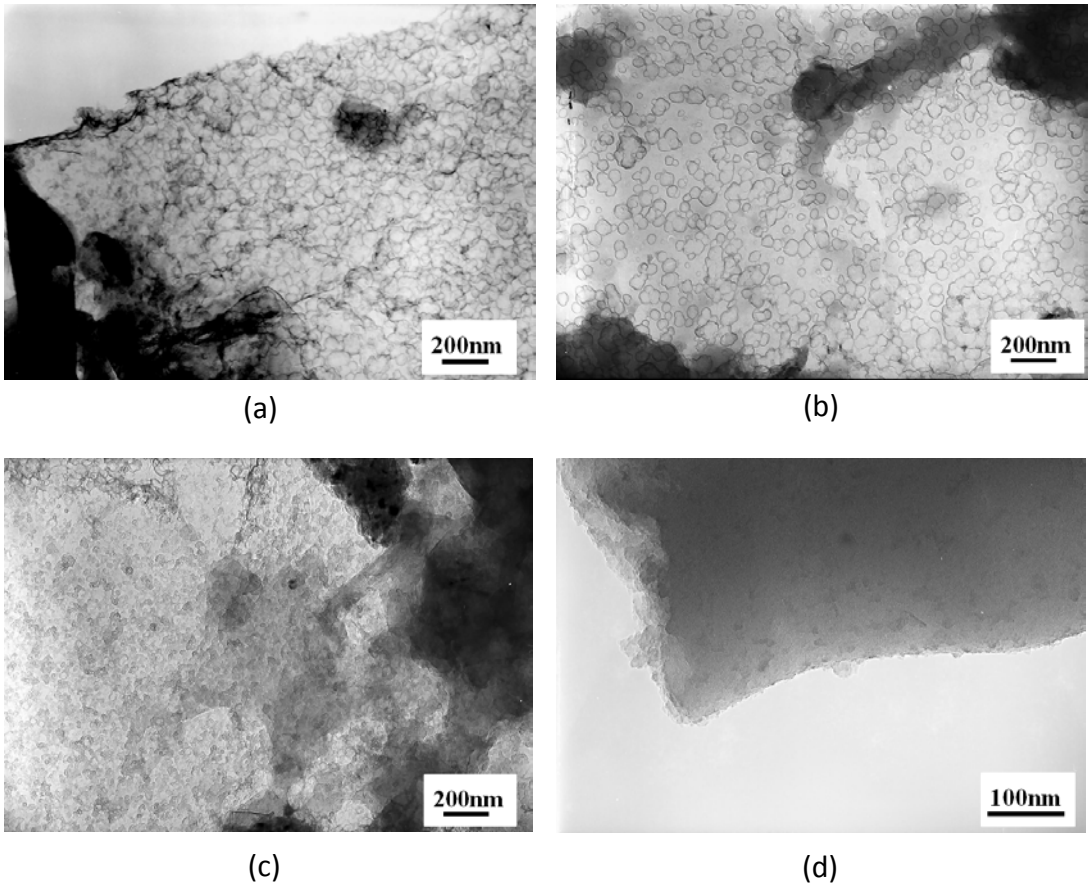

(a) (b)

(c) (d)

Fig. 5-18. TEM micrographs showing different film morphology

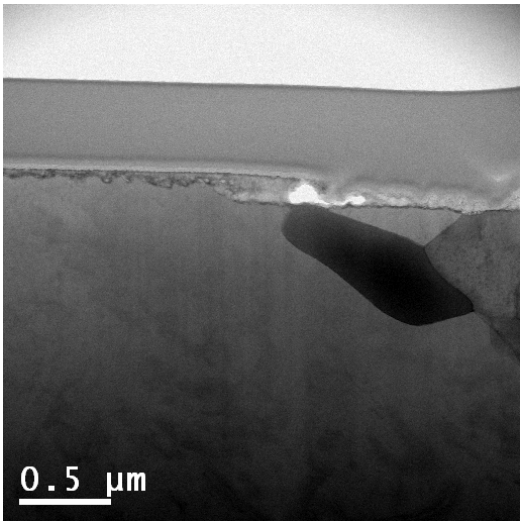

(a)

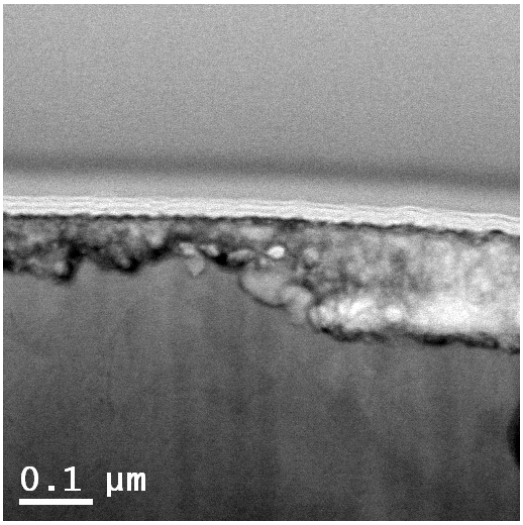

(b)

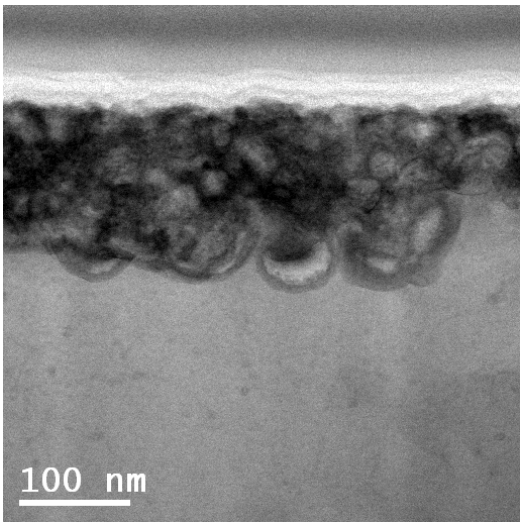

(c)

Fig. 5-19. Cross section of the film observed by STEM.

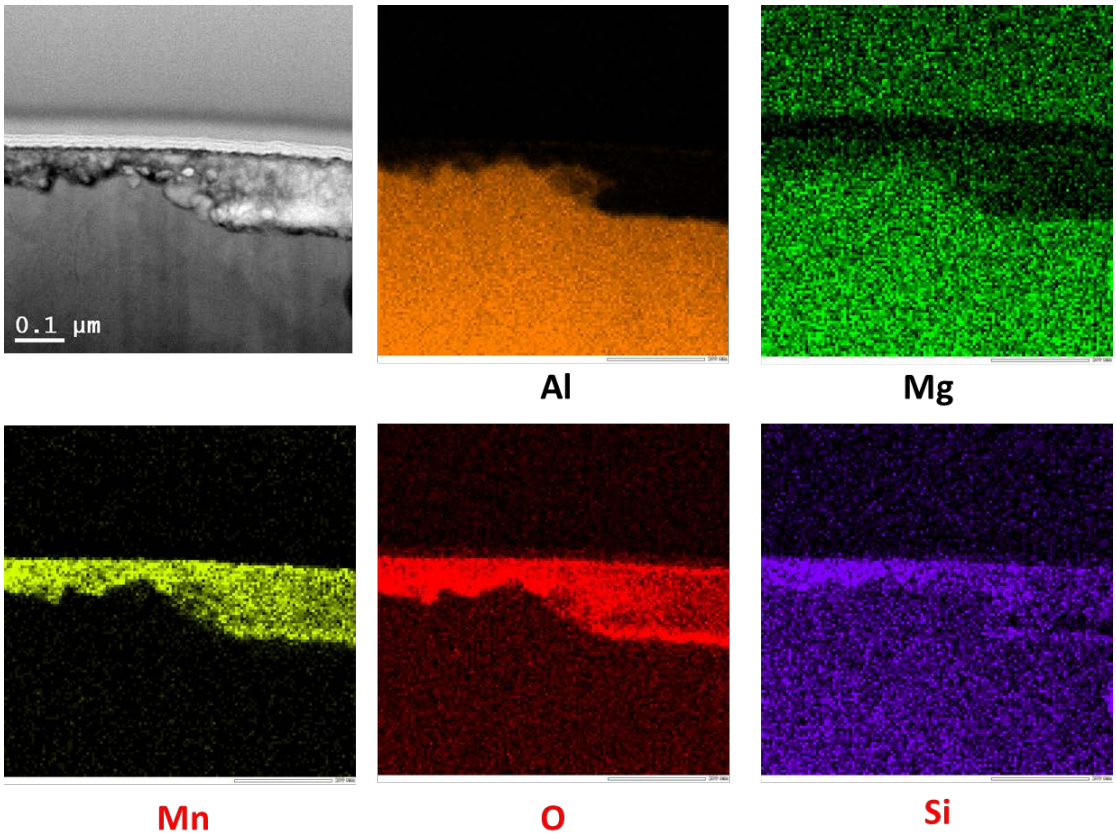

(a)

Fig. 5-20. Composition analysis of the film by STEM equipped with EDS.

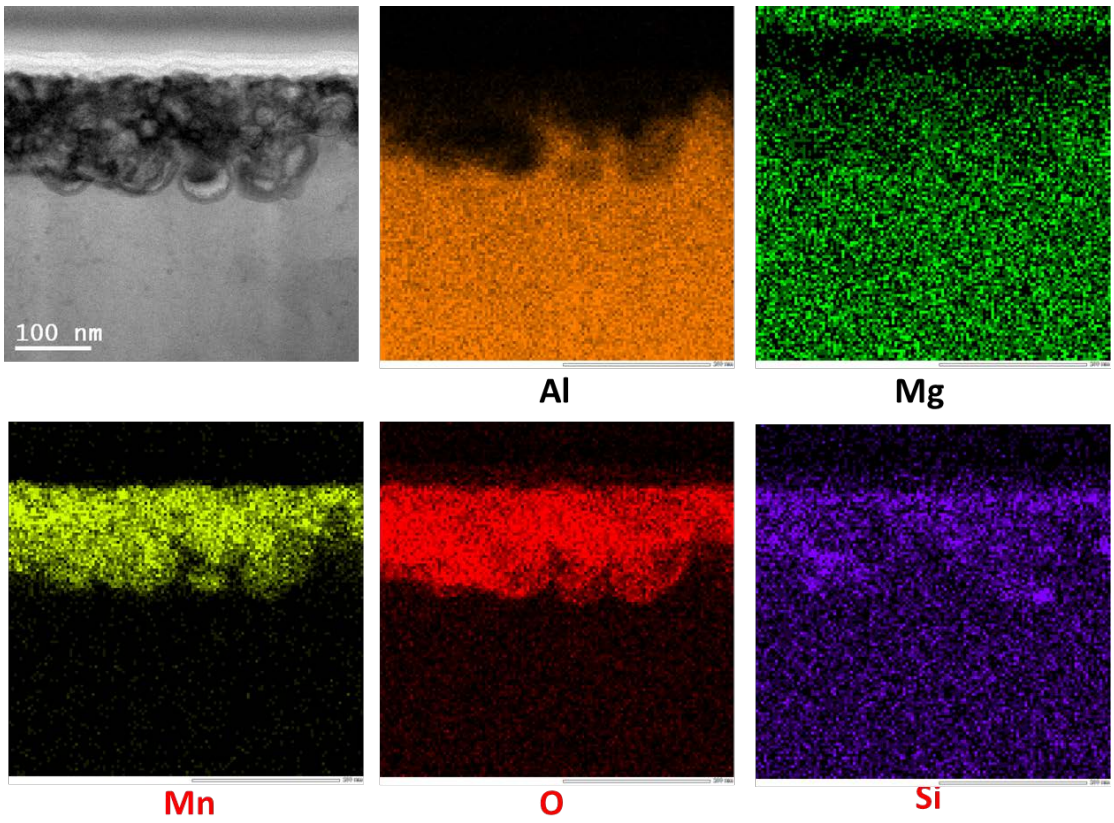

(b)

Continued

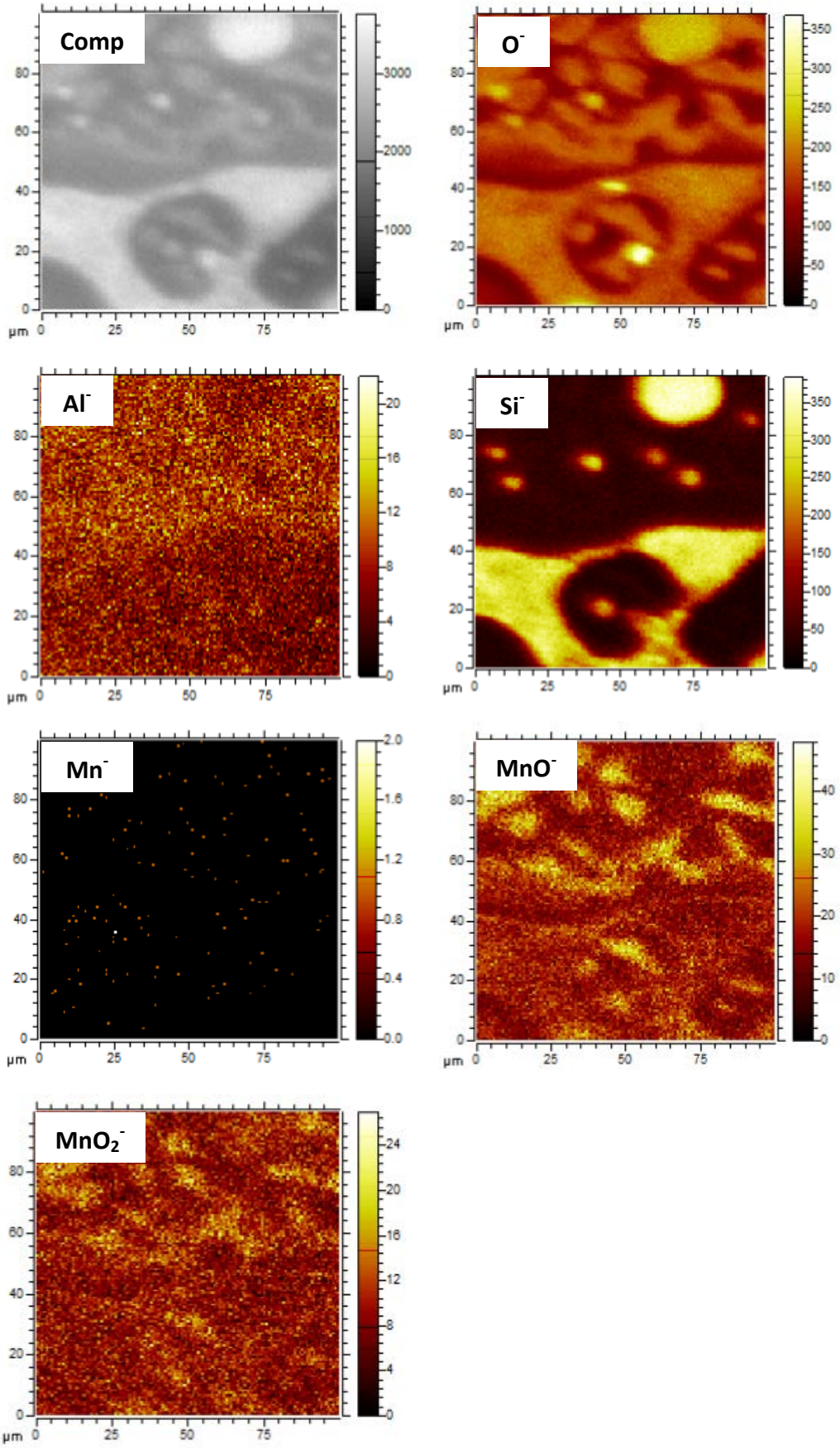

Fig. 5-21. Mapping of negative irons came out from the film analyzed by TOF-SIMS

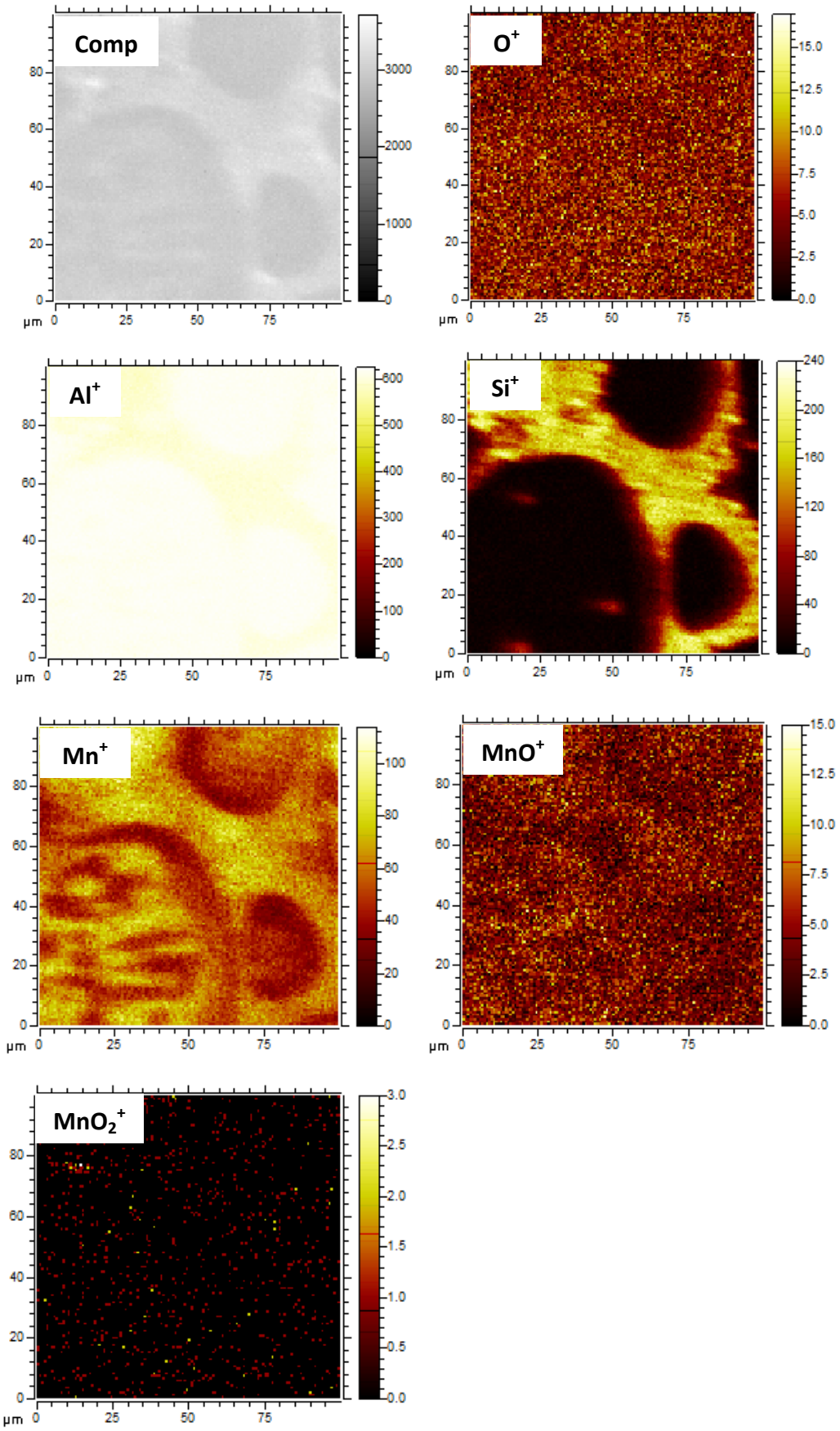

Fig. 5-22. Mapping of positive irons came out from the film analyzed by TOF-SIMS

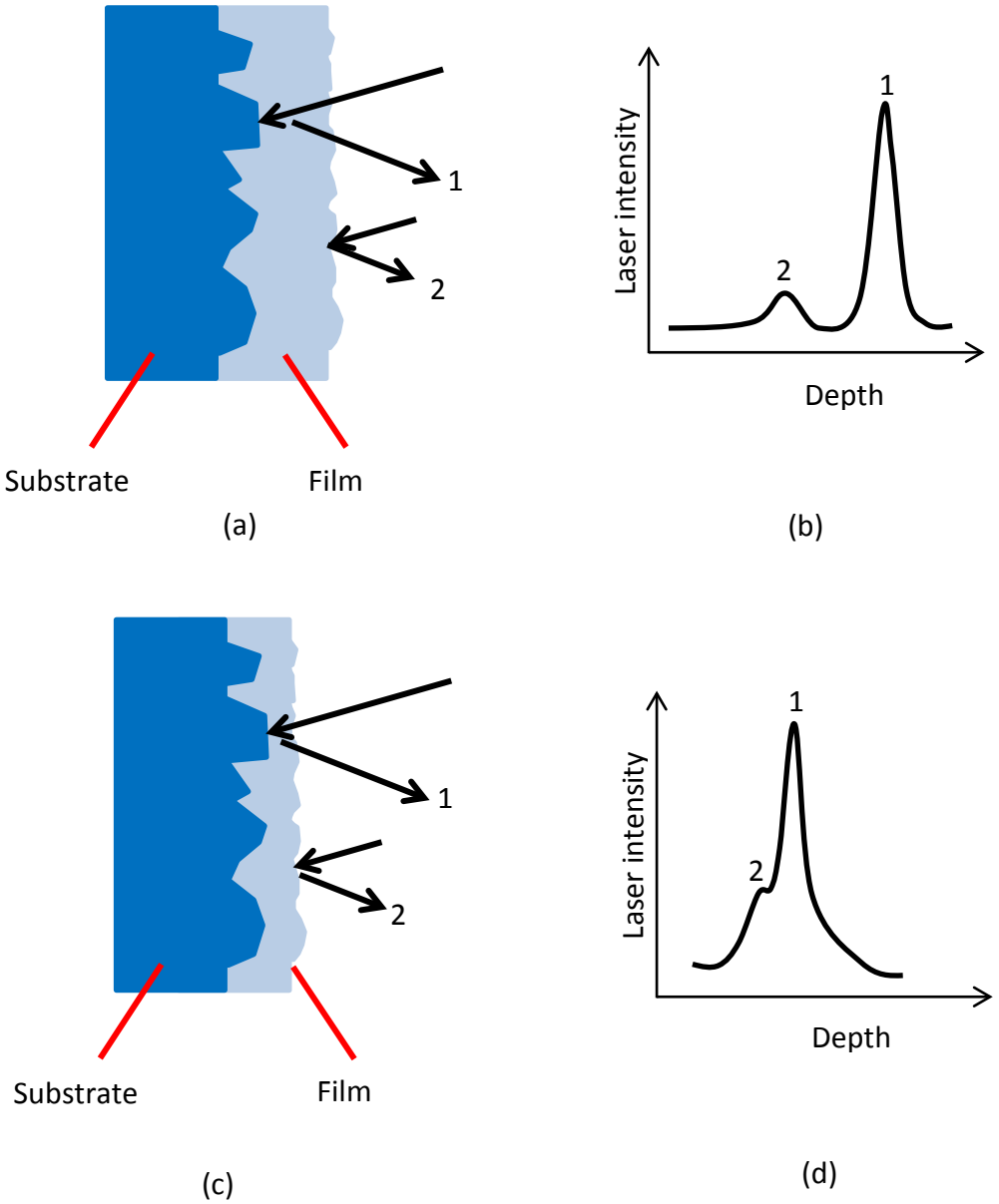

Fig. 5-23. Schematic graph showing the double reflecting of laser when characterizing a transparent film. (a, b) thick(> 1 μm) film, (c, d) thin(< 1 μm) film.

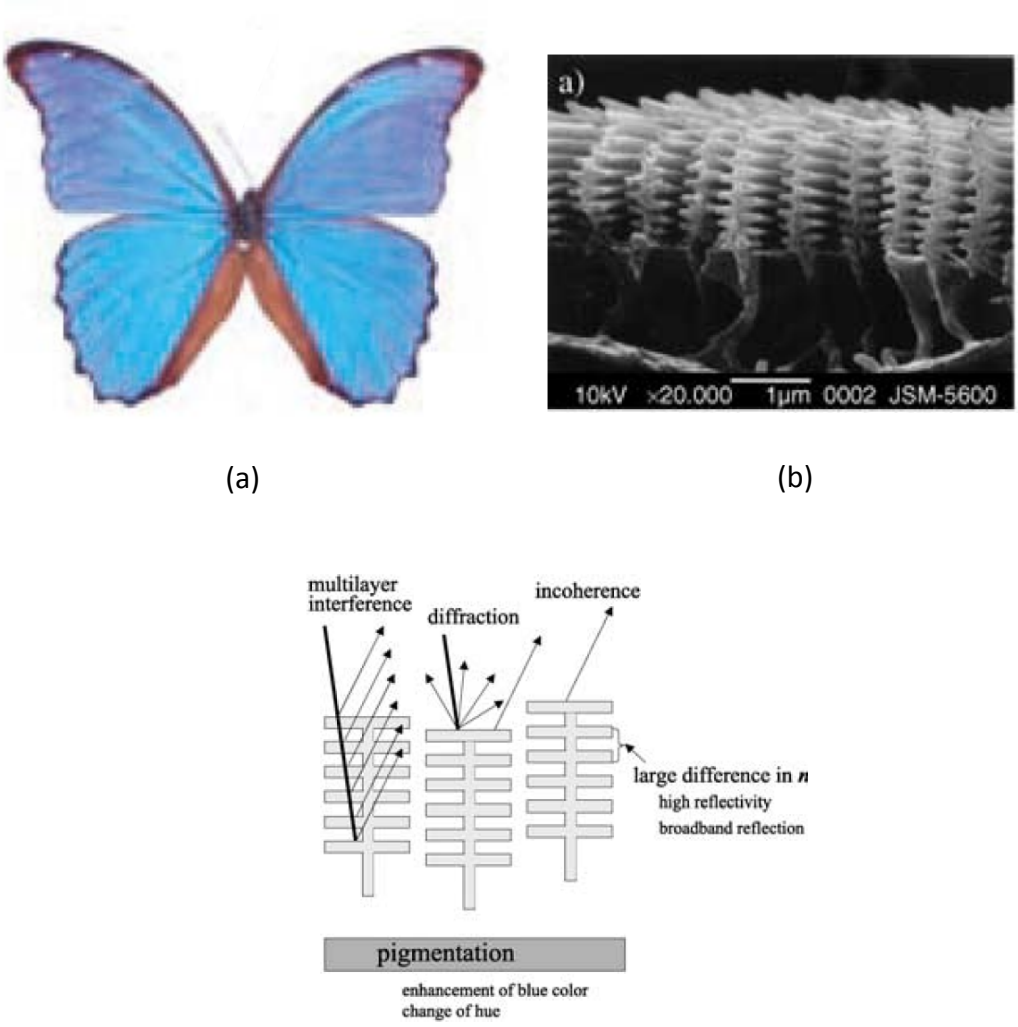

(a) (b)

(c)

Fig. 5-24. The example of coloring mechanism of morpho butterfly [6]. (a) the blue color of the butterfly (b) microstructure of the wing's surface (c) possible coloring mechanisms produced by the microstructure.

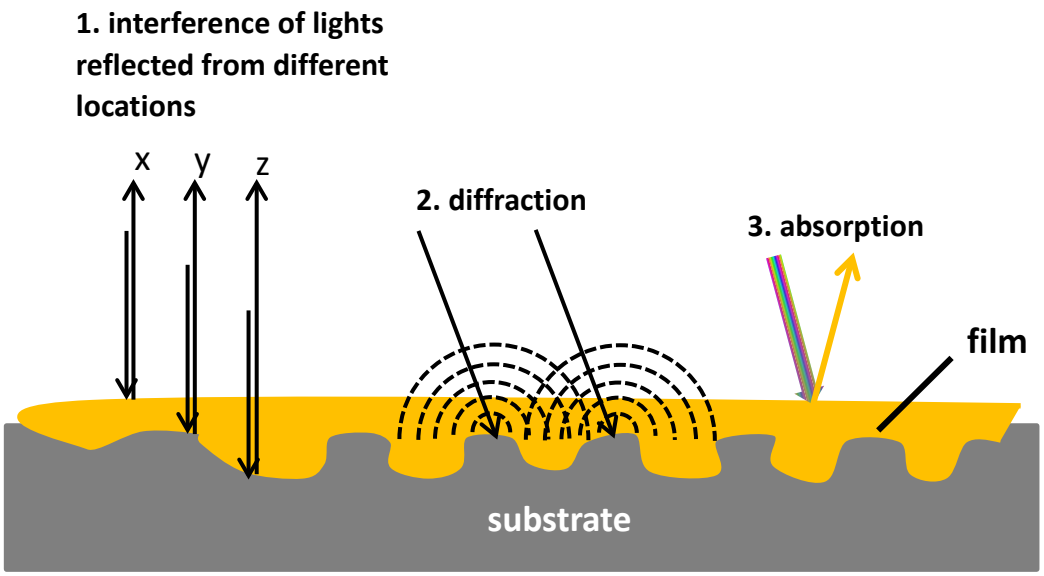

Fig. 5-25. Schematic graph showing the cross section of the specimen after etching as well as three proposed coloring mechanisms

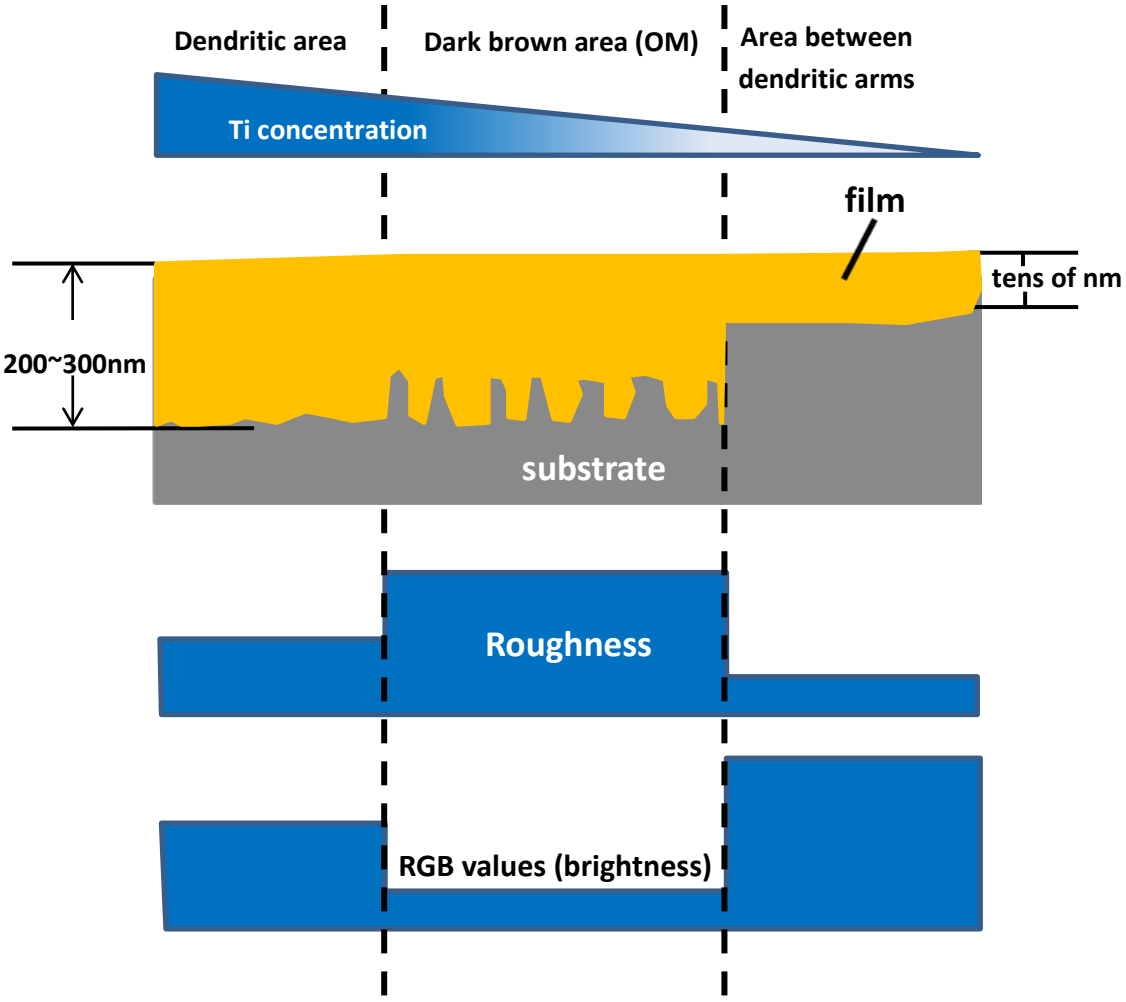

Fig. 5-26. Schematic graph showing the cross section of the specimen after 12 s etching with correlation to the change of Ti concentration

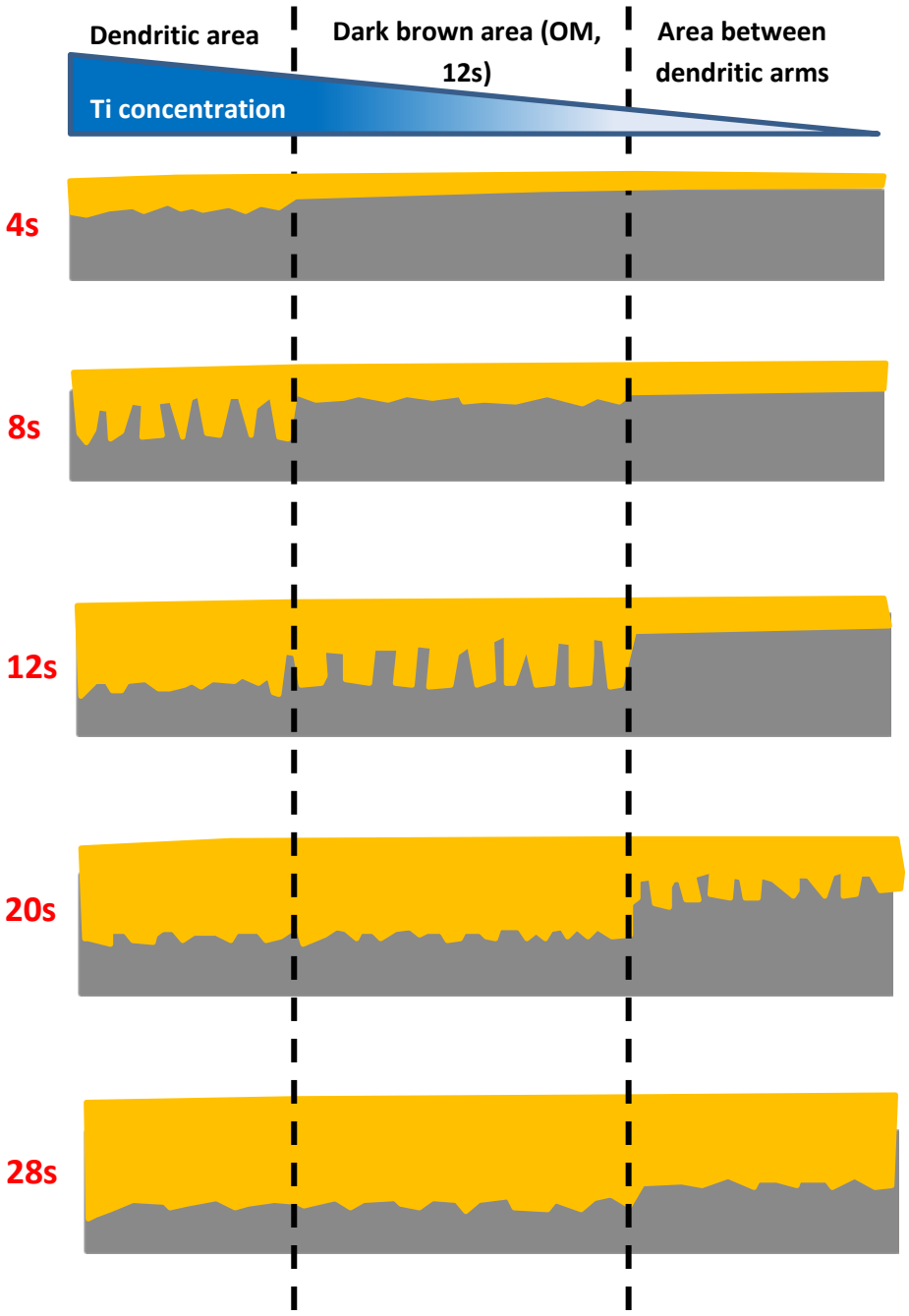

Fig. 5-27. Schematic graph showing the cross section of the specimen after different time of etching with correlation to the change of Ti concentration

Chapter 6

Summary and general conclusions

In this thesis titled “Color metallography of Al alloys using Weck’s reagent: applications and coloring mechanism”, the color etchant named Weck’s reagent was used to reveal the color metallography of various Al alloys. The first task of this thesis was to study the detailed relationship between micro-segregation in Al and the color difference revealed by Weck’s reagent. After that, using this ability of detecting micro-segregation, Weck’s reagent was used for the evaluation of solid fractions and the study of microstructure evolution for semi-solid processed Al alloy. Finally, the coloring mechanism of Weck’s reagent was studied through various characterizations of the etched surface.

In Chapter 1, an introduction of both color metallography and Weck’s reagent was given. Some accepted coloring mechanisms were also introduced by referring to recent published studies. The objectives and construction of this thesis were also given in this chapter.

In Chapter 2, focus was paid on the detailed correlation between micro-segregations in Al and the color difference revealed by Weck’s reagent. By using Al-7%Si and Al-5%Mg binary alloys, the color

difference was revealed inside dendritic Al grains after etching by Weck's reagent. The binary composition of the specimen has proved that micro-segregation of either Si or Mg can be visualized by Weck's reagent.

If the material is multi-component, the color revealed by Weck's reagent should be the result of the all the micro-segregations inside Al phase. In the case of Ti-contained A356 Al alloy, both micro-segregations of Ti and Si existed in dendritic Al grain.

Not only dendritic structure, micro-segregations in spheroidal grains can also be characterized by Weck's reagent. However, in the case of Ti-contained A356 Al alloy, Si's micro-segregation disappeared while Ti's micro-segregation still remained, which could be revealed by Weck's reagent. The extremely low diffusion speed of Ti contributed to the preservation of Ti's micro-segregation at semi-solid state. In the case of Ti-free spheroidal grain, no micro-segregations could be detected by EPMA. But color difference could still be seen after etching although the contrast was low.

In Chapter 3, accurate evaluation of solid fractions for the commercial A356 Al alloy was realized using Weck's reagent to visualize the grain growth during water quenching.

When evaluating the solid fraction, the grain growth revealed by Weck's

reagent was excluded and the area fraction of the original solid phase was calculated as the solid fraction. The solid fractions were measured for the entire semi-solid temperature ranging from 575 ^{o}C to 615 ^{o}C. The results obtained by excluding the grain growth using Weck's reagent agreed well with the values calculated from Al-Si binary phase diagram. The overestimation of those values obtained without excluding the grain growth was also exhibited. It was found that the overestimation was larger in the higher temperature side because at higher temperature, the grain growth during water quenching was also thicker, so without excluding the growth layer, more overestimation will be caused.

Solid fraction evaluation by using Weck's reagent is an improved image analysis. Comparing with in-situ observation technique, the present method is time saving and economical. Furthermore, this color etching method can be applied to both equilibrium and unequilibrium state without influence of the experiment conditions.

In Chapter 4, A356 aluminum alloy was RAP processed to produce semi-solid slurry with spheroidal Al grains. Optical microstructure observation was carried out by using Weck's reagent to visualize the inner microstructure of ripening Al grains with attention paid on the microstructure evolution and ripening behavior of Al dendritic grains.

In contrast to the coarse grains which could not be spheroidized in the

strain free specimen after partial re-melting, the strain induced specimen showed a much finer and spheroidal structure at semi-solid state. Microstructures before complete spheroidization showed that the dendritic Al grains were ripened gradually. At the same time, eutectic Si particles were also coarsened at first and then melted when the temperature became higher than eutectic melting temperature. After that, liquid phase penetrated toward grain boundaries, which contributes to the spheroidization of Al phase.

By optical observation after etching using Weck's reagent, Al dendrites were found separated during heating before liquid was formed, which contributed to the refinement and spheroidization of Al grains. This phenomenon was compared with EBSD observation, which leads to the conclusion that the separating lines were actually HAGBs. This comparison proves that Weck's reagent can also be used to reveal grain boundaries in Al alloys. The EBSD analysis found that numbers of those HAGBs was decreasing during heating due to the connection of them resulted from migration inside dendrites.

In Chapter 5, coloring mechanism of Weck's reagent was focused. Various characterization methods were applied to understand more about the film in terms of surface topography, cross section observation and chemical composition.

In the beginning of this chapter, the reproducibility of the color revealed by Weck's reagent was tested first by repeating the 12 s etching for four times in total. The results showed that the reproducibility of the color revealed by Weck's reagent was quite good, with stable color microstructure obtained every time.

The etched (12 s) surface topography of Ti-contained and Ti-free A356 Al alloy was observed by both SEM and FE-SEM. In the case of Ti-contained A356 Al alloy, the surface topography changed from location to location inside the spheroidal Al grain. Comparing the topography with color optical micrograph, it can be seen that the topography was in strong correlation with the color difference revealed by Weck's reagent. Furthermore, the topography was also in correlation with Ti micro-segregation inside Al grain. Higher concentration of Ti in Al phase resulted in the formation of smooth film. On the contrary, lower concentration of Ti led to a rough surface. The Ti-free A356 Al alloy showed a low color contrast after etching with Weck's reagent. However, in the region corresponding to the grain growth during water quenching, due to the simultaneous segregation of Si and Ti, the film was smooth and well formed. But the morphology was different from the smooth film in the dendritic region in Ti-contained Al alloy. Color micrographs obtained with other etching time were also shown. Compared with 12 s etching, their color contrast was decreased. According to surface observation by

SEM, 12 s etching showed the best contrast in topography inside Al grains.

The relationship between surface condition and color was investigated quantitatively by laser microscopy. The results showed that the reflected laser intensity and RGB values decreased as the average surface roughness increases. However, AFM analysis conflicted with laser microscopy by which the surface roughness seems to be low and constant. Considering the fact that the film is probably transparent, the rough surface detected by laser microscopy might be actually the interface of film and substrate, which was in agreement with cross section observation of STEM.

TEM observation of film also detected difference in the film morphology from location to location. The halo pattern indicated that the film is amorphous. Some locations containing “bubble” like structure with different density were found, which might be in accordance with the SEM observations at dendritic and dark brown areas.

Cross section observation by STEM revealed that the film thickness ranged from tens of nanometers to 200 nm. It was also interesting that the interface between film and substrate was rougher than the surface of film, which supported the viewpoint that the rough surface observed by laser microscopy was actually the interface of film and substrate. Composition analysis carried by EDS equipped showed that the film was rich in Mn, O

and Si in spite of the difference in morphology. This result proved that the film was actually manganese oxide. Si had higher concentration in the film than the substrate probably due to the consumption of Al reacted with Weck's reagent.

SIMS analysis further helped to understand the chemical composition of the film. The existence of MnO_2 was confirmed. MnO^- ions were also detected that probably come from MnO_2 due to the ionization. The ion mapping also indicated that the concentration of manganese oxide differed in different location, which could also have an influence on the color observed by optical microscope.

Coloring mechanism was proposed with consideration of the structure of the film formed during etching with Weck's reagent. The surface of the film and the rough interface between film and substrate could both reflect incident light, which led to the interference of light. Diffraction can also happen but it was not confirmed. At the same time, the absorption of light with a certain wavelength by manganese oxide can also contribute to the coloration. The color observed by optical microscope should be the combination of those effects.

The concentration of Ti in Al has a strong influence on the film formation. Higher concentration of Ti can promote the film growth. 12 s showed the best color contrast because that the difference of film thickness and morphology among difference locations in the Al grain is

the biggest. As the etching time increases, in spite of the location or Ti concentration, the color tends to be brown and the morphology of film also becomes homogeneous.

Color metallography using Weck's reagent has already been invented for about 30 years. However, the understanding of this characterization method has never been enough. As a result, the application has also been limited. The present thesis has included the four years' study of this color etchant. Various applications in Al alloys have been demonstrated in this thesis and a wider use of this etchant is expected. Also, the coloring mechanism was studied as another main topic of this thesis. The color comes from a manganese oxide film formed during etching, which has smooth surface but a rough interface with the Al substrate. Coloring mechanism should be a combination of several effects including light interference, diffraction and absorption.

Appendix

1. Manual of color etching with Weck's reagent

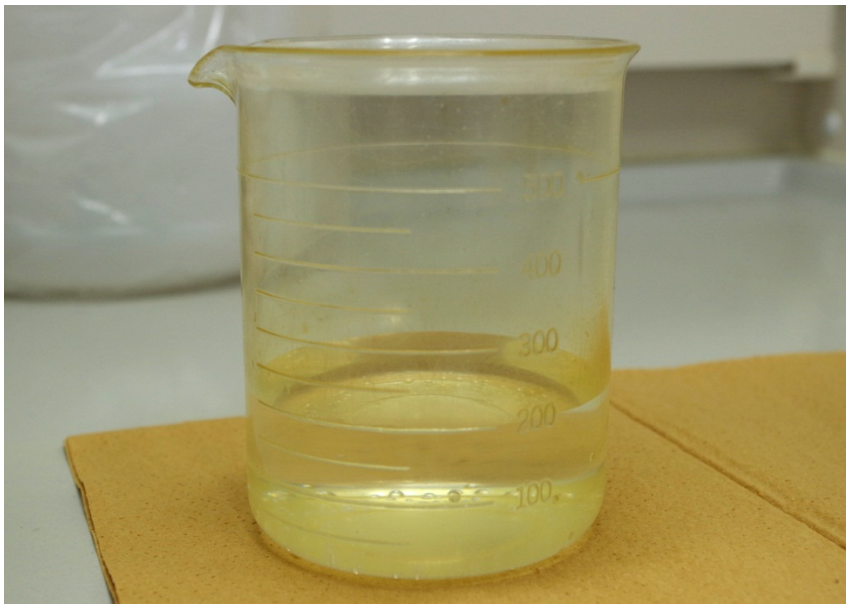

200 mL distilled water, use plastic beaker

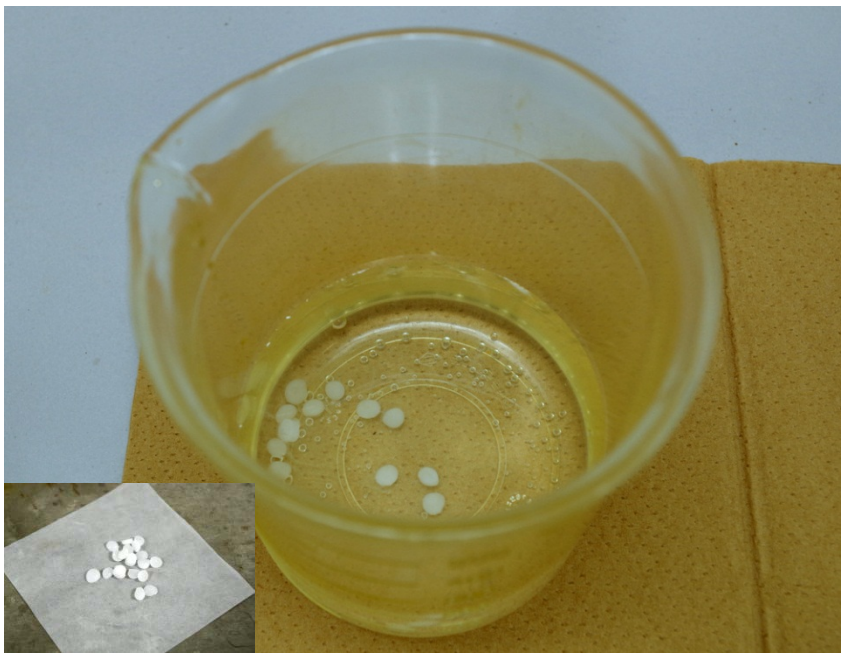

Add 2.0 g NaOH, wait until it all dissolved.

Add 8.0 g $KMnO_4$ after NaOH is all dissolved. Stirring is also OK.

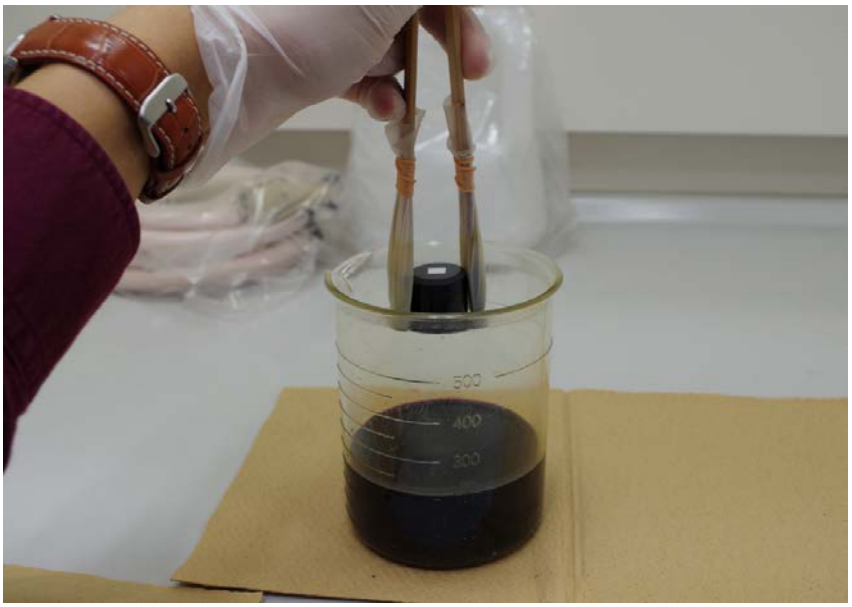

After $KMnO_4$ is all dissolved, etch the specimen for 12 s. The specimen should not be shaken vigorously in the reagent.

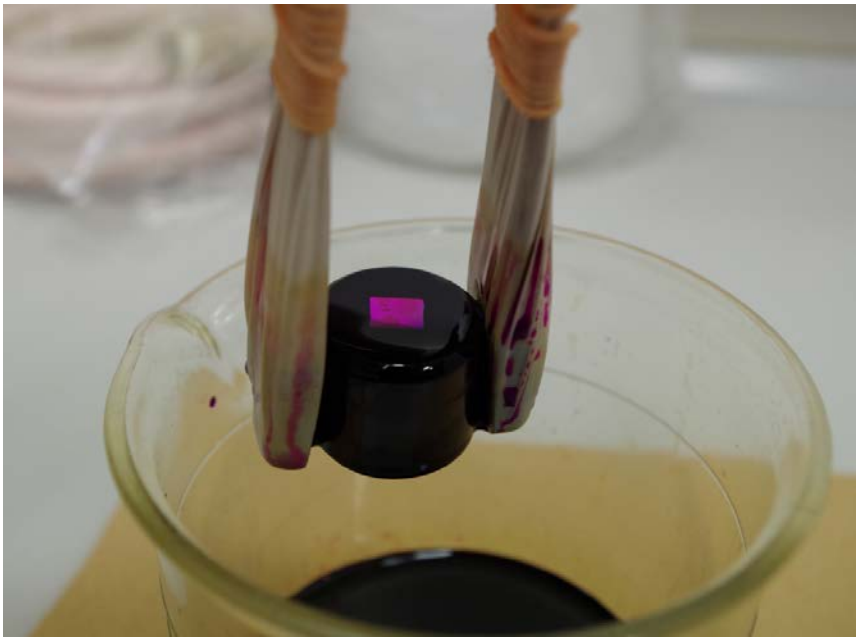

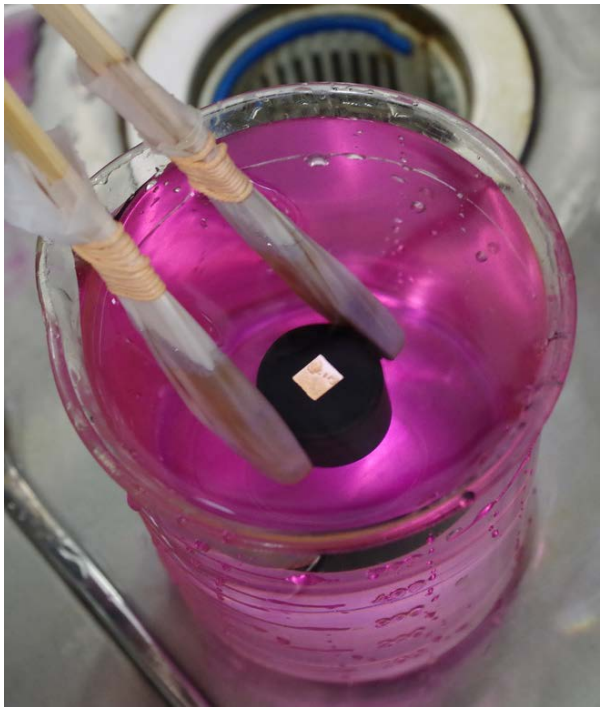

After etching, wash the specimen gently in a beaker with tap water in. Do not wash it using running water. After washing, dry the specimen.

2. Various applications of Weck's reagent

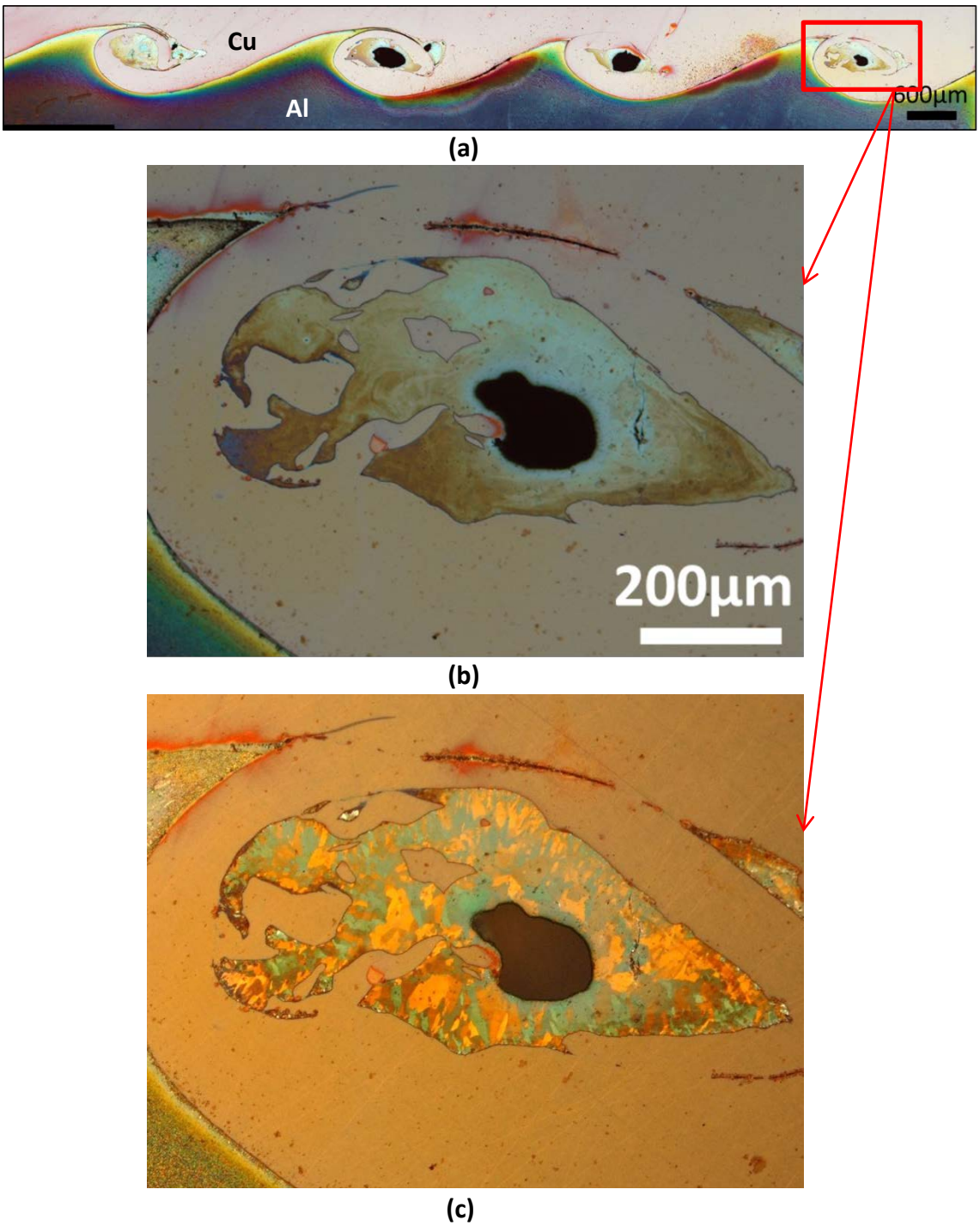

Microstructure of a joint of Cu and Al obtained by explosive welding. Note the color change in the Al side near the wavy interface (a). The microstructure of the vortex after etching is shown in (b) and (c), with grain structures visualized in (c) under polarized light.

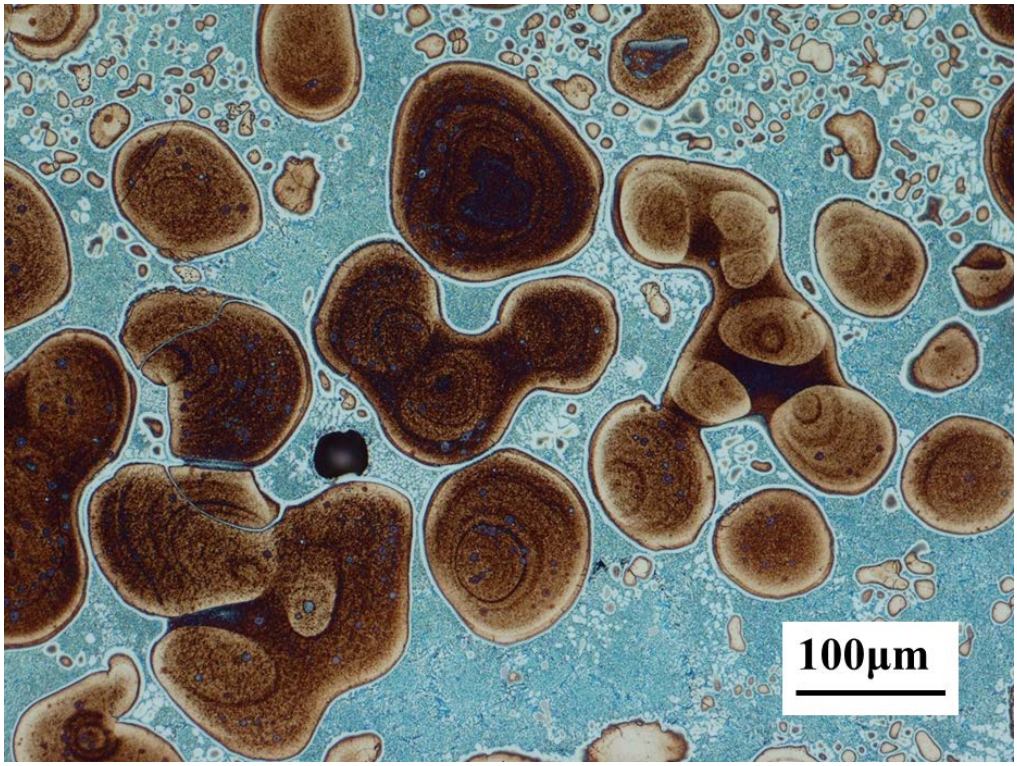

Using Weck’s reagent to etch a rheocast A356 Al alloy. The “annual ring” structure observed indicates the growing history of the coarse Al grain.

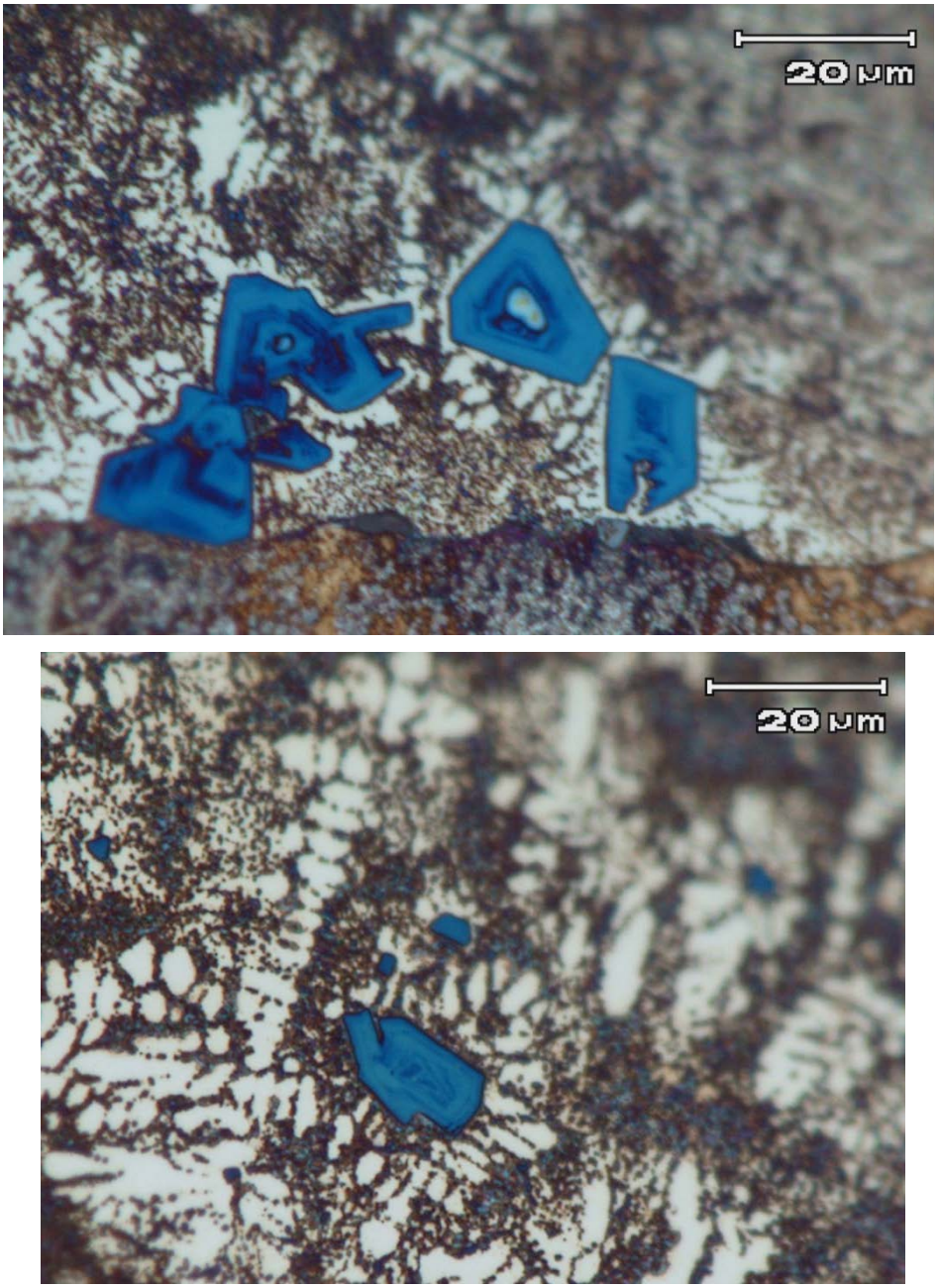

As cast microstructure of an Al-10%Si alloy. Note the structure revealed inside primary Si particles.

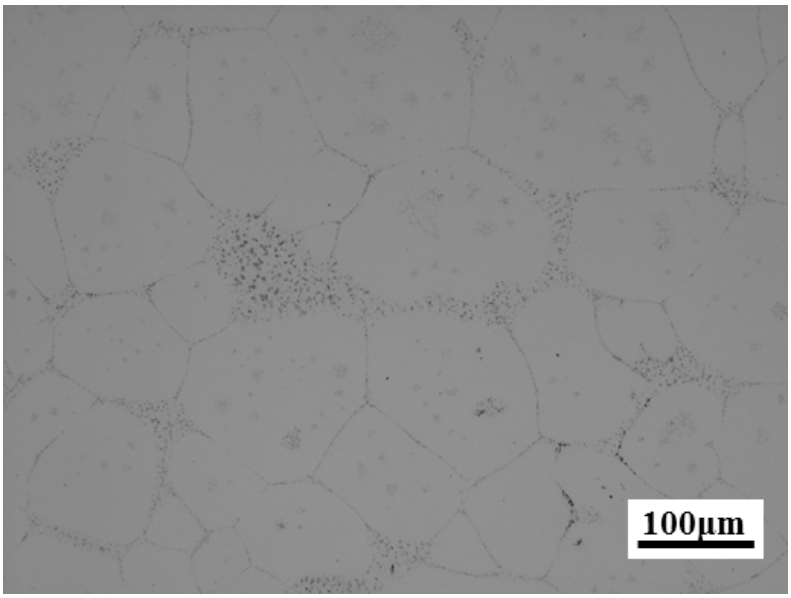

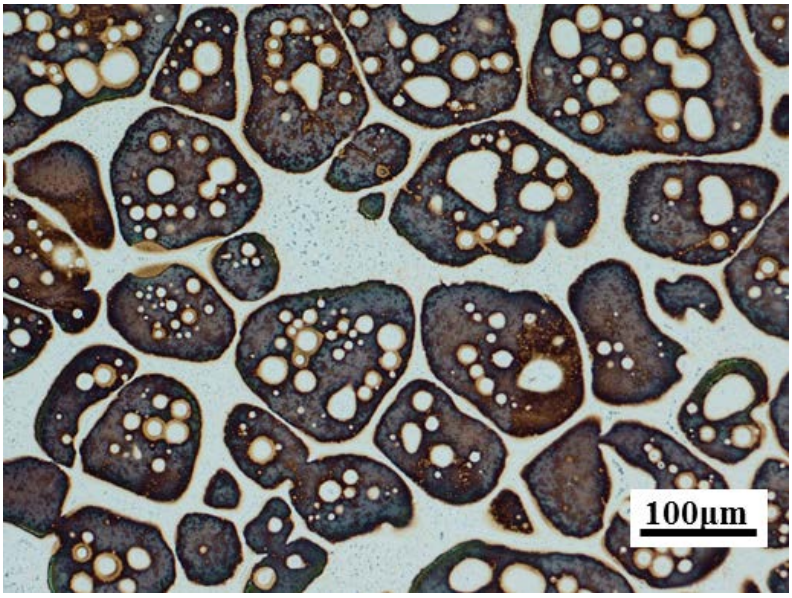

Microstructure of an Al-5%Mg alloy after cold compression and partial re-melting. After etching, it becomes easier to observe the size and shape of spheroidal Al grains.

Acknowledgements

I would like to express my special appreciation and thanks to my advisor Professor Dr. Shinji Kumai who has been a great mentor for me. I would like to thank you for your kind support and encouraging for both my life and research in Japan. As a foreign student, I love the lab and the atmosphere that you have made and kept. I want to tell you that I ENJOYed my life both in this lab and Japan. You also have allowed me to think freely and tried to let me do various experiments outside our lab. When I felt difficulties in some accesses to experiments, you have always helped me out by contacting companies or technicians by yourself. I know you have put much effort on my research, too. Recently, Associate Professor Dr. Shinji Muraishi also joined our lab. Although there is only limited time remained before my graduation, I am sure that you will be a great advisor.

Also, I want to thank sincerely Assistant Professor Dr. Yohei Harada. You have been helping me from the beginning since I came to Japan by moving my heavy luggage to my dormitory. I also remember clearly the time we did experiments together. You were always patient in explaining everything and every detail to me who is not good at reading manual in Japanese. When I had questions about my experiments, you were always very kind to me and tried to help me. It is my great honor and luck to have such a supporter in my research.

Besides the above faculties in my lab, I also want to give my thanks to Professor Tatsuo Sato, Professor Yoshisato Kimura and Professor Masato Sone who belong to this thesis committee. Thank you very much for your interest in my thesis. I would like to thank other professors in the Department of Materials Science and Engineering as well. I have learned a lot from your lectures and the colloquium of this department. I hope I had been a good student in your lectures. I also want to express appreciation to Mr. Hiroyasu Tezuka who has retired from Tokyo Institute of Technology. The discussion about Ti micro-segregation in Al inspired me a lot.

My special thanks go to my lovely lab mates including my *Douki*, *Senpai* and *Kouhai* who have been in this lab from 2010 to 2015. You are all my dearest friends in Japan. When I was not good speaking Japanese, you have helped me a lot in explaining Japanese. I always said to others that “I have not been to any Japanese language school because I have a lot of good Japanese teachers (you guys) around me”. I also enjoyed

nomikai and traveling with you guys. When I was job hunting, Mr. Yusuke Takayama, Mr. Hiroki Yamada and Mr. Hiroaki Yamamoto gave me lots of useful advice and helped me with my job interviews. I really appreciate all the things you have done for me and I hope all of you have a bright future after master's graduation. I also want to thank Mr. Kamolwat Prapasajchavet who has done a lot experiments with me. I hope you also enjoyed your life in Japan and become stronger against the cold winter here.

A lot of people have contributed to the experiments in this thesis. I received my materials from Nissan Motor Co., Ltd and Kyushu Mitsui Aluminium Co., and the cold compression was carried also in Nissan Motor Co., Ltd. I would like to thank all staffs in these two companies. Not only the supplement of materials and compression experiments, but also the discussions with people in Nissan should be appreciated. From next year, I will a member of Nissan Co., Ltd, I hope I will also become an excellent engineer like you in the future. In chapter 5 of this thesis, laser microscopy and AFM measurements were carried out with the help of Keyence Corporation and Olympus Corporation, respectively. I want to thank them for their kind corporation of my experiments.

My study in Japan has been constantly supported by Ministry of Education, Science and Culture with the MEXT Scholarship. I think the money comes from the public revenue of Japan, which means being from all the Japanese people. Therefore, I would like to thank all the people in Japan for providing this scholarship for me and other foreign students like me. Although these four years have been the coldest season for China-Japan relationship, I felt warm welcome and received kind help from everywhere and everyone in this university. I appreciate everyone who helped me in Japan.

Not only people in Japan, but also my friends in China gave me a lot support. Mr. Xu Gong and Mr. Shaoxin Zhu have been my best friends for many years. Discussion with them about experimental methods gave me a lot of inspirations. Thank you very much.

Finally, I would like to deeply thank my parents who have been supporting me these years. Whatever decision I made, you have been on my side, which has given me a lot encouragement. I would like to dedicate this work to you.